2021

An Accuracy and Precision Analysis of the VELYS™ Robotic Assisted Solution for Total Knee Arthroplasty

Gary Doan

An Accuracy and Precision Analysis of the VELYS™ Robotic Assisted Solution for Total Knee Arthroplasty

_____

A Thesis

Presented to

the Faculty of the Daniel Felix Ritchie School of Engineering and Computer Science

University of Denver

_____

In Partial Fulfillment

of the Requirements for the Degree

Master of Science

_____

by

Gary Doan

August 2021

Advisor: Chadd W. Clary, PhD

Author: Gary Doan
Title: An Accuracy and Precision Analysis of the VELYS™ Robotic Assisted Solution for Total Knee Arthroplasty
Advisor: Chadd W. Clary, PhD
Degree Date: August 2021

Abstract

Total knee arthroplasty (TKA) is a procedure where the arthritic surfaces of the knee is removed and replaced with a combination of metal and polymer implants that recreates the joint line to restore function and quality of life. Implant alignment is important in the success of a TKA. Modern day conventional instrumentation can be cumbersome in the operating room and can be inaccurate when resecting bone and aligning implants. Patients with large errors in resections and implant orientation are more prone to experience mechanical failures with their TKA. Mechanical failures in primary TKA require revision surgeries which can lead to further iatrogenic effects. New technology has been created to reduce these errors such as computer-aided surgery and robotic assisted total knee arthroplasty (RATKA). The purpose of this study was to measure the accuracy and precision of femoral and tibial osteotomies and implant alignment between RATKA and conventional total knee arthroplasty (CTKA). The results showed that coronal plane resection errors improved from 1.39° ± 0.95° to 0.65° ± 0.50° and implant alignment absolute errors improved from 1.42° ± 1.15° to 0.91° ± 0.83° for RATKA cases. Improvements were also seen for sagittal plane implant alignment and femoral relative resections for RATKA cases. Other measures reported non-inferiority and there was no statistical difference in the flatness of the proximal resection ($p = 0.36$) between CTKA and RATKA.

Table of Contents

List of Figures

List of Tables

Chapter 1 : Introduction

1.1 Introduction

Knee osteoarthritis (OA) is the degeneration of articulating cartilage in the knee joint that causes inflammation, pain, and/or joint stiffness due to wear. Treatments for mild knee OA include physical therapy and anti-inflammatory medication, but in severe cases, osteotomies and arthroplasties are common procedures.

As the current population ages and rates of osteoarthritis increases, more people are in need for a total joint replacement. Data from 2000 to 2014 shows that total hip arthroplasty (THA) is projected to grow 71% to 635,000 procedures and total knee arthroplasty (TKA) is projected to grow 85% to 1.26 million procedures by 2030 [1]. The age of traditional recipients for TKA range from 60 – 70, but the mean patient age for a total joint arthroplasty has been getting younger [2]. As younger patients are more physically active, revision rates among the younger population have increased [2]. Because revision surgery is expensive and often results in worse outcomes, increasing implant survivability is pertinent to offset the increasing rates of revision surgery. At the moment, studies have shown that implant survivorship ranges from 92 – 97% at 10 years postoperative of the primary TKA [3]. Implant survivorship decreases dramatically to 82% at 25 years postoperatively [4]. This is a problem as younger patients are expected to outlive the life of the implant; thus, requiring revision TKA after implant failure.

Today, common causes for revision surgery are infection, loosening, instability, periprosthetic fracture, etc. [5,6]. Following short term failures due to infection are mechanical failures such as: loosening, instability, anterior knee pain and periprosthetic fracture. There are various reasons behind mechanical failures, but evidence suggests that inaccurate resections and implant malalignment are contributing causes [7,8].

Currently the most popular way to perform TKA is using conventional tools where the surgeon uses a series of cutting jigs, pins, and rods to align the resection relative to anatomical landmarks. These methods have been shown to be prone to errors and less accurate when preparing the femur and tibia [9]. Error prone tools reconstruct a poorly balanced knee, defined by Babazadeh et al. as a knee with a combination of one or more of the following factors: limited range of motion, asymmetrical medial-lateral balance at full extension and 90° of flexion resulting in trapezoidal tibiofemoral gaps, incorrect varus-valgus (V-V), flexion-extension (F-E), and internal-external (I-E) alignment, a maltracking patella, and excessive rollback of the femur on the tibia [10]. Newer technology has been developed in hopes of improving conventional tools, resulting in more accurate results. Robotic surgery has been proposed as a method to resect bone and align implants accurately and precisely for a balanced knee.

1.2 Objectives

The objective of this thesis is to compare the accuracy and repeatability between robotic assisted (RATKA) and conventional TKA (CTKA). It is hypothesized that RATKA cases will have greater resection accuracy and implant alignment and less outliers compared to CTKA.

1. Compare angular and depth resection errors during femoral and tibial preparation between the robotic surgical system and conventional tools.
2. Compare femoral implant fit between the robotic surgical system and conventional tools.
3. Compare final implant alignment errors between the robotic surgical system and conventional tools.
4. Compare the flatness of the proximal tibial resection between the robotic surgical system and conventional tools.

1.3 Thesis Overview

The purpose of this thesis is to document the methods and results for the work performed and further the field of biomechanics specifically for robotic surgical systems for TKA. Chapter Two provides information from previous studies through a thematic review starting with osteoarthritis, TKAs, common failures in TKAs, patient specific instrumentation, and finally robotic surgical systems. Chapter Three outlines a study that quantified the resection and implant alignment accuracy and precision for the femur and tibia between RATKA and CTKA. Chapter Four describes a study that assessed the proximal tibial resection flatness between RATKA and CTKA using two different metrics. Chapter Five concludes the thesis with a summary of important findings from Chapters Three and Four and presents ideas for future work. This is ended with references, additional figures, as well as the MATLAB code used for the resection angle analysis.

Chapter 2 : Literature Review and Background

2.1 Osteoarthritis

Osteoarthritis (OA) is an inflammatory condition of the synovial joint when articular cartilage wears down. OA is characterized by joint stiffness, pain, and inflammation. It is estimated that 27 million US adults have clinical OA [11,12]. Among the estimated population of adults who suffer from OA, 10% of men and 13% of women aged 60 or older suffer from knee OA [13]. Popular treatments for mild osteoarthritis include physical therapy and anti-inflammatory medication, but in the case of severe degenerative osteoarthritis, osteotomies and joint arthroplasties are common procedures.

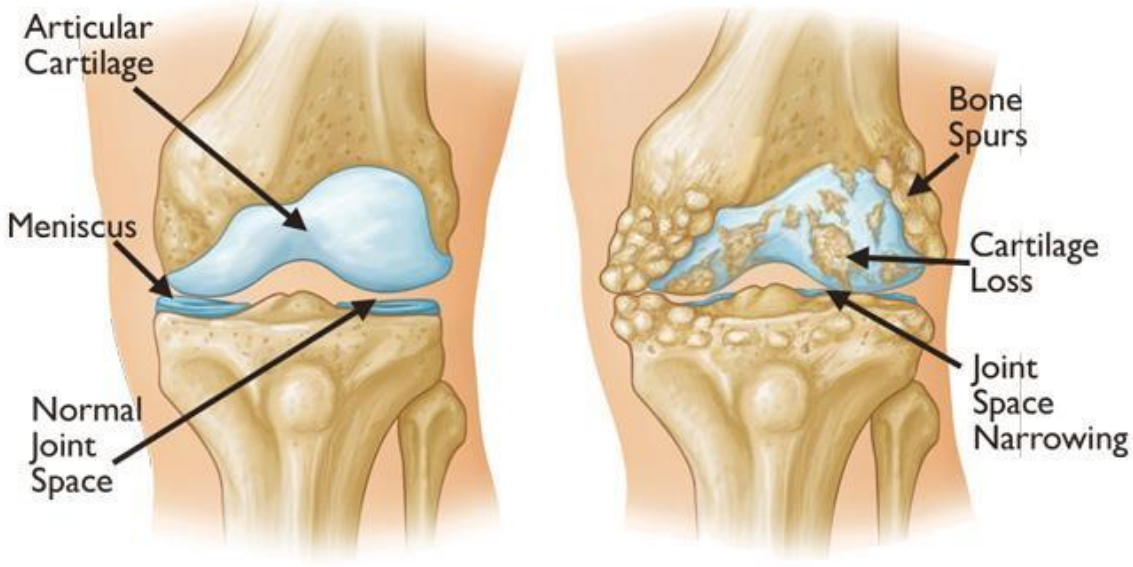

Figure 2.1: Pre-arthritic knee (left) and arthritic knee (right) (orthoinfo.aaos.org)

2.2 Total Knee Arthroplasty

Knee arthroplasty can be partial or total and is a procedure to remove and replace the inflamed articulating surface of the knee. During this procedure, the joint line is restored using one of the many alignment philosophies: anatomic, mechanical, adjusted mechanical, kinematic, or restricted kinematic [14]. The resected bone is restored by a combination of metal and polyethylene protheses that attach to the distal end of the femur and proximal end of tibia. TKA procedures have become more popular as the number of procedures increased by 161.5% from 1991 to 2010 and is projected to increase another 143% from 2012 to 2050 [15,16]. But despite the recent overall success of total knee arthroplasty (TKA), there are still an unacceptable number of patients dissatisfied with their TKAs. Choi et al. reported that patient satisfaction after TKA ranges from 75% to 92% with the most common causes of patient dissatisfaction being residual pain and limited function [17].

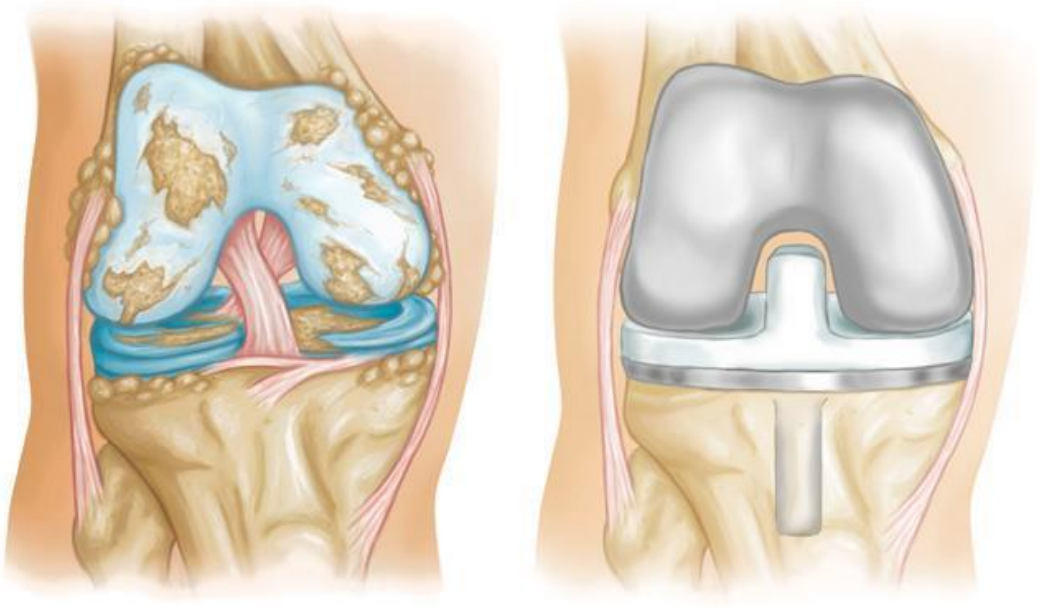

Figure 2.2: Arthritic knee (left) and post-TKA (right) (orthoinfo.aaos.org)

Poor outcomes of TKA may be attributed to intraoperative factors such as surgical technique and prostheses alignment. Bone cutting errors can influence implant alignment and can cause the prostheses to experience increased loads which accelerate polyethylene wear, mechanical loosening, instability, and unbalanced knee kinematics. In these cases, a revision surgery is necessary to replace the failed prostheses. Poor reproducibility using conventional instrumentation can be derived from errors in locating anatomical landmarks, pinning cutting jigs, and intraoperative movement of instrumentation and fixation devices.

Locating the anatomical landmarks can be difficult even for experienced surgeons. A study found that the mean dispersion of locating the medial and lateral femoral epicondyles were 2.8 ± 1.5 mm and 1.7 ± 0.9 mm respectively and locating the femoral and tibial centers had a dispersion of 1.3 ± 1.3 mm and 1.7 ± 1.5 mm [18]. These errors influence the identification of the transepicondylar axis (TEA), a frequently used landmark, and consequently the rotational alignment of the knee. Errors in rotational alignment have also been shown to affect the coronal and sagittal alignment as well [19]. In the study, when the maximum deviations of the anatomical landmarks were used, an error of 5.5° was calculated for the TEA which corresponds to resection errors of 0.7° in the coronal plane and 2.2° in the sagittal plane.

Intraoperative movement of conventional instrumentation also attributes to a large percent of resection and implant positioning error [9]. Slight movements of the cutting jigs due to slip or external forces between the cutting jig and the bone can contribute 10% to 40% of the total resection error [9]. Plaskos et al. reported bone cutting errors vary

with surgical experience, type of cutting guide, and intraoperative guide movement. The authors reported that high volume orthopaedic surgeons resect bone more precisely than trainee surgeons in the coronal plane (0.4° vs 0.8°), and a slotted cutting guide compared to an open cutting guide reduced variability and bias for sagittal alignment. The authors also estimate the variability associated with oscillating saws contribute 0.6° to 1.1° and 1.8° of SD in coronal and sagittal alignment, respectively. While bone cutting errors can be reduced with more precise tooling such as a slotted cutting guide, standards for optimal implant alignment are still being debated [9].

Because implant alignment determines the loading of the underlying bone, correct implant alignment is strongly associated with greater stability, a lower rate of loosening, and higher clinical scores, but precise range of values for implant alignment have not been determined [20]. A preponderance of studies has found a correlation between excessive malalignment and revision surgeries [7,8]. Studies suggest that a coronal alignment of less than 2.0° or greater than 8.0° valgus for the femoral component and any variation other than neutral for the tibial component results in increased failure rates. Tibial coronal alignment other than neutral creates an unequal loading distribution at the tibiofemoral joint which increases shear forces, resulting in increased wear. Similarly, sagittal alignment of the femoral component of more than 3.0° flexed and deviations outside 0° and 7° of posterior tibial slope increased failure rates. Femoral and tibial components rotated externally outside of the 2° - 5° range increased failure rates significantly as well [20,21].

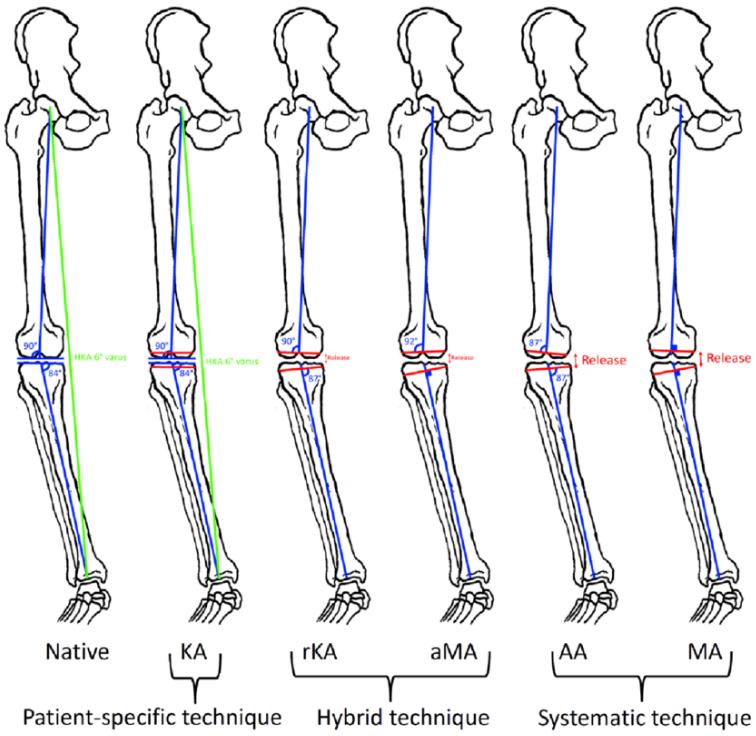

Figure 2.3: Knee alignment philosophies. KA, Kinematic Alignment; rKA, Restricted Kinematic Alignment; aMA, Anatomical Mechanical Alignment; AA, Anatomical Alignment; MA, Mechanical Alignment [22]

2.3 Common Failures

Implant alignment outside of the above-mentioned ranges significantly increases mechanical failures. Malalignment in the coronal plane creates an abnormal force distribution through the medial and lateral compartments of the polyethylene insert and subsequently accelerates polyethylene wear. The increased tractive-rolling forces generated from contact mechanics within the tibiofemoral joint during activities associated with daily living creates small particles and eventually delaminates and pits the polyethylene surface [23]. The same forces at the bone-implant interface, for cemented implants, can fatigue the cement mantle and release wear particles as well. These wear particles perpetuate particle disease, such as osteolysis, through a series of biological pathways and responses such as inflammation. Chronic inflammation

stimulates the patient's auto-immune system and increases osteoclast formation [23]. The accumulation of osteoclasts contributes to the resorption of the periprosthetic bone bed compromising implant fixation and furthering implant loosening. This further perpetuates micromotion of the implant and osteolysis until implant instability or another form of failure occurs, and a revision surgery is needed.

Another form of failure associated with inaccurate resections and implant alignment is instability. While a precursor to long term instability is osteolysis and implant loosening, a precursor to short term instability is inaccurate osteotomies, mal-aligned components, and soft tissue damage. A goal of TKA is to achieve balanced soft tissue tension through the knee's range of motion and is often characterized with balanced rectangular flexion and extension gaps. A trapezoidal gap exhibits unequal tension on the medial or lateral compartment; therefore, a subsequent resection or ligament release is performed to achieve a rectangular gap and is followed with an increase in polyethylene thickness to compensate for the increased gap. Loose knees are a resultant of unbalanced gaps which increase the chance of excessive displacement of the articular components. Unbalanced gaps can be the result of over or under resection of the distal femur with respect to the proximal tibia as well as over or under release of one collateral ligament relative to the contralateral collateral ligament. Accurate osteotomies and maintaining the structural integrity of stabilizing soft tissue structures is necessary to prevent short term instability.

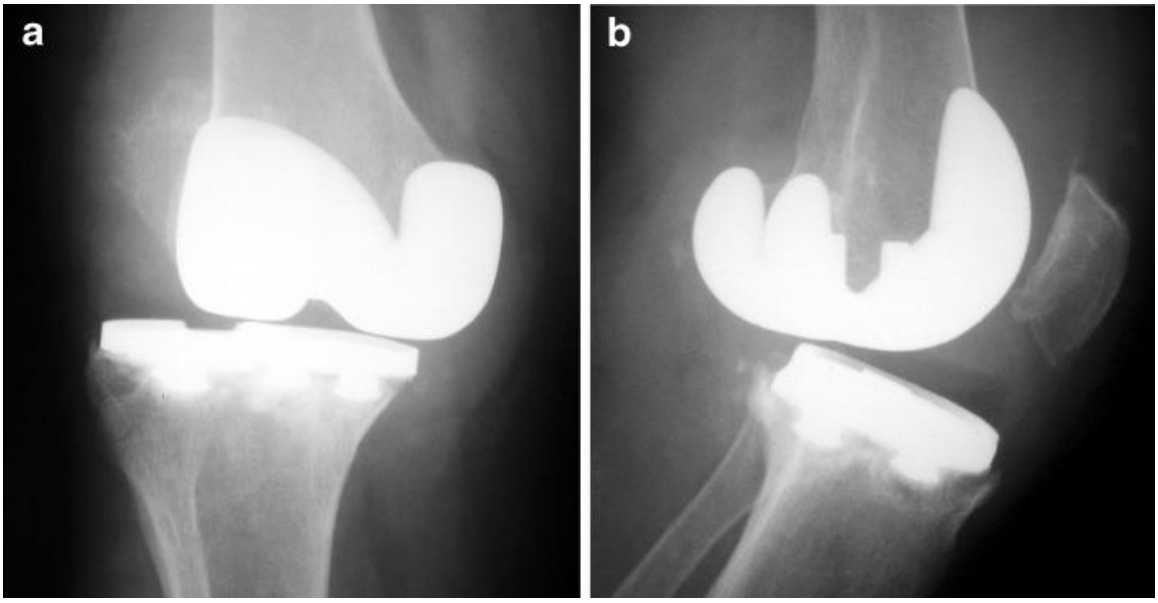

Figure 2.4: Frontal (left) and sagittal (right) plane views of an unstable TKA [24]

Anterior knee pain is one of the most common types of chronic pain after TKA. Causes of anterior knee pain can be a combination of functional (muscular insufficiencies or imbalances) and mechanical (malalignment of prosthetic, poor lower limb balance, instability, loosening, etc.) problems. Studies have shown that an internally rotated femoral component increases the quadriceps angle (Q-angle), the angle formed between a line connecting the anterior superior iliac spine and the center of the patella and a line connecting the tibial tuberosity and the center of the patella and can cause an increased lateral tilt angle as well as patella lateralization (Figure 2.5) [25]. A lateralized patella increases lateral contact forces, and the change in the extensor mechanism causes pain in the lateral retinaculum where densely packed nociceptors exist [25].

Figure 2.5: Radiograph of patella lateralization (boneandspine.com)

Surgeons must also avoid Anterior-Posterior (A-P) offset errors when aligning the femoral component. A large overhang due to an oversized femoral component or under resection of the anterior femoral cortex can cause “overstuffing” of the patellofemoral joint. This increased pressure due to increased shear forces during patellofemoral movement causes pain. The opposite must be taken into consideration as well since an over resection of the anterior cortex causes the patella to sit posteriorly relative to the natural anatomy and may cause quadricep weakness and instability. Because the patella provides a moment arm to increase the efficiency during knee extension, a posterior translation of the patella decreases the moment arm thus increasing the required quadriceps force to extend the knee. While conservative measures can be taken to restore functional causes of mild anterior knee pain, in cases of severe pain due to mechanical causes, revision surgery is needed but should be prevented by resecting bone and aligning

implants more accurately. Care should be taken when performing a revision surgery for anterior knee pain as studies have shown success rates to be around 50% [25].

Although rare, inaccurate implant alignment and bony resections can cause the periprosthetic bone to fracture. One risk factor for femoral fracture is anterior notching. Anterior notching occurs when there is an excessive resection of the femoral anterior cortex. An anterior notch creates a local stress concentration and predisposes the femur to fracture when experiencing high energy trauma. A study has reported that femoral fracture occurs in 10 – 46% of notched femurs [26]. On the tibial side, a similar phenomenon occurs. A tibial component in varus is associated with medial bone collapse due to severe comminution of the medial compartment. When the tibial tray is placed in severe varus, an uneven distribution of load on the periprosthetic bone bed causes increased localized stress on the medial compartment of the tibia [27]. The resection inaccuracy in the coronal plane has been attributed to conventional instrumentation where one study showed that extramedullary and intramedullary rods have shown accuracies of ± 2° 71 – 94% and 82 – 88% of the time respectively [28]. Medial bone collapse will occur once the stress exceeds the fatigue strength of the bone. Authors have found that periprosthetic fractures corresponding with the tibia range from 0.4% - 1.7% and 0.3% – 2.5% for the femur [26]. Inaccurate resections should be avoided to prevent fracture of the periprosthetic bone.

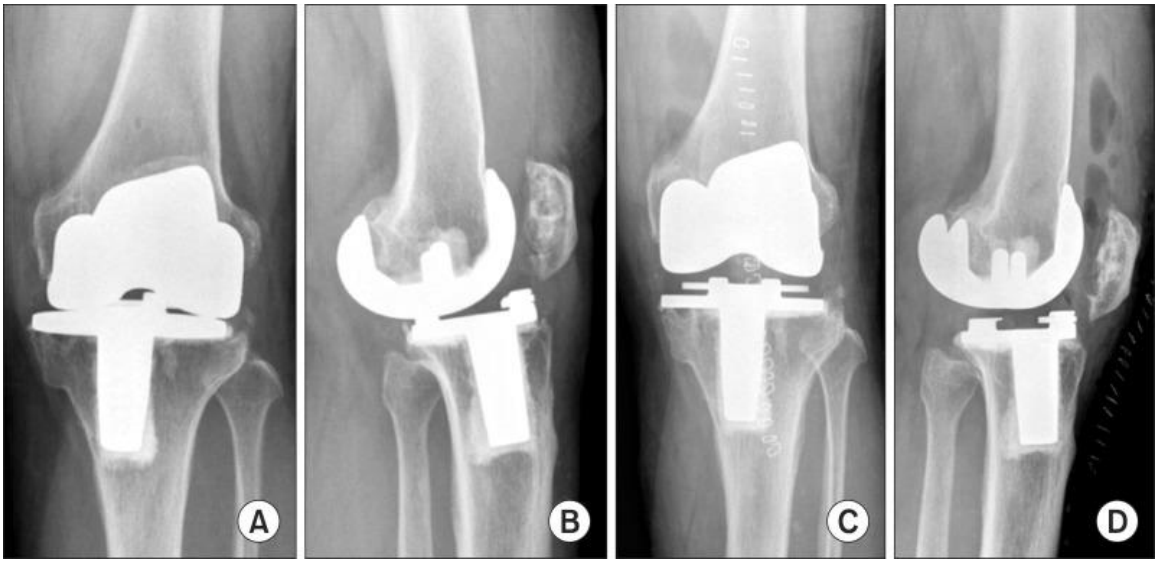

Figure 2.6: Radiographs of polyethylene failure (A, B) and radiographs of revised TKA (C, D) [7]

2.4 Patient Specific Instrumentation

In order to more precisely align implants, the distribution of bone cutting errors must be reduced and conventional instruments must be improved. Improvements in technology such as patient specific instrumentation (PSI) have been implemented as a potential solution. In PSI, customized cutting jigs are created from a preoperative computed tomography (CT) or magnetic resonance imaging (MRI) scan. The series of 2D images of the lower limb are turned into a 3D model where anatomical landmarks are located, and a preoperative plan is created. The preoperative plan consists of the depth of resection, coronal, sagittal and rotational alignment for femoral and tibial components. The PSI are then manufactured and sent to the surgeon. The patient specific cutting guides are used primarily for the distal femoral and proximal tibial resection, then standardized instrumentation is used to perform the subsequent cuts [29]. Recent research has debated the efficacy of PSI in clinical settings. In a literature review conducted by Sassoon et. al., the authors found mixed results when using PSI in comparison to conventional

instrumentation. Out of 16 studies, 10 of the studies reported no significant differences in improved mechanical alignment, four studies reported fewer alignment outliers, one study reported an increased amount of alignment outliers, and one study reported improved alignment [30]. There has not been enough evidence to support PSI achieving greater neutral alignment when performing TKAs and improved patient reported outcomes compared to conventional instrumentation.

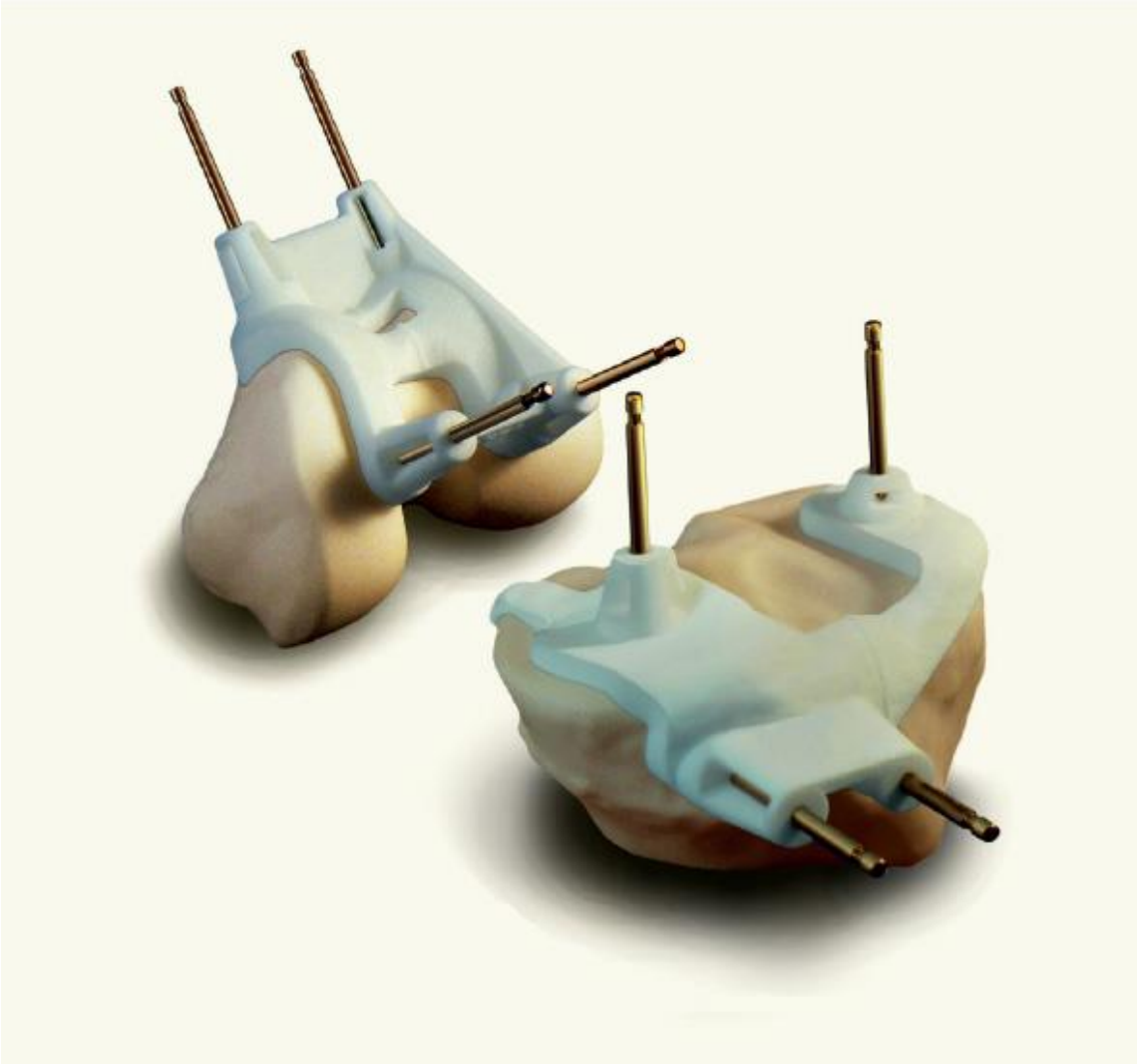

Figure 2.7: Patient specific instrumentation (PSI) for the distal femoral and proximal tibia resection (consultqd.clevelandclinic.org)

2.5 Robotic Assisted Surgical Systems

Recently there has been a wide adoption of robotic assisted surgical systems. From 2012 to 2018, the use of robotic surgery for all general surgery procedures has increased from 1.8% to 15.1% [31]. As new technology is expanding, orthopaedic surgeons are now turning to RATKAs and computer navigation to achieve more precise osseous resections and implant alignment. Commercially available surgical robots in TKA come with a wide range of autonomy from creating 3D models of the patient's lower limb to orienting cutting guides and performing osteotomies. Surgical robots in TKA can be fully active and perform a set of surgical steps programmed preoperatively, or semi-active and allow surgeon control while providing haptic, audible, and/or visual feedback. Passive systems such as computer navigation have been implemented in tandem to increase surgical accuracy providing real time visual information, such as the location and orientation of the femur and tibia for the operating surgeon. This information significantly improves surgeon visualization of the joint allowing for better knee alignment [32]. Computer navigation systems can be image-based or imageless. Image-based navigation uses a preoperative CT or MRI scan or intraoperative fluoroscopy while imageless navigation uses strictly intraoperative information such as anatomical landmarks and surfaces. The intraoperative information collected during imageless navigation is used to analyze the morphology and alignment of the knee. Clinical studies have shown that CT-based navigation results in more neutral tibiofemoral alignment, but preoperative radiography increases patient radiation exposure and well as costs and time [33]. On the other hand, imageless navigation has been shown to yield equivalent implant

positioning in the coronal and sagittal planes as well as reconstruction of the mechanical axis of the limb without the need to predispose the patient to radiation [34,35].

The process of a semi-active imageless robotic surgical system can be broken into three major steps: planning, bony registration, and bony preparation. First, the surgeon performs an arthrotomy to obtain adequate exposure of the joint. Rigid body arrays, a constellation of markers, are pinned into the femur and tibia which are tracked by a camera located opposite from the robotic arm. The computerized system is able to calculate the position of the femur and the tibia by creating a coordinate system from the markers. The surgeon then characterizes the bony surface by creating point clouds around specific anatomical landmarks and articulating surfaces with a stylus that is tracked by the camera system. An anatomical coordinate system is created based on the registered landmarks, and a 3D model of the patient's bony anatomy is generated. The robotic system then plans the resection angles and depths, and the surgeon verifies and modifies the plan for acceptable knee balance. Once the plan has been finalized, the surgeon controls the end effector which is equipped with an instrument to remove bone such as an oscillating saw or rotating burr. The bony resections and ligament balance are based on the surgeon's methodology (measured resection or gap balancing) [36]. After the bony resections, trial prostheses are implanted, the joint space and surrounding soft tissue are assessed for an acceptable balanced knee. If the results are unsatisfactory, the surgeon may continue to release soft tissue and/or resect bone. Once results are satisfactory, the final components are implanted and standard TKA procedures are followed to close the wound.

Even though the underlying concept of robotic surgical systems is the same for many currently marketed surgical robots, the execution varies with manufacturer. The Mako system (Stryker, Kalamazoo, MI), a semi-active image based robotic surgical system, uses patient specific information from a preoperative CT scan in order to plan the resections. This system orients the end effector, an oscillating saw, to the correct position and allows the operating surgeon to control and resect bone [37]. Systems such as the OMNIBot surgical robot (Corin, Cirencester, UK), a semi-active imageless robotic surgical system, will orient the end effector, a slotted cutting guide, to the correct location where a manual oscillating saw is then used to perform each resection of the femur. A separate cutting jig is then pinned to the anterior cortex of the tibia where screws are tightened to orient the resection plane and a manual oscillating saw is used to perform the resection [38]. The NAVIO surgical system (Smith & Nephew, London, UK), a semi-active imageless system, uses a rotating bur to perform the femoral distal resection and holes are bored for the placement of a cutting block. Holes are also bored in the anterior cortex of the tibia, for the tibial cutting jig, where pins are used to secure the device and a manual oscillating saw is used for the tibial proximal resection and the subsequent resections of the femur [39]. The ROSA knee system (Zimmer Biomet, Warsaw, IN), an image-based or imageless semi-active robotic surgical system, shares aspects with both the OMNIBot and NAVIO surgical systems where the end effector, a slotted cutting guide, orients the femoral distal resection angle and locates the position of the pins for the femoral and tibial cutting block which is used for the subsequent resections. Once the

cutting guide is oriented, a manual oscillating saw is then used to perform the resections [40].

The VELYS™ Robotic Assisted Solution (Depuy Synthes, Warsaw, IN), is a semi-active imageless robotic surgical system. The surgical system, a three degree of freedom (DOF) articulated robotic arm, utilizes three revolute joints to span a workspace, the total volume swept out by the end effector. The revolute joints are oriented such that transformations from the base to the end effector can be parameterized by three Euler Angles. The system consists of three critical components: a satellite station equipped with an optical system, a cart that houses the detachable robotic arm, and a detachable robotic arm that is attached to the surgical table during operation. Prior to operation, the surgical system is calibrated through a series of motions to track the rigid body arrays. Similar to currently available imageless robotic surgical systems designed for TKA, bicortical pins attached with a constellation of three reflective markers are implanted into the femur and tibia. Markers are also attached to the end effector of the surgical unit. The VELYS™ Robotic Assisted Solution surgical unit can generate the 3D bony anatomy of the patient's lower limb through the identification of anatomical landmarks using a stylus that is optically tracked. Using intraoperative data and a series of coordinate transformations, the surgical unit can estimate the relative distance between the femur and the tibia. This information is displayed onto the screen as a function of knee angle. Because the robotic surgical system is semi-active, the operating surgeon is able to control the end effector, equipped with an oscillating saw, to resect bone while the system rejects any positional and angular deviations from the procedure. After trial components

have been impacted, the operating surgeon can use the relative distance between the femur and tibia as a function of knee angle information to check for correct knee balance from full flexion to extension. Once satisfactory results have been achieved, standard procedures are performed to replace the trial components with the final components and to close the wound.

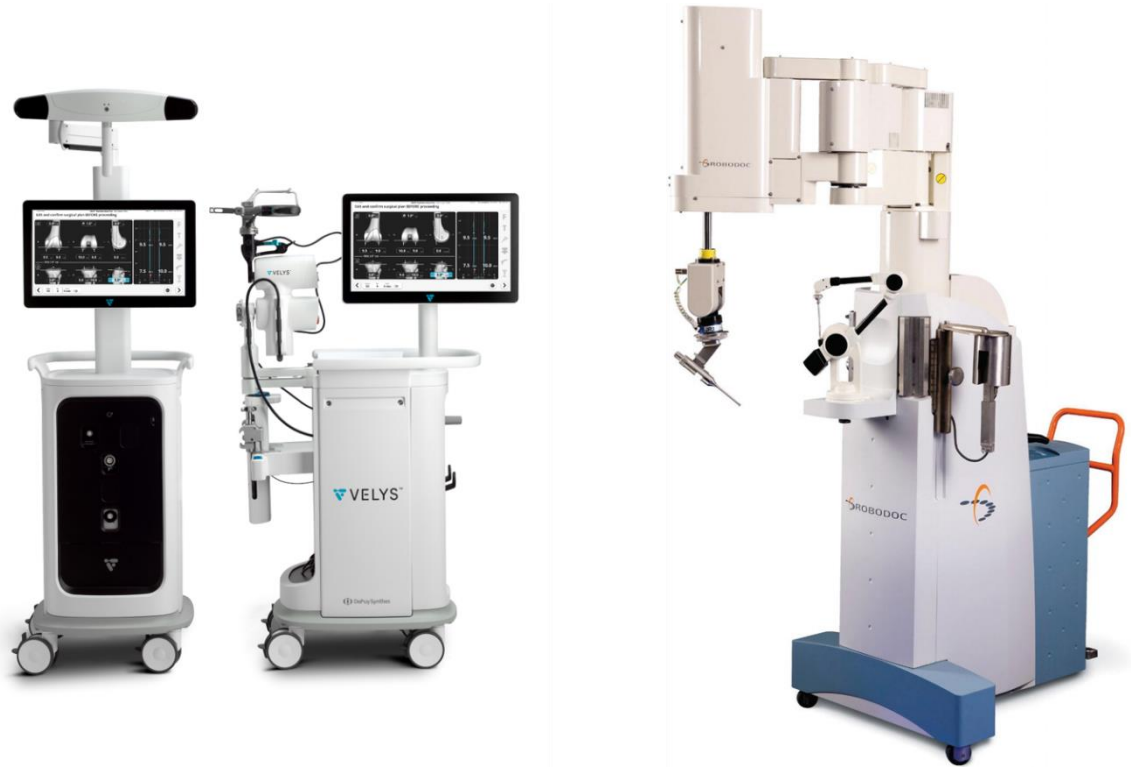

Figure 2.8: VELYS™ Robotic Assisted Solution (DePuy Synthes, Warsaw, IN) (Left) and T-Solution One® (THINK Surgical®, Fremont, CA) (Right) [41]

Previous studies have explored the accuracy and precision of commercially available surgical systems. Many studies have shown that robotic surgical systems can recreate resection errors of less than ± 1° or ± 1 mm [37,39,40,42]. A study conducted by Hampp et al. investigated the difference in accuracy of bone resection and implant positioning between the Mako system and conventional instrumentation. The authors found that the

robotic-assisted surgical system is capable of resecting bone at a highly accurate and significantly different level than the conventional instrumentation in all anatomic planes except for the sagittal plane. The Mako system also demonstrated highly accurate implant placement in all planes except for the tibial sagittal plane [37]. Casper et al. investigated the implant placement accuracy of the Navio system. The authors calculated that the Navio is highly accurate in all planes of alignment except for the femoral sagittal plane [39]. Figueroa et al. assessed the in-vivo accuracy achieved with the OMNIBot surgical robot (Corin, Cirencester, UK). In this clinical study, the authors discovered that the OMNIBot was accurate in all planes except for the sagittal plane. For both the femur and the tibia, the resections were on average 1.5 ± 0.3° and 1.3 ± 1.5° more flexed [38]. In three separate studies with three different robotic systems, the results showed accurate resections and/or implant alignment in all planes except for the sagittal plane. In a study conducted by Plaskos et al. the authors reported that an oscillating saw blade can contribute to 0.6° to 1.1° and 1.8° of SD in the coronal and sagittal planes [9]. This is possible due to small vibrations of the equipment which can deviate the resection, or the deflection of the blade as a resection is performed because an oscillating blade can deflect more easily as the blade travels posteriorly where sclerotic bone tends to exist.

It is often difficult to directly compare accuracy and precision metrics between studies because measurements and calculations vary between studies. In a couple studies, authors measured the resection surface using a planar probe [37,40]. A rigid body array was attached to the probe, where the camera system calculates the orientation of the instrument, and the final cuts were measured relative to the fiducial markers attached to

the femur or tibia. Although this measurement technique is accurate in the surgical system's model of the bones, it may not be an accurate representation of the actual resection error in the femoral or tibial anatomic coordinate system. Because the surgical system's model is based on surgeon-determined anatomical landmarks, inaccuracies associated with locating anatomical landmarks will deviate the true femoral or tibial anatomical reference frames from the model. Amanatullah et al conducted a study where inaccurate registrations of the femoral epicondyles, femoral and tibial centers, and malleoli were correlated to rotational errors in the robotic surgical system's model. The authors found that incorrect registration of the femoral and tibial centers of 6 mm in the Medial-Lateral (M-L) and A-P directions caused a 1° change in the Varus-Valgus (V-V) and Flexion-Extension (F-E) angle respectively [18]. The study found that the most sensitive anatomical landmarks were the medial and lateral epicondyles, where 2 – 4 mm of error in the A-P direction caused 1° change in Internal-External (I-E) angle [18]. A study encompassed the registration error into the resection error by including a preoperative CT scan, which was independent of the surgical technique, and defined the anatomic coordinate system for measurements [38]. A postoperative CT scan was taken and registered to the preoperative scan, and the resection was measured relative to the anatomical coordinate system. The measurement was independent from the coordinate system created from the robotic model and includes the registration error of the system.

Authors agree that diminutive improvements of fractional degrees and millimeters will show little clinical significance, but the reduction of outliers will translate to improved clinical outcomes [37]. Current research demonstrates that RATKAs are

capable of achieving highly accurate and precise implant alignment than conventional methods, but in order to correctly determine other potential benefits and long-term outcomes of robotic assisted TKAs, larger volume studies and more clinical data is needed. There are also various sources of error for RATKA such as: software, hardware calibration, pin array placement, registration of anatomic landmarks, intraoperative pin array movement, incorrect bone cuts, and incorrect final implant placement, and it is pertinent to explore each source of error and their individual contributions to the overall system error of RATKA.

Chapter 3 : Resection Angle and Implant Orientation Accuracy

3.1 Introduction

During CTKA, errors can occur such as intraoperative movement of cutting jigs, due to poor fixation, locating anatomic landmarks, and resection and implantation techniques which are all dependent on surgical experience [9]. The sum of these errors can amount to large deviations of the final implant orientation and an unbalanced knee.

Instruments are aligned using anatomical landmarks which are determined by palpating and identifying bony points. Points on the malleoli, femoral condyles, and tibial plateau can be used to create anatomic axes where instruments are used to estimate the alignment of the knee. Intra and extra medullary rods estimate the anatomic axis for both the tibia and the femur based on patient natural anatomy which is then used to set the distal femoral and proximal tibial resection angle. It has been shown that these tools can be inaccurate especially when patients suffer from severe valgus or varus deformities [19].

The aim of RATKA is to reduce intraoperative errors that exist with CTKA resulting in more accurate bony resections, implant placement, and a balanced knee. Theoretically, by replacing the initial tools used to set the angles of the resections with a computer, capable of motions of fractional degrees, intraoperative errors can be reduced.

This study was performed to compare the resection and implant alignment errors between the robotic assisted surgical system and conventional instrumentation. In order

to quantify the resection error metric, the angle of the anterior, distal, and posterior surface of the femur and proximal tibial surface were determined. To quantify the implant alignment errors, the final orientation of the implant was determined.

3.2 Methodology

In this study, bilateral TKA was performed on forty pelvis-to-toe cadaveric specimens (Age: 70.4 ± 8.2 years, Height: 67.1 ± 4.1 in., Weight: 132.4 ± 35.8 lbs., BMI: 20.6 ± 4.9). Five board certified orthopaedic surgeons performed all TKAs using either conventional tools or the robotic surgical system. For a given knee, the surgical method was randomly selected, and the contralateral knee would receive the alternative method to avoid side or handed bias. The orthopaedic surgeons were familiar with the ATTUNE INTUITION™ conventional instrumentation and were also familiar with either computer assisted surgery or RATKA and were also trained on the VELYS™ Robotic Assisted Solution surgical system prior to the study. For all cases, the ATTUNE® Cementless Cruciate Retaining Femur and ATTUNE® Cemented Tibial Base was impacted onto the femur and tibia, respectively.

Prior to the study, CT scans were taken of each specimen with a 0.6 mm slice thickness. The CT scans were used to measure the resection accuracy after TKA but was independent of the surgical procedure.

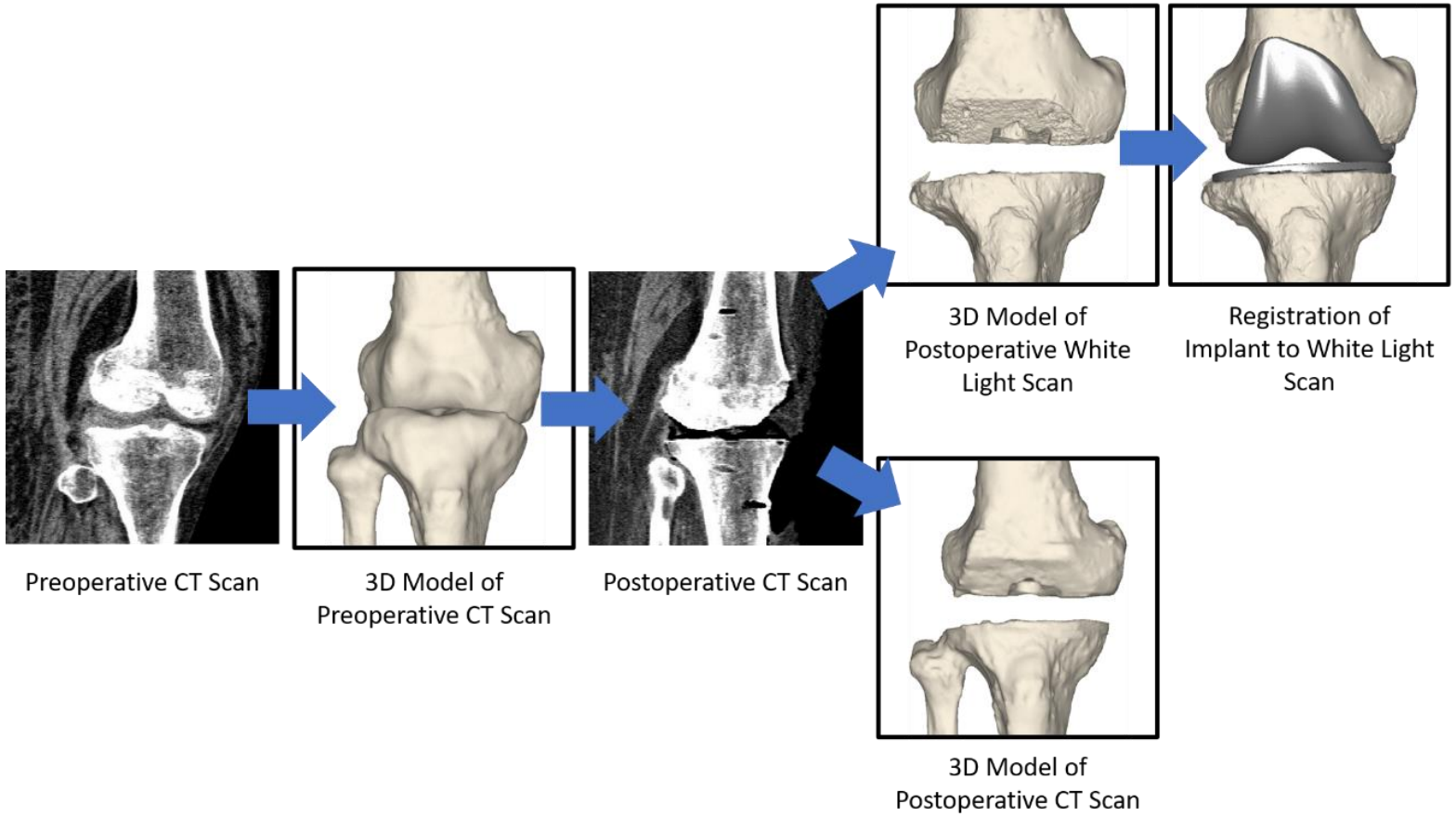

Figure 3.1: CT and white light imaging workflow

For the robotic assisted cohort, rigid body arrays were attached to the femur and tibia using bicortical screws. Standard workflow was performed to expose the knee joint as well as to mark, define, and register anatomical landmarks on the femur and tibia using a stylus with a rigid body array. The imageless robot is then capable of creating a 3D model from the locations of the registered anatomical landmarks and surface point clouds. Surgeons subsequently plan the resection angle and depth based on the knee balance using the system's software. The robotic surgical system orients the end effector to the correct angle relative to the resected bone and allows the surgeon to perform the resection while rejecting positional or angular error. The femoral sagittal angle (FSA), femoral coronal angle (FCA), femoral rotational angle (FRA), tibial sagittal angle (TSA), tibial coronal angle (TCA), as well as the medial femoral distal thickness, medial femoral posterior thickness, and tibial resection thickness target values were recorded.

For the conventional cohort, a standard arthrotomy was performed to expose the knee joint and the surgical technique for the ATTUNE® Knee System was followed.

Figure 3.2: VELYS™ Robotic Assisted Solution (DePuy Synthes, Warsaw, IN) (Left) and Conventional Instrumentation Trays (Right) (jnjmedicaldevices.com)

After each primary resection, bone remnant thicknesses were measured using a calibrated digital caliper. The thicknesses of the femoral resections were measured from

the resection plane to the most prominent point on the articular surface and the thickness of the tibial resection was measured from the resection plane to an electrocautery mark on the tibial plateau.

After the resections, another CT scan was taken to capture the resection surface of the postoperative knees. The specimens were returned, and the distal 300 mm of the femur and proximal 300 mm of the tibia were extracted (Figure 3.3). The bones were exposed, and all soft tissue was stripped. The Artec Space Spider (Artec3D, Luxembourg), white/structured light scanner, was then used to accurately capture the resection surfaces of the bone. The extracted bones were implanted with their respective components and measured again using the white light scanner. The scanning process can be seen in Figure 3.1.

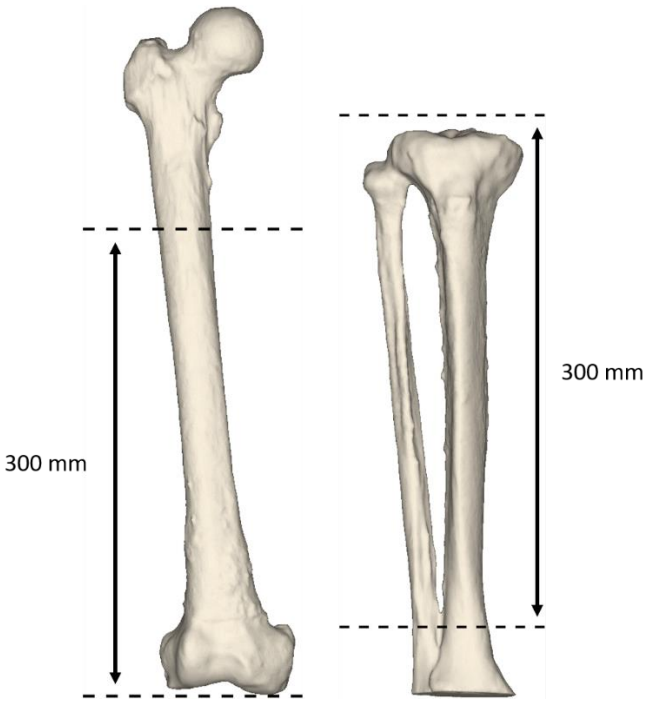

Figure 3.3: Extraction length (300 mm) for the femur and tibia.

A team of engineers at TruMatch® Personalized Solutions (DePuy Synthes) segmented each preoperative and postoperative CT scan and created 3D models along with the locations of anatomical landmarks of the preoperative model.

All white light scans were fused using the Artec Studio 15 (Artec3D, Luxembourg) software and all postoperative (CT and white light) scans were manually registered by matching the topology of the non-implanted regions to the preoperative CT scan in HyperMesh (Altair Engineering Inc, Troy, MI). An iterative closest point (ICP) algorithm was applied to finalize the registration between the postoperative and preoperative scans (Figure 3.4).

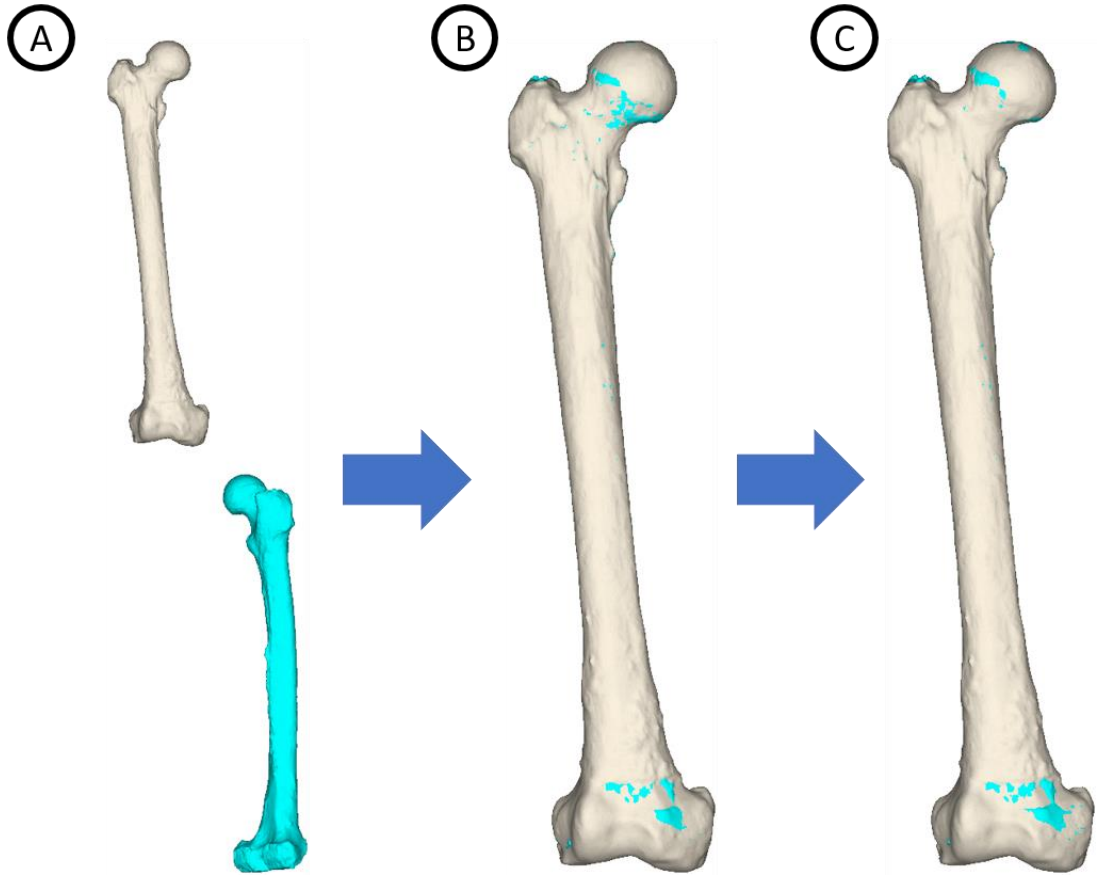

Figure 3.4: Registration steps between preoperative and postoperative CT scans. A: no transformation. B: manual registration. C: ICP algorithm.

3.2.1 Femoral Definitions

Anatomic coordinate systems were constructed from the preoperative CT scan anatomical landmarks. The origin was defined as the most distal point on the femoral sulcus. The femoral Superior-Inferior (S-I) axis was aligned to the mechanical axis of the femur, a vector from the origin pointing to the center of the femoral head. The coordinate system was then rotationally aligned to the posterior condylar axis (PCA), an axis between the most posterior points on the posterior femoral condyles, pointing laterally for right knees and pointing medially for left knees. The vector product between the femoral mechanical axis and the PCA creates the A-P axis. A final vector product between the S-I and A-P axes forms the M-L axis (Figure 3.5).

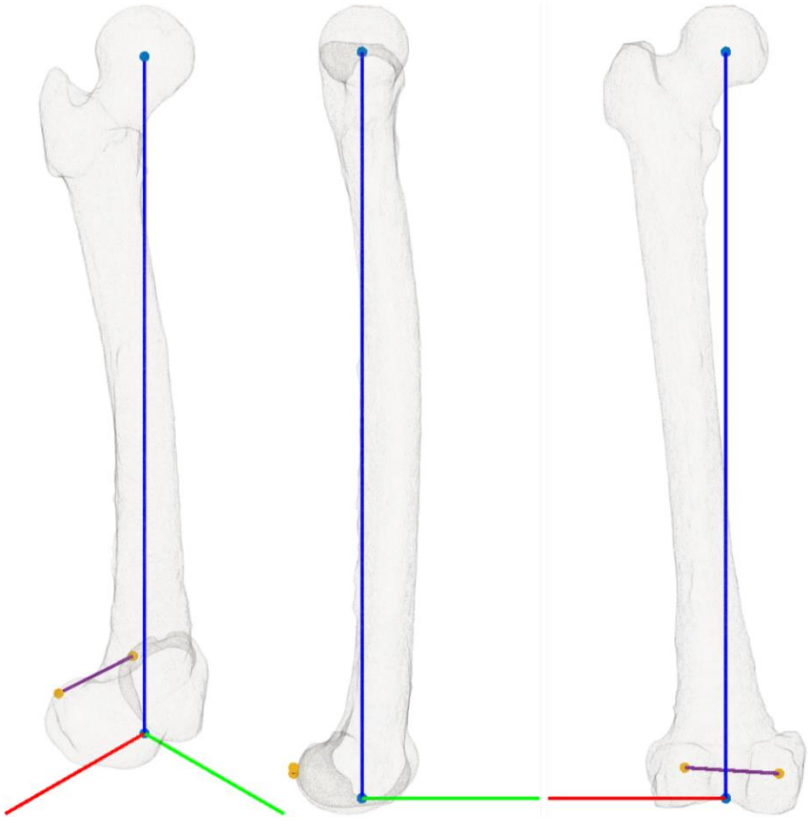

Figure 3.5: Femoral anatomic coordinate system. Posterior condylar axis (purple), Femur mechanical axis (blue), A-P axis (green), and M-L axis (red)

The femoral sagittal angle (FSA) is defined as the angle between the femoral mechanical axis and the distal femoral resection or implant surface in the sagittal plane. The femoral coronal angle (FCA) is defined as the angle between the mechanical axis and the distal femoral resection or implant surface in the coronal plane. The femoral rotational angle (FRA) is defined as the angle between the PCA and the posterior resection or implant surface in the transverse plane (Figure 3.6).

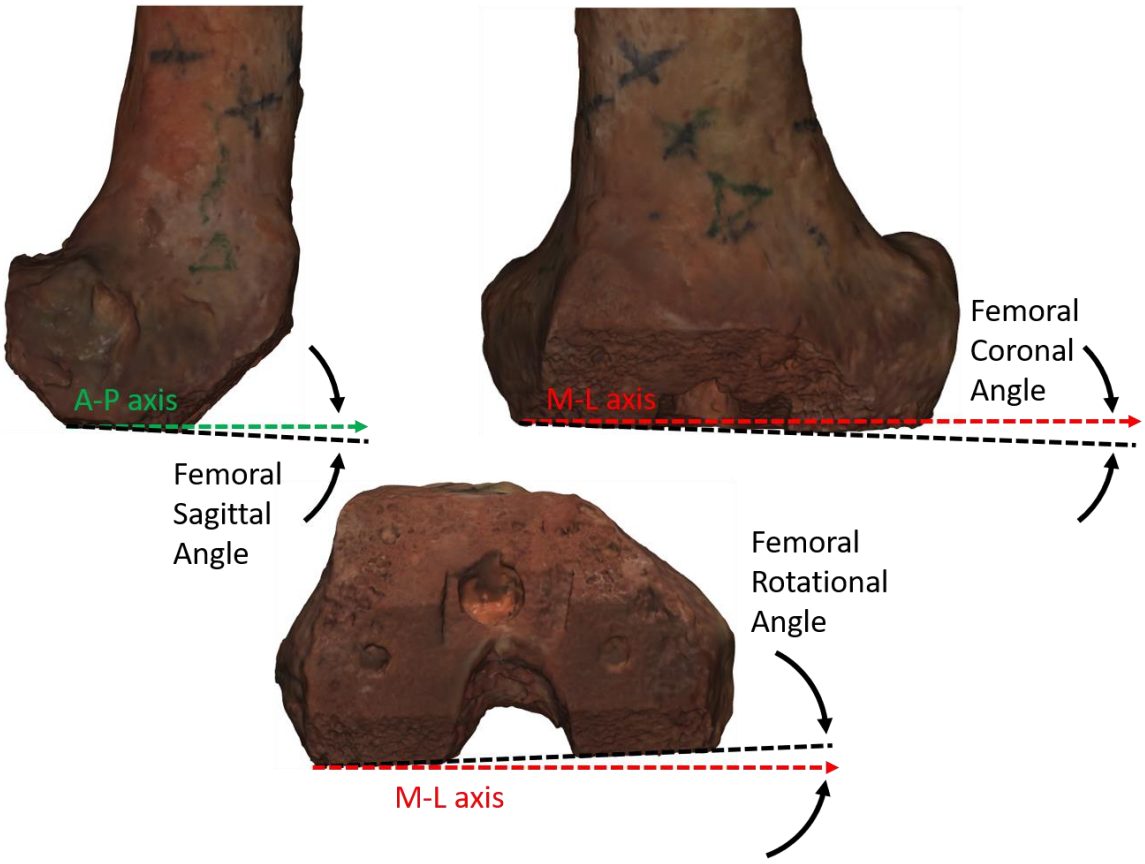

Figure 3.6: Femoral rotations relative to anatomic axes. Femoral sagittal angle (FSA) (top left). Femoral sagittal angle (FSA) (top right). Femoral rotational angle (FRA) (bottom). A-P axis (green) and M-L axis (red).

3.2.2 Tibial Definitions

The tibial S-I axis was aligned to the mechanical axis of the tibia, a vector from the malleoli center to the tibial intercondylar eminence. The coordinate system was

rotationally aligned with a vector from the medial third of the tubercle to the tibial center. A vector product was performed between the tibial S-I axis and the medial third of the tubercle axis to form the M-L axis. A final vector product between the S-I and M-L axis to form the A-P axis (Figure 3.7).

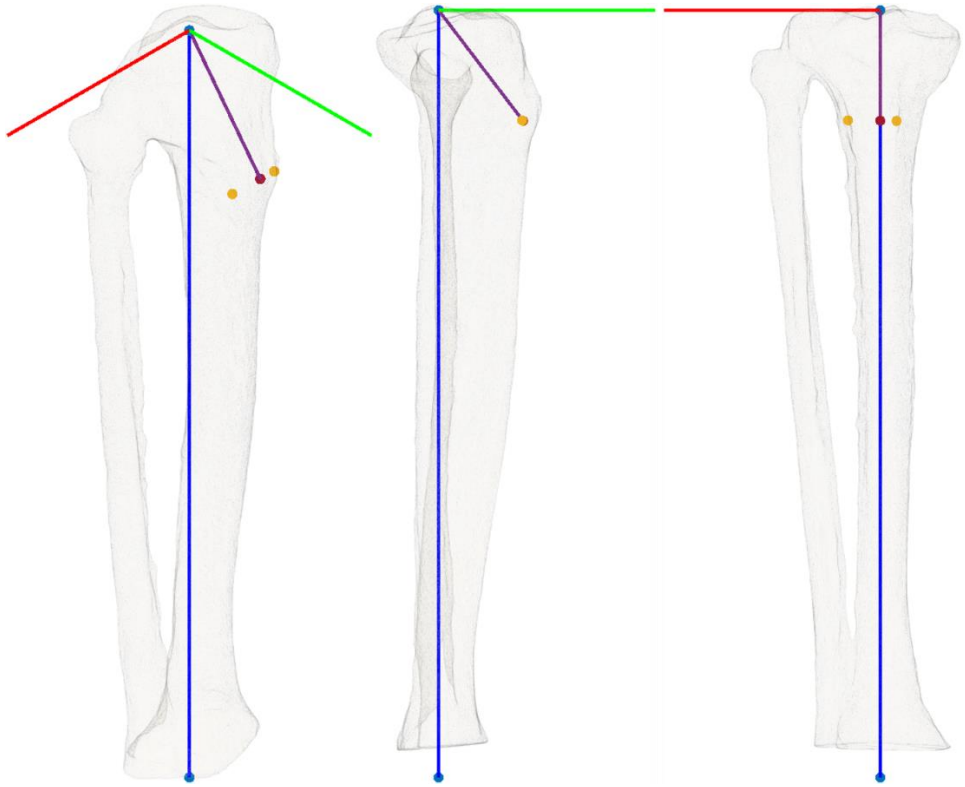

Figure 3.7: Definition of tibial anatomic coordinate system. Medial third of tubercle axis (purple), tibial mechanical axis (blue), A-P axis (green), and M-L axis (red).

The tibial sagittal angle (TSA) is defined as the angle between the tibial mechanical axis and the proximal resection surface in the sagittal plane. The tibial coronal angle (TCA) is defined as the angle between the tibial mechanical axis and the proximal resection surface in the coronal plane (Figure 3.8).

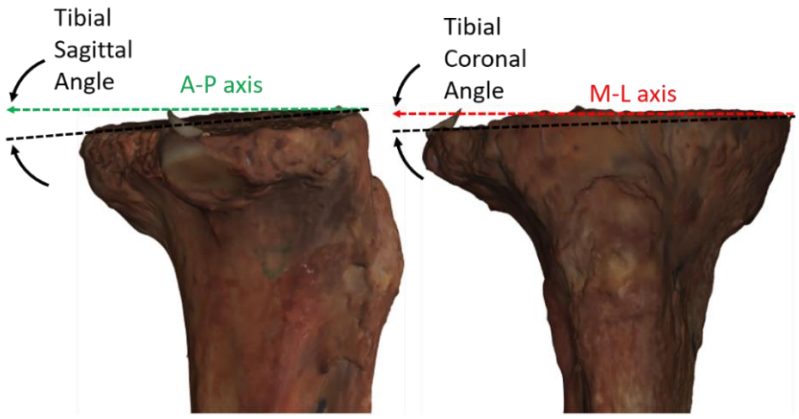

Figure 3.8: Tibial rotations relative to anatomic axes. TCA (Left) and TSA (Right). A-P axis (green) and M-L axis (red).

3.2.3 Sign Convention

In the sagittal plane, flexion is considered positive (+), and extension is considered negative (-). In the coronal plane, varus is considered positive (+), and valgus is considered negative (-). In the transverse plane, internal is considered positive (+), and external is considered negative (-).

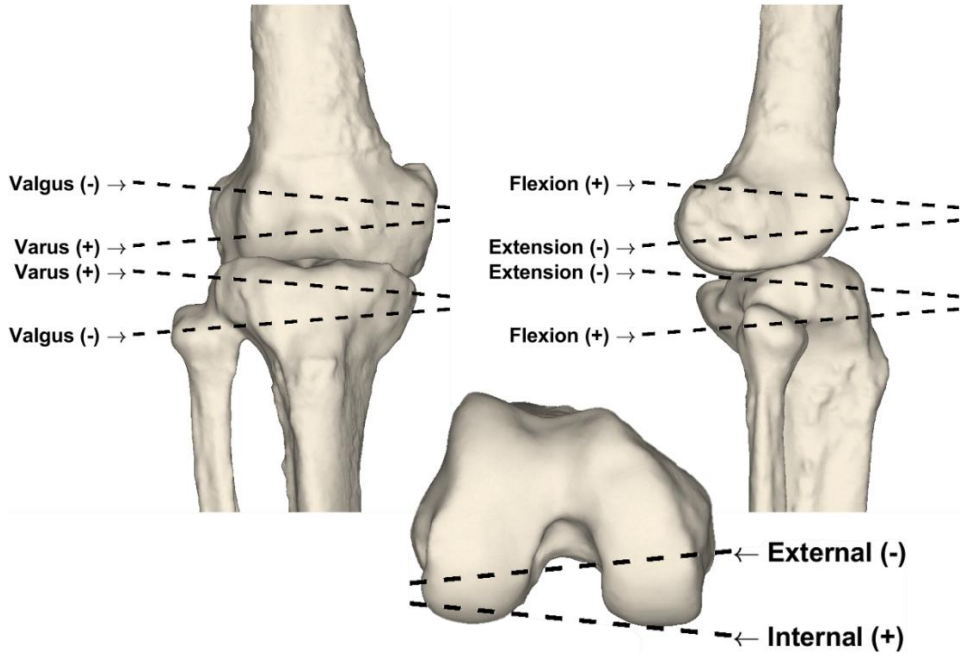

Figure 3.9: Sign conventions for a right knee. Flexion (+), Extension (-), Varus (+), Valgus (-), Internal (+), and External (-).

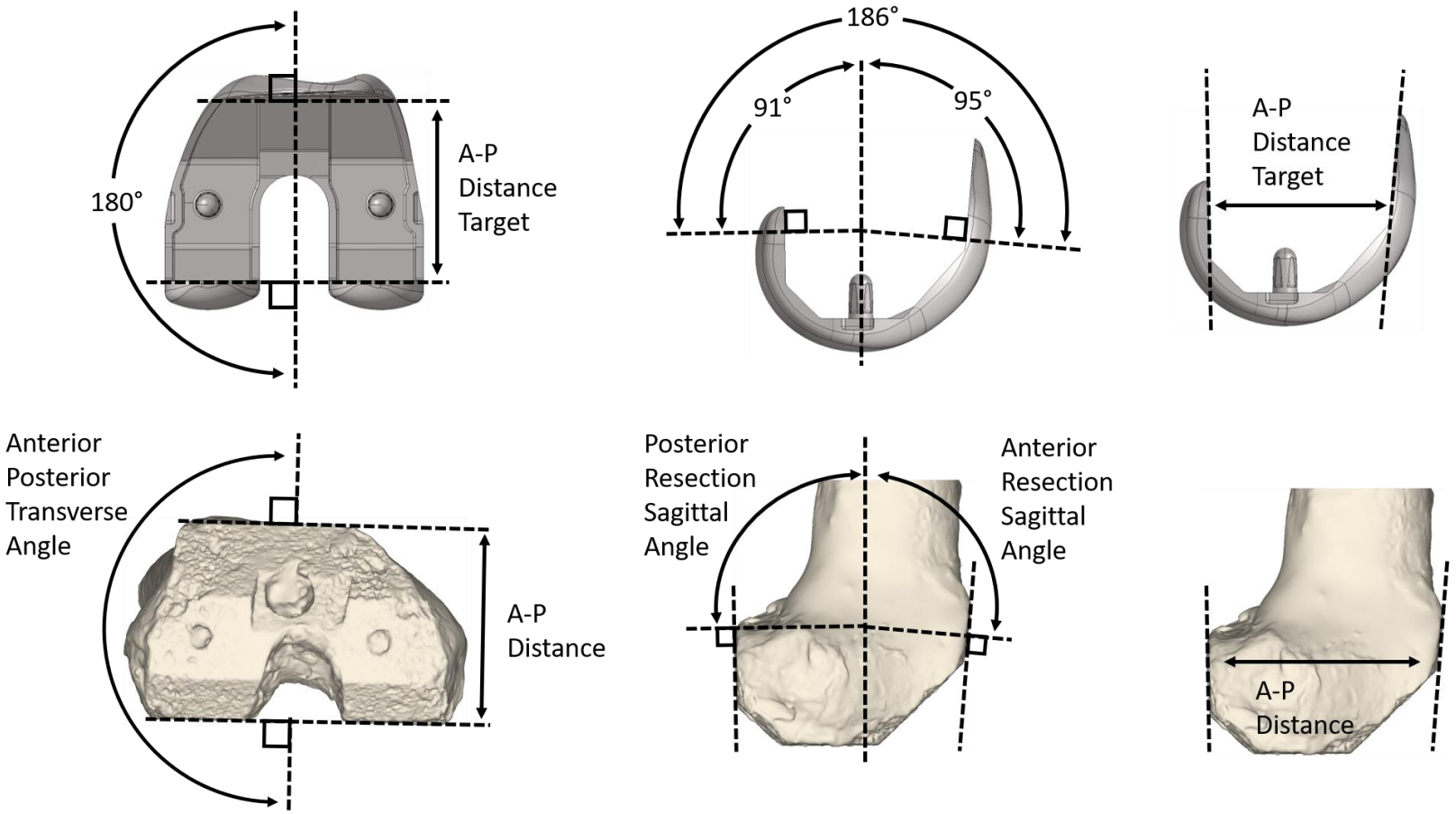

Figure 3.10: Femoral Relative Angle and A-P Distance Targets (Top) and Measures (Bottom). Anterior Posterior Transverse Angle (Left), Anterior and Posterior Resection Sagittal Angle (Center), and Anterior-Posterior Distance (Right).

3.2.4 Resection Angle Calculations

The bones were then transformed to their respective anatomic coordinate systems where the measurements are calculated. A custom MATLAB (MathWorks, Natick, MA) script was used to fit a plane to the distal femoral, posterior femoral, and proximal tibial resections (Figure 3.11).

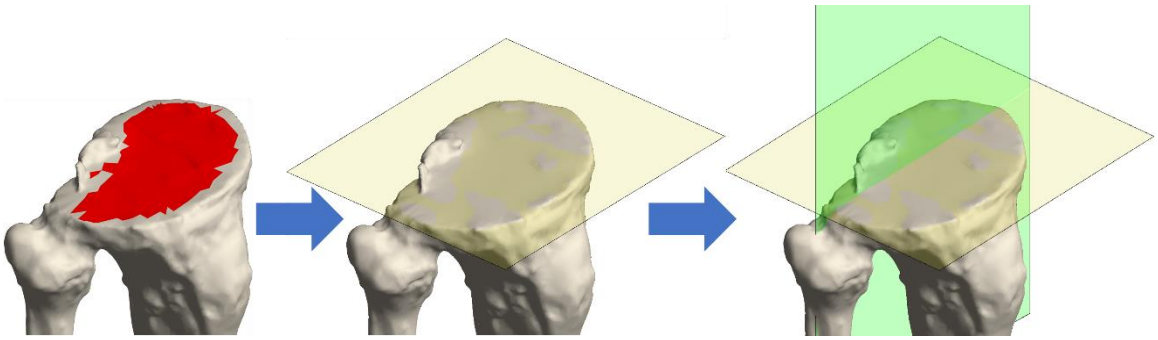

Figure 3.11: Extracted surface (Left), and plane fit (Middle), surface intersection (Right).

A set of points on each resection surface was extracted from the solid models generated from the postoperative CT or white light scans. A covariance matrix was formed and the eigenvalues and eigenvectors were computed. The smallest eigenvalue and its associated eigenvector returns the principal direction with the highest variability. This principal direction is associated with the normal vector to the resection surface. This is because for a set of distinct eigenvalues the eigenvectors are orthogonal. With this property, the other two eigenvectors are in-plane to the set of points extracted from the solid models. The calculated normal vectors of each resection plane are projected to the anatomic planes and the FSA, FCA, FRA, TSA, and TCA are calculated using the dot product definition (Figure 3.12).

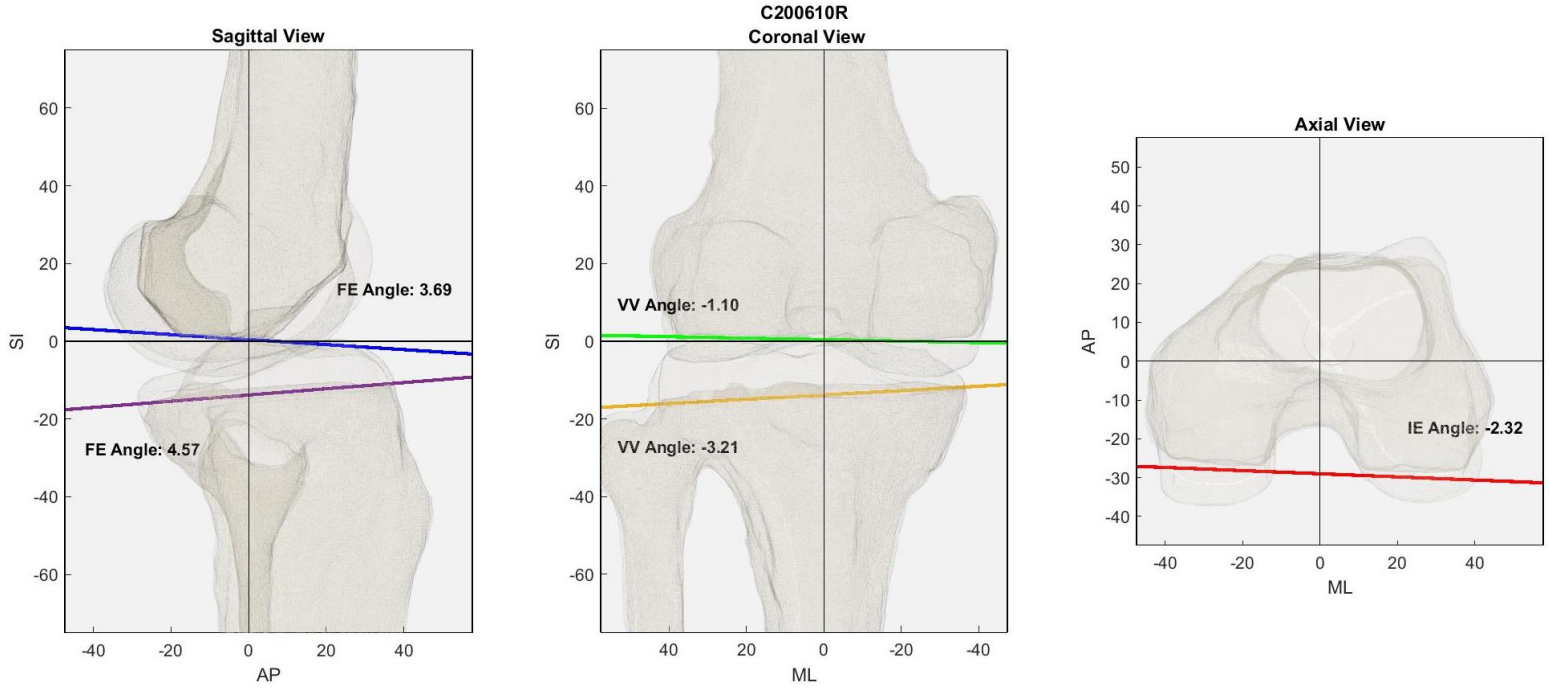

Figure 3.12: Calculated resection angles in the sagittal (Left), coronal (Center), and transverse (Right) planes.

3.2.5 Implant Angle Calculations

To quantify the implant orientation error, a homogenous transformation between the implant Computer Aided Drawing (CAD) geometry and the white light scan of the implanted prosthesis was calculated. The CAD geometry of the femoral component was oriented such that a line connecting the center of the medial and lateral posts correlates with the M-L axis, a line normal to the distal surface correlates with the S-I axis, and the vector product between the two lines correlates with the A-P axis. The CAD geometry for the tibial component was oriented such that a line connecting the most lateral and most medial points correlates with the M-L axis, a line normal to the proximal surface of the tray correlates with the S-I axis, and the vector product between the two lines correlates to the A-P axis (Figure 3.13).

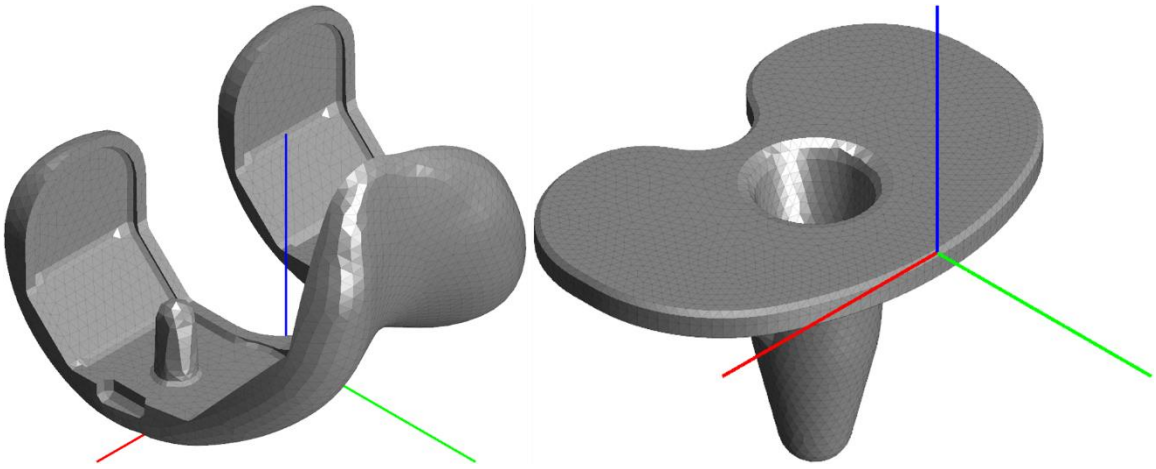

Figure 3.13: Implant Coordinate System. Z-axis (blue), A-P axis (green), and M-L axis (red)

An iterative closest point (ICP) algorithm was implemented to minimize the difference between the CAD geometry and white light scan. The basis of this algorithm minimizes an error metric such as the sum of squared differences, by comparing a point on the source point cloud (fixed) to points on the reference point cloud. A transformation

is estimated to minimize the error metric and is iteratively repeated. The output of the ICP algorithm returns a homogenous transformation matrix which linearly maps the initial position and orientation of the CAD implant geometry to the final implanted position and orientation (Figure 3.14).

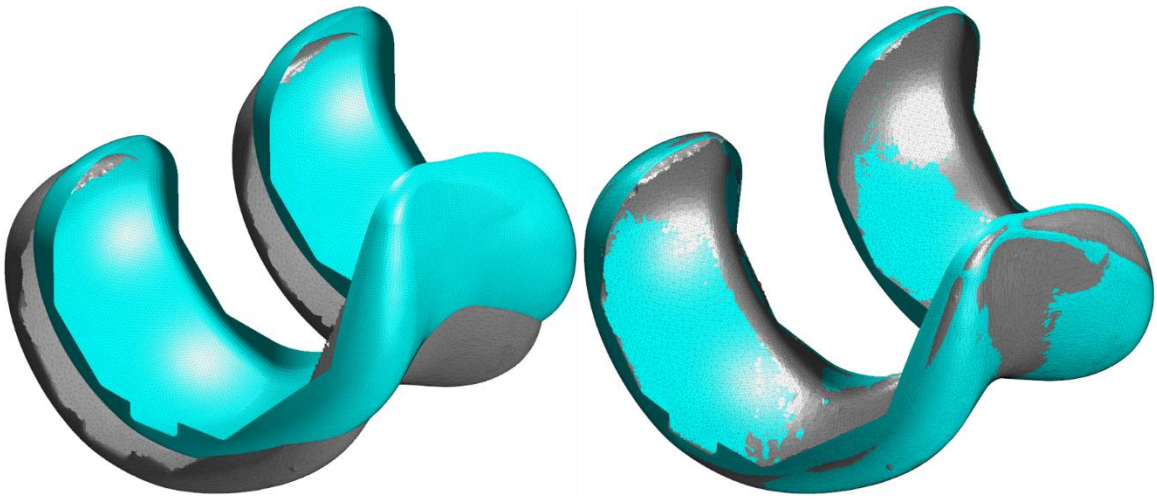

Figure 3.14: Registration of femoral implant using ICP. Before ICP (Left) and After ICP (Right)

The homogenous transformation matrix was converted to Cardan Angles, so the transformation can be interpreted as rotations, in degrees, about the fixed implant axes. The femoral implant sagittal angle (FISA), femoral implant coronal angle (FICA), femoral implant rotational angle (FIRA), tibial implant sagittal angle (TISA), and tibial implant coronal angle were calculated (TICA).

3.2.6 Femoral Relative Resection and Anterior Posterior Average Distance Calculations

The preoperative and postoperative scans of the femur were transformed to a distal resection coordinate system where the normal vector of the distal resection was aligned with the z-axis, and then rotationally aligned with the A-P axis defined in Chapter 3.2.1. This consists of creating a temporary vector by taking the vector product between the A-P

axis and z-axis. Another vector product is taken between the z-axis and temporary axis to form the y-axis, and a final vector product is taken between the y-axis and z-axis to form the x-axis.

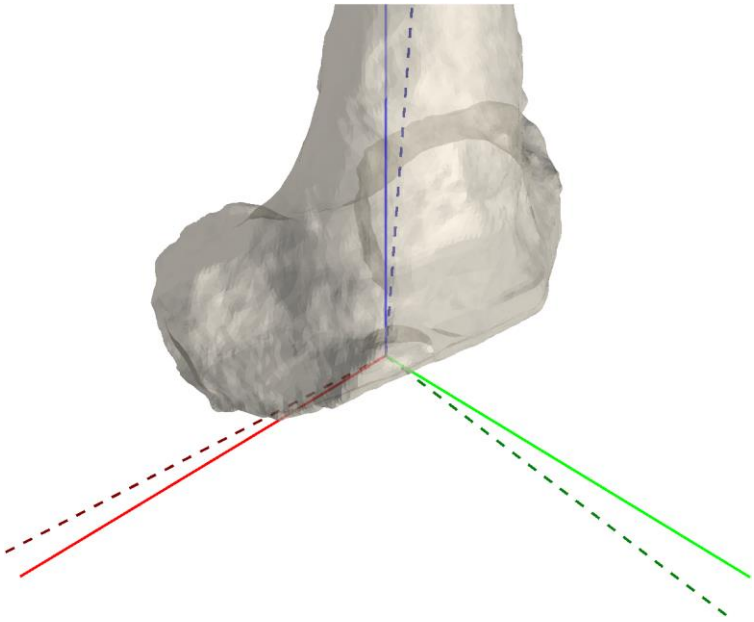

Figure 3.15: Femur in distal resection coordinate system (solid = anatomical, dotted = distal resection coordinate system)

Similar to the resection angle calculations, a plane was fit to the anterior, distal, and posterior resection surfaces and the normal vectors were projected onto the three orthogonal planes (X-Y, Y-Z, and X-Z). The anterior resection sagittal angle, posterior resection sagittal angle, and A-P transverse angle are then calculated (Figure 3.16).

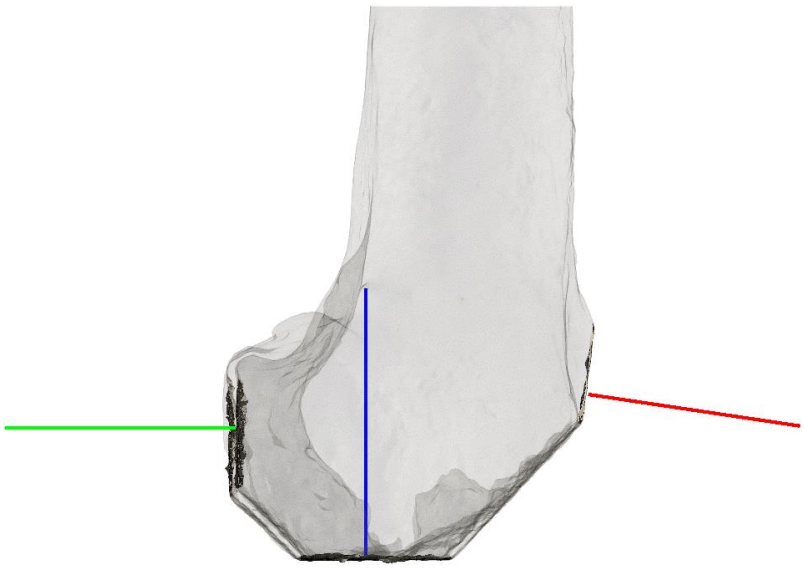

Figure 3.16: Sagittal view of the femur in the distal resection coordinate system and projected resection normal vectors.

To measure the A-P distance between the anterior and posterior resection, an average of distances was calculated. A plane, normal to the z-axis, was created on the most proximal point on the posterior resection. Then, another plane was created on the most distal point on the anterior resection, and the last plane was created equidistant between the two planes (Figure 3.17).

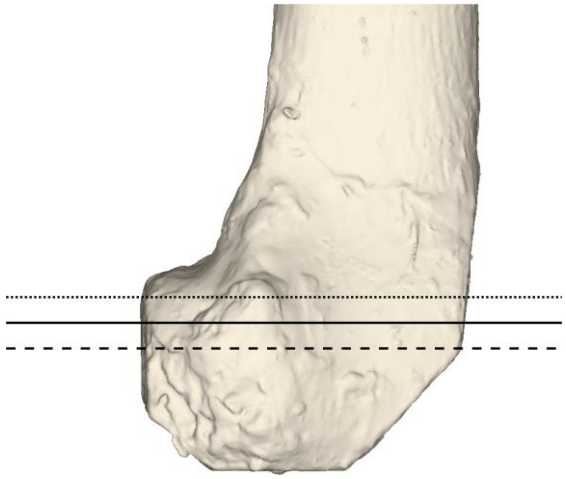

Figure 3.17: Sagittal view of the femur with a plane on the most proximal point on the posterior resection (dotted), most distal point on anterior resection (dashed), and equidistant between the proximal and distal planes (solid).

The anterior and posterior resections were then intersected by the equidistant plane. When two surfaces intersect, the result is a line. Two lines for the posterior resection are extracted and one line for the anterior resection is extracted. Points on the posterior resection line are projected onto the anterior resection line in the y-direction. If a point exists on the anterior resection line, then a distance can be calculated. The workflow is shown in Figure 3.18.

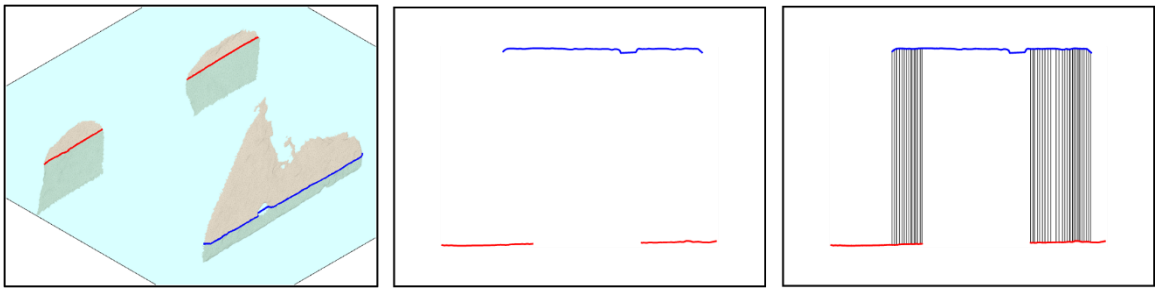

Figure 3.18: A plane (light blue) intersects both the posterior and anterior resections creating a posterior resection line (red) and anterior resection line (blue) (Left). Extracted posterior and anterior resection lines (Middle). Distance measurement line (black) between posterior and anterior resection lines.

3.2.5 Statistical Methodology

Errors were calculated as the difference between the measured alignment metric and corresponding target. Summary statistics were calculated which include: mean and standard deviation of the errors, median errors, and mean and standard deviations of the absolute errors for each metric across the RATKA and CTKA cohorts. After testing for normality and constant variances, 2-sample one tailed t-tests with a significance level of 5% ($\alpha = 0.05$) were performed to determine superiority (or non-inferiority) of the absolute error from the RATKA cohort compared to the CTKA cohort using a minimal clinically important difference of 0.5° or 0.5-mm ($p \leq 0.05$) where appropriate. For a superiority test, a two sample one tailed t-test was performed with the alternative hypothesis stating: The mean error in the CTKA cases is significantly greater than the

mean error in RATKA cases. If we reject the alternative hypothesis for the superiority test, we can perform a non-inferiority test with an alternative hypothesis stating: The mean error in RATKA cases is not significantly greater than the CTKA cases by 0.5 mm or 0.5°. One tailed t-tests were performed because the absolute values of the errors limit the lower tail in the distribution.

In a previous power analysis, a necessary sample size of 34 specimens was determined to achieve a minimum statistical power of 80% with a significance level of 5% ($\alpha = 0.05$). By using a sample size of 40 specimens, an error margin is created in the case of excluding specimens based on the circumstances of the experiment. Specimens were initially included based on the following criteria:

- Both extremities without prior knee surgery and trauma
- No retained hardware in the lower limb
- Intact ligaments
- Radiographs without evidence of advanced osteoporosis or advanced arthritis that would affect screw fixation or inhibit the planning process.

To quantify the presence of resection or alignment outliers, specimens were categorized into accuracy errors less than 3° or 3-mm, less than 2° or 2-mm, and less than 1° or 1-mm. Since accuracy of the primary resections were calculated using both the CT scans and white light scans, mean absolute differences and correlation coefficients were calculated between the redundant measures. Finally, mean absolute differences and

correlation coefficients were calculated between the resection alignments and final implant alignments.

A linear regression model was created to verify the results generated from t-tests as well as to compare the resection angle results between the white light and CT scan. From the linear regression model, an adjusted correlation coefficient (R^2), goodness-of-fit measure, can be used to quantify variances between the two scans. If the R^2 value is high, the variances between the resection angle calculated from the white light and CT scans are explained by the linear model.

3.3 Results

Out of the forty RATKA performed, intraoperative movement caused the femoral rigid body array to dislodge in two cases. These two cases were excluded from the analysis. The resection thickness was not measured in one RATKA case and one conventional case. These were also excluded from the analysis. The mean absolute resection angle error between the robotic surgical system and conventional instrumentation in FSA distal reference was 1.65° ± 1.11° and 1.92° ± 1.50°, in FCA was 0.65° ± 0.50° and 1.39° ± 0.95°, in FRA was 1.08° ± 0.81° and 1.00° ± 0.70°, in TSA was 1.62° ± 1.13° and 1.63° ± 1.39°, and in TCA was 0.93° ± 0.72° and 1.66° ± 1.29° respectively. The mean absolute resection depth error between RATKA and CTKA for the femoral distal resection was 0.62 mm ± 0.60 mm and 0.88 mm ± 0.96 mm, for the femoral posterior distal resection was 0.54 mm ± 0.43 mm and 0.77 mm ± 0.83 mm, and for the tibial proximal resection was 0.67 mm ± 0.69 mm and 1.66 mm ± 1.38 mm, respectively. The resection accuracy results of the study are also presented in Table 1.

A white light scan of the femoral component and tibial tray were corrupted for the CTKA group. These cases were also excluded from the analysis. When comparing the implant alignment results between RATKA and CTKA, the implant orientation was measured. The mean absolute implant orientation error between the robotic surgical system and conventional instrumentation in FISA was 1.51° ± 1.08° and 2.49° ± 2.10°, in FICA was 0.91° ± 0.83° vs 1.42° ± 1.15°, in FIRA was 1.14° ± 0.76° vs 0.98° ± 0.90°, in TISA was 1.37° ± 1.11° vs 1.65° ± 1.51°, and in TICA was 1.31° ± 0.84° vs 2.03° ± 1.44° respectively. The results of the study are also presented in Table 2.

Table 3.1: Resection accuracy descriptive statistics for CT scans. All results are statistically significant ($p < 0.05$) FSA, femoral sagittal alignment, distal or posterior reference; FCA, femoral coronal alignment; FRA, femoral rotational alignment; TSA, tibial.

	RATKA			CTKA				
Metric	**Mean ± SD**	**Median**	**Abs. Mean ± SD**	**Mean ± SD**	**Median**	**Abs. Mean ± SD**	**Result**	**p-value**
FSA, Dist. Ref. (°)	1.18 ± 1.62	1.20	1.65 ± 1.11	0.47 ± 2.41	0.56	1.92 ± 1.50	Non-Inferior	0.006
FSA, Post. Ref. (°)	0.65 ± 1.37	0.71	1.21 ± 0.90	0.15 ± 4.15	0.19	3.27 ± 2.51	Superior	0.000
FCA (°)	0.00 ± 0.82	-0.01	0.65 ± 0.50	-0.21 ± 1.69	-0.25	1.39 ± 0.95	Superior	0.000
FRA (°)	-0.26 ± 1.33	0.07	1.08 ± 0.81	-0.04 ± 1.23	0.16	1.00 ± 0.70	Non-Inferior	0.009
TSA (°)	0.69 ± 1.86	1.07	1.62 ± 1.13	0.59 ± 2.07	0.64	1.63 ± 1.39	Non-Inferior	0.036
TCA (°)	-0.04 ± 1.18	0.11	0.93 ± 0.72	0.92 ± 1.90	0.97	1.66 ± 1.29	Superior	0.001
FDR (mm)	0.01 ± 0.87	-0.03	0.62 ± 0.60	-0.56 ± 1.18	-0.30	0.88 ± 0.96	Non-Inferior	0.000
FPR (mm)	-0.08 ± 0.69	-0.28	0.54 ± 0.43	-0.69 ± 0.89	-0.46	0.77 ± 0.83	Non-Inferior	0.049
TPR (mm)	-0.44 ± 0.86	-0.30	0.67 ± 0.69	-1.21 ± 1.79	-1.30	1.66 ± 1.38	Superior	0.000

Table 3.2: Implant alignment accuracy descriptive statistics. All results are statistically significant ($p < 0.05$) FISA, femoral implant sagittal alignment; FICA, femoral implant coronal alignment; FIRA, femoral implant rotational alignment; TICA, tibial implant.

	RATKA			CTKA				
Metric	**Mean ± SD**	**Median**	**Abs. Mean ± SD**	**Mean ± SD**	**Median**	**Abs. Mean ± SD**	**Result**	**p-value**
FISA (°)	-0.53 ± 1.79	-0.36	1.51 ± 1.08	-2.22 ± 2.39	-1.75	2.49 ± 2.10	Superior	0.006
FICA (°)	-0.29 ± 1.20	-0.30	0.91 ± 0.83	-0.62 ± 1.73	-0.42	1.42 ± 1.15	Superior	0.014
FIRA (°)	-0.13 ± 1.38	-0.32	1.14 ± 0.76	0.13 ± 1.33	0.01	0.98 ± 0.90	Non-Inferior	0.039
TISA (°)	0.10 ± 1.77	0.37	1.37 ± 1.11	0.13 ± 2.25	0.36	1.65 ± 1.51	Non-Inferior	0.005
TICA (°)	0.47 ± 1.50	0.51	1.31 ± 0.84	1.54 ± 1.97	1.68	2.03 ± 1.44	Superior	0.004

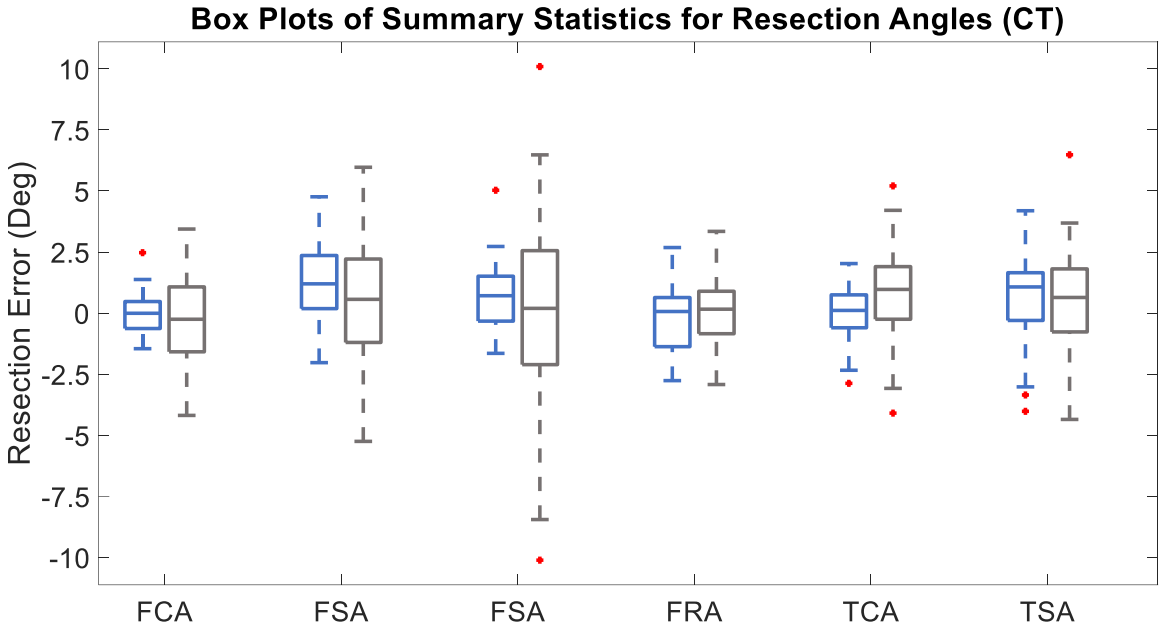

Figure 3.19: Box plots showing summary statistics of resection angles (CT). Central mark represents the median and red dots denote outliers (Data outside 1.5 IQR)

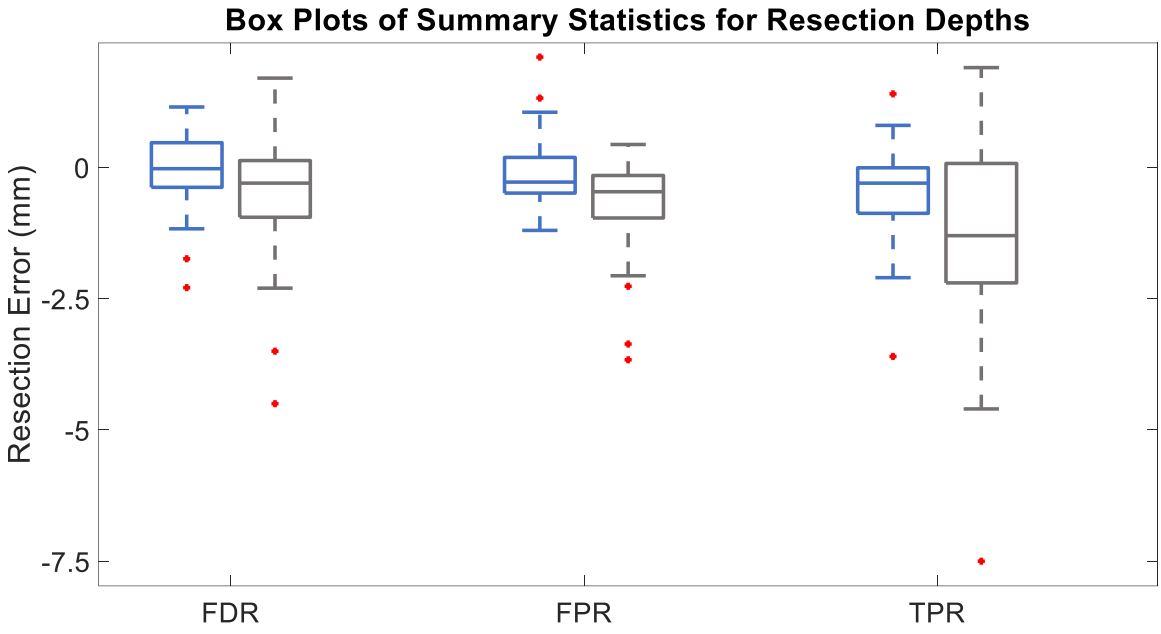

Figure 3.20: Box plots showing summary statistics of resection depths. Central mark represents the median and red dots denote outliers (Data outside 1.5 IQR).

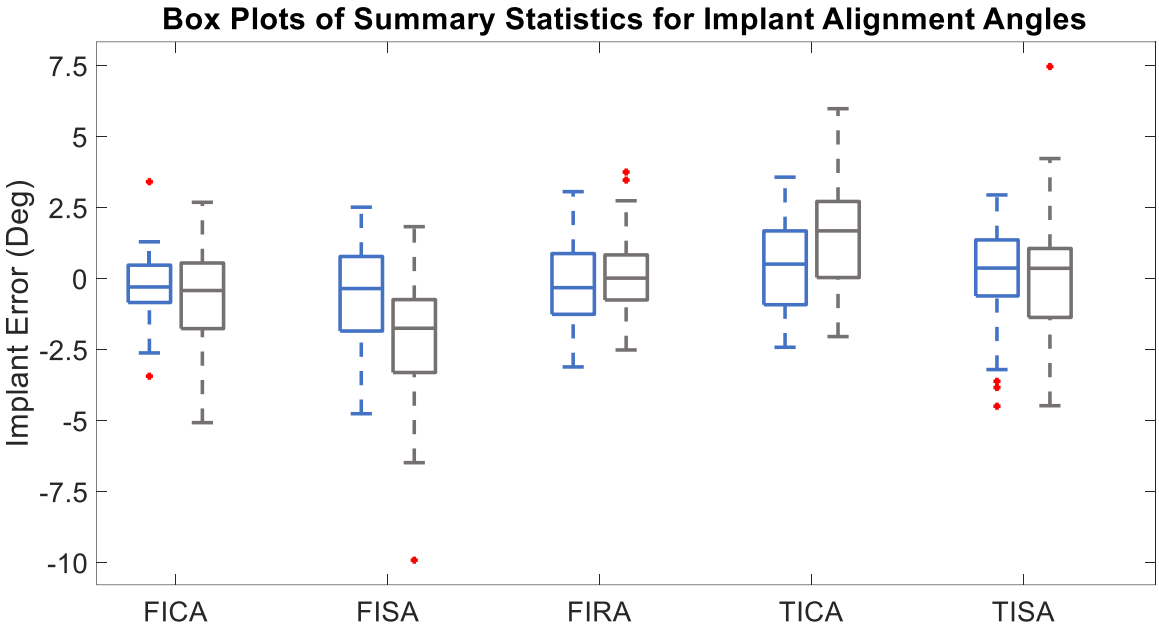

Figure 3.21: Box plots showing summary statistics of implant alignment angles (CT). Central mark represents the median and red dots denote outliers (Data outside 1.5 IQR).

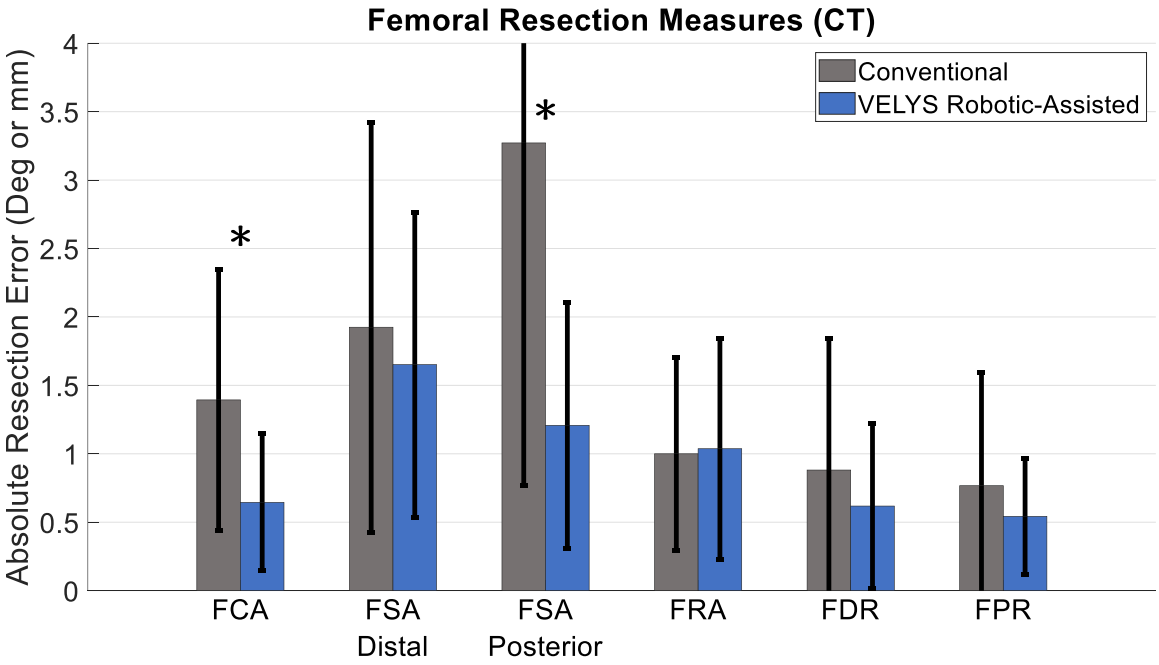

Figure 3.22: Femoral resection accuracy measures based on postoperative CT scans (indicates RATKA superiority at a 95% CI).*

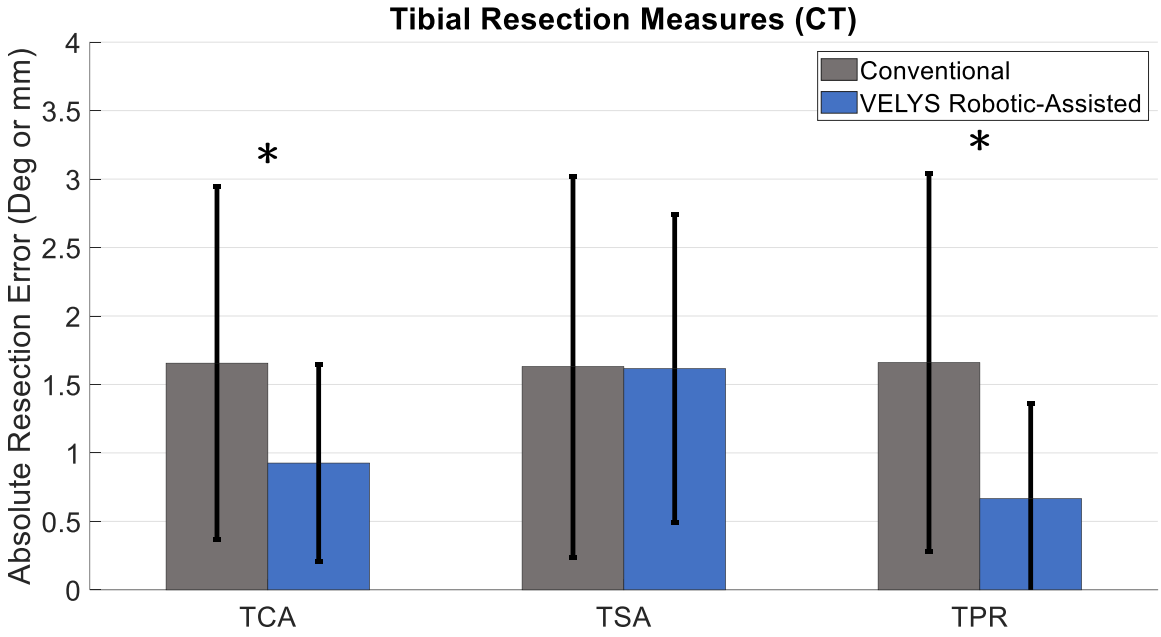

Figure 3.23: Tibial resection accuracy measures based on postoperative CT scans (indicates RATKA superiority at a 95% CI).*

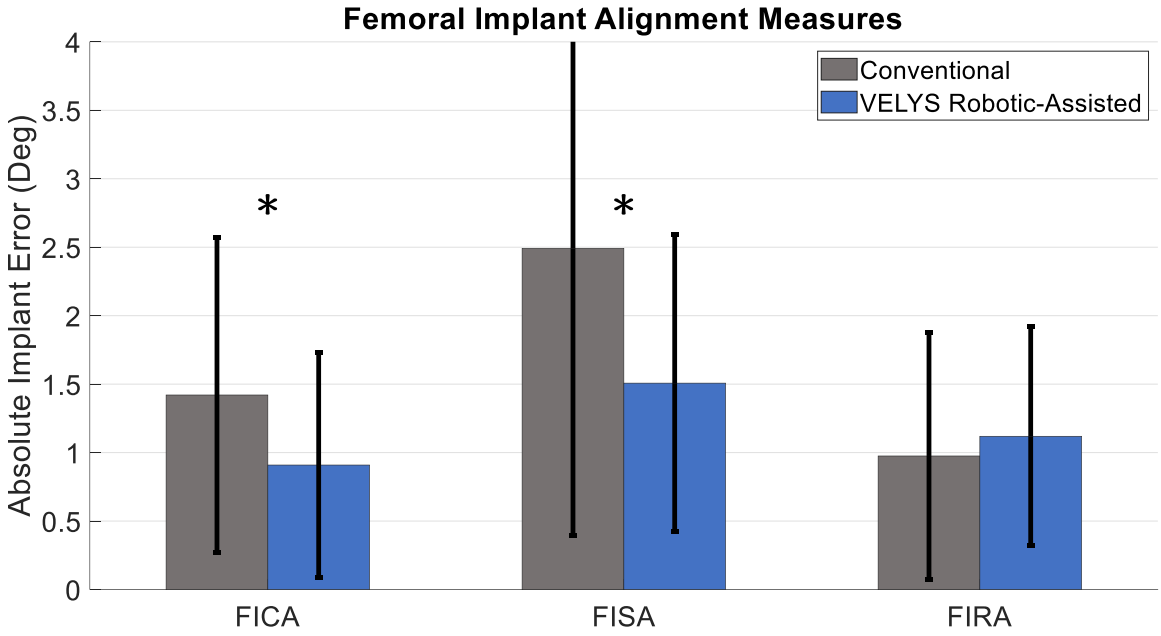

Figure 3.24: Femoral implant alignment measures (indicates RATKA superiority at a 95% CI).*

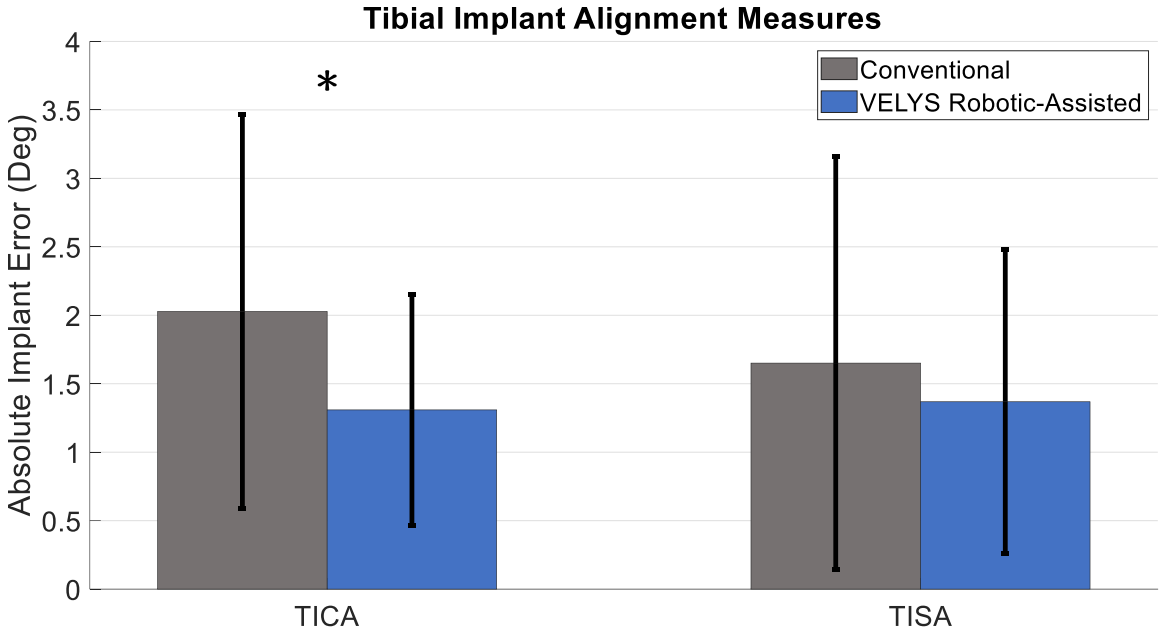

Figure 3.25: Tibial implant alignment measures (indicates RATKA superiority at a 95% CI).*

Outliers were reported by calculating the number of cases between two different bounds. It was found that for RTKA and CTKA, 89.5% (34/38) and 85% (34/40) of cases were within ± 3° and 31.6% (22/38) and 35% (14/40) of cases were within ± 1° in FSA, Distal Reference. For TSA, 85% (34/40) and 80% (32/40) of cases were within ± 3° and 35% (14/40) and 42.5% (17/40) of cases were within ± 1° for RTKA and CTKA respectively. For FCA, 100% (38/38) and 92.5% (37/40) of cases were within ± 3° and 86.8% (33/38) and 42.5% (17/40) of cases were within ± 1° for RTKA and CTKA respectively. For TCA, 100% (40/40) and 80% (32/40) of cases were within ± 3° and 60% (24/40) and 37.5% (15/40) of cases were within ± 1° for RTKA and CTKA respectively. For FRA, 100% (38/38) and 97.5% (39/40) of cases were within ± 3° and 52.6% (20/38) and 60% (24/40) of cases were within ± 1° for RTKA and CTKA respectively. The results are summarized in Table 3.

It was found that for RATKA and CTKA, 92.1% and 69.2% of implants were aligned within ± 3° and 42.1% and 20.5% were aligned within ± 1° for the FISA metric respectively. 94.7% and 87.2% of cases were aligned within ± 3°, and 68.4% and 46.2% of RATKA and CTKA cases were aligned within ± 1° in FICA. 94.7% and 94.9% of RATKA and CTKA cases were aligned within ± 3°, and 52.6% and 66.7% of cases were aligned within ± 1° for FIRA. 90.0% and 84.6% were aligned within ± 3°, and 42.5% and 46.2% of cases were aligned within ± 1° for RATKA and CTKA cases in the TISA metric. For the TICA metric, 95.0% and 82.1% of cases were within ± 3°, while 35.0% and 28.2% of cases were within ± 1° for RATKA and CTKA cases respectively.

Table 3.3: Resection angle and resection depth precision summary for CT scans expressed as a percentage of sample size (Number of subjects are expressed in parentheses).

	RATKA			CTKA		
Metric	**Inside ± 1° or 1 mm**	**Inside ± 2° or 2 mm**	**Inside ± 3° or 3 mm**	**Inside ± 1° or 1 mm**	**Inside ± 2° or 2 mm**	**Inside ± 3° or 3 mm**
FSA, Dist. Ref.	31.6% (12/38)	63.2% (24/38)	89.5% (34/38)	35.0% (14/40)	60.0% (24/40)	85.0% (34/40)
FSA, Post. Ref.	44.7% (17/38)	92.1% (35/38)	97.4% (37/38)	10.0% (4/40)	35.0% (14/40)	57.5% (23/40)
FCA	86.8% (33/38)	97.4% (37/38)	100% (38/38)	42.5% (17/40)	85.0% (34/40)	92.5% (37/40)
FRA	52.6% (20/38)	78.9% (30/38)	100% (38/38)	60.0% (24/40)	90.0% (36/40)	97.5% (39/40)
TSA	35.0% (14/40)	70.0% (28/40)	85.0% (34/40)	42.5% (17/40)	70.0% (28/40)	80.0% (32/40)
TCA	60.0% (24/40)	90.0% (36/40)	100% (40/40)	37.5% (15/40)	72.5% (29/40)	80.0% (32/40)
FDR	78.9% (30/38)	94.7% (36/38)	100% (38/38)	77.5% (31/40)	90.0% (36/40)	95.0% (38/40)
FPR	84.2% (32/38)	97.4% (37/38)	100% (38/38)	75.0% (30/40)	90.0% (36/40)	95.0% (38/40)
TPR	79.5% (31/39)	94.9% (37/39)	97.4% (38/39)	41.0% (16/39)	71.8% (28/39)	92.3% (36/39)

Table 3.4: Implant alignment precision summary expressed as a percentage of sample size (Number of subjects are expressed in parentheses).

	RATKA			CTKA		
Metric	**Inside ± 1° or 1 mm**	**Inside ± 2° or 2 mm**	**Inside ± 3° or 3 mm**	**Inside ± 1° or 1 mm**	**Inside ± 2° or 2 mm**	**Inside ± 3° or 3 mm**
FISA	42.1% (16/38)	68.4% (26/38)	92.1% (35/38)	20.5% (8/39)	56.4% (22/39)	69.2% (27/39)
FICA	68.4% (26/38)	89.5% (34/38)	94.7% (36/38)	46.2% (18/39)	71.8% (28/39)	87.2% (34/39)
FIRA	52.6% (20/38)	92.1% (35/38)	94.7% (36/38)	66.7% (26/39)	84.6% (33/39)	94.9% (37/39)
TISA	42.5% (17/40)	77.5% (31/40)	90.0% (36/40)	46.2% (18/39)	61.5% (24/39)	84.6% (33/39)
TICA	35.0% (14/40)	85.0% (34/40)	95.0% (38/40)	28.2% (11/39)	56.4% (22/39)	82.1% (32/39)

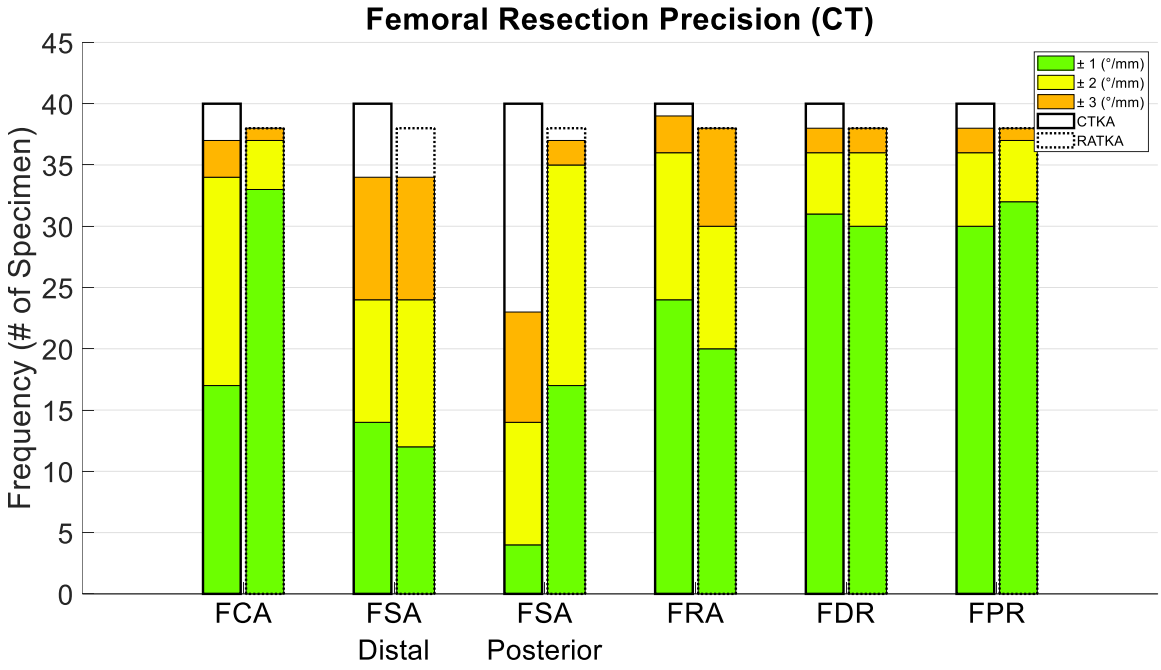

Figure 3.26: Stacked bar chart of femoral resection accuracy metrics within ±1 (green), ±2 (yellow), and ±3 (orange) degrees or mm.

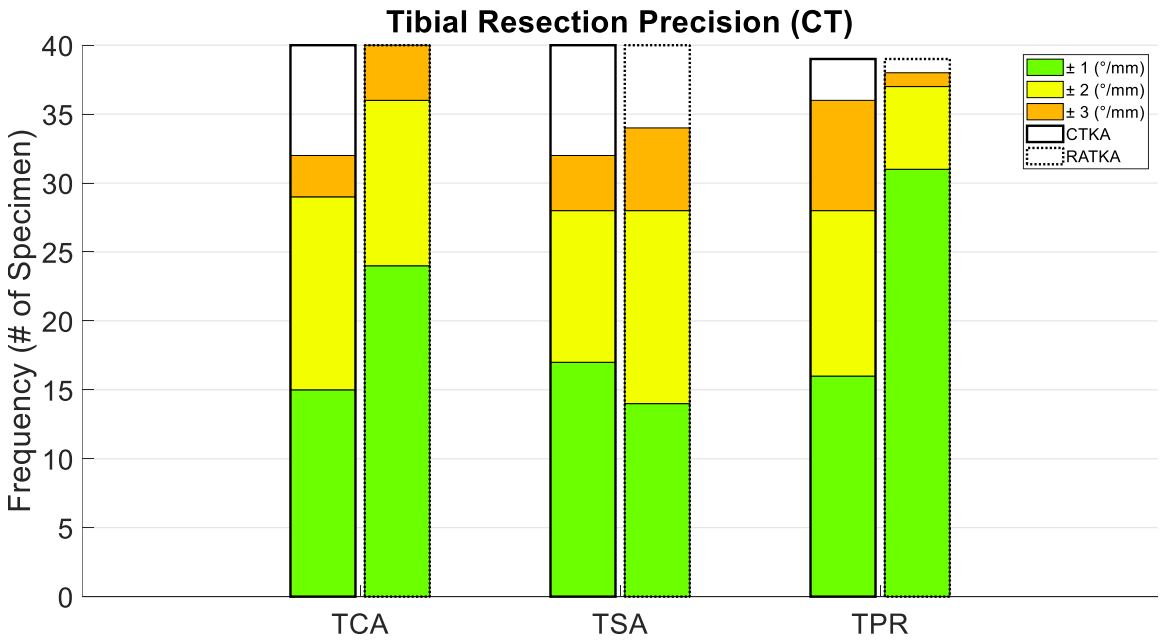

Figure 3.27: Stacked bar chart of tibial resection accuracy metrics within ±1 (green), ±2 (yellow), and ±3 (orange) degrees or mm.

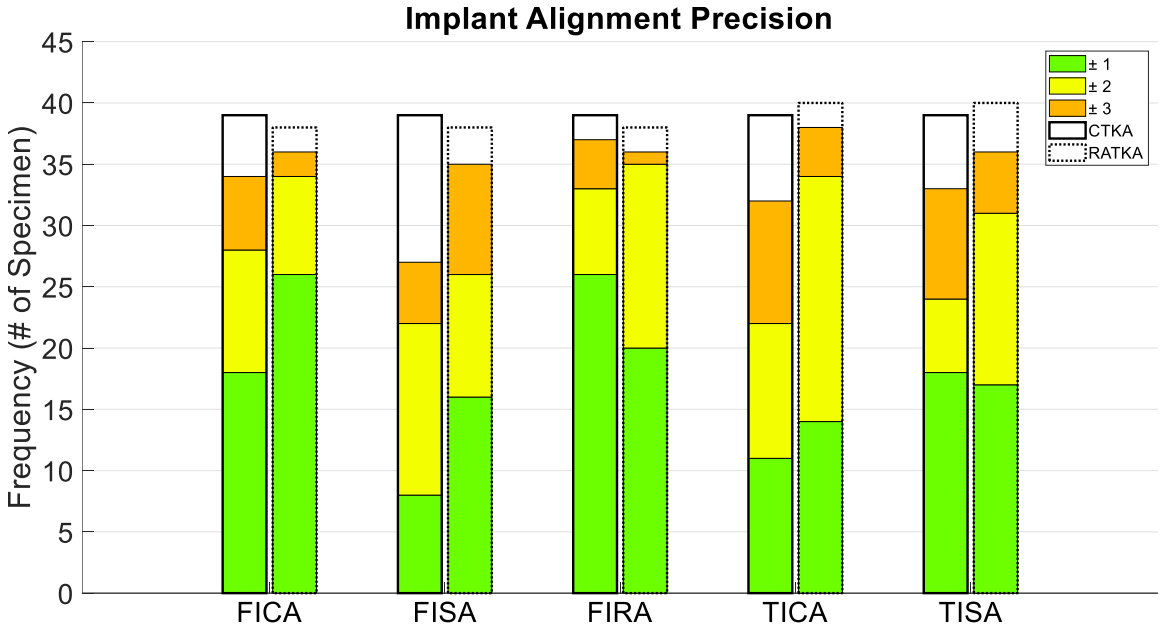

Figure 3.28: Stacked bar chart of implant accuracy metrics within ±1 (green), ±2 (yellow), and ±3 (orange) degrees.

The absolute resection error mean for Posterior Resection Sagittal Angle (PRSA) was 0.95 ± 0.96 and 2.08 ± 2.05 for RTKA and CTKA, respectively. The Anterior Resection Sagittal Angle (ARSA) showed absolute mean error values of 1.91 ± 1.05 and 1.92 ± 1.27 for RTKA and CTKA, respectively. For the Anterior Posterior Transverse Angle (APTA) the absolute mean resection error was 0.85 ± 0.70 and 0.71 ± 0.58 for RTKA and CTKA. The Anterior Posterior Resection Distance (APRD) showed absolute mean errors of 0.56 ± 0.63 and 0.97 ± 0.82.

The linear regression between the CT and white light scan resection angles describes a R^2 value of 0.644 for the femoral F-E (distal reference) resection angle, 0.946 for the femoral V-V resection angle, 0.911 for the femoral I-E resection angle, 0.834 for the tibial F-E resection angle, and 0.915 for the tibial V-V resection angle.

A linear regression model between the resection angle and the implant alignment angle for femoral F-E (distal reference) describes a R^2 value of 0.354. For the femoral V-V, femoral I-E, tibial F-E, and tibial V-V metrics, the adjusted R^2 values were 0.754, 0.775, 0.760, and 0.841.

Table 3.5: Resection angle agreement between CT and white light scans expressed as an adjusted correlation coefficient.

Metric	**Correlation Coefficient (R^2)**
Femoral F-E (Distal Ref.)	0.644
Femoral F-E (Posterior Ref.)	0.833
Femoral V-V	0.946
Femoral I-E	0.911
Tibial F-E	0.834
Tibial V-V	0.915

Table 3.6: Angle agreement between CT scan resection and implant alignment expressed as an adjusted correlation coefficient.

Metric	**Correlation Coefficient (R^2)**
Femoral F-E (Distal Ref.)	0.354
Femoral F-E (Posterior Ref.)	0.291
Femoral V-V	0.754
Femoral I-E	0.775
Tibial F-E	0.760
Tibial V-V	0.841

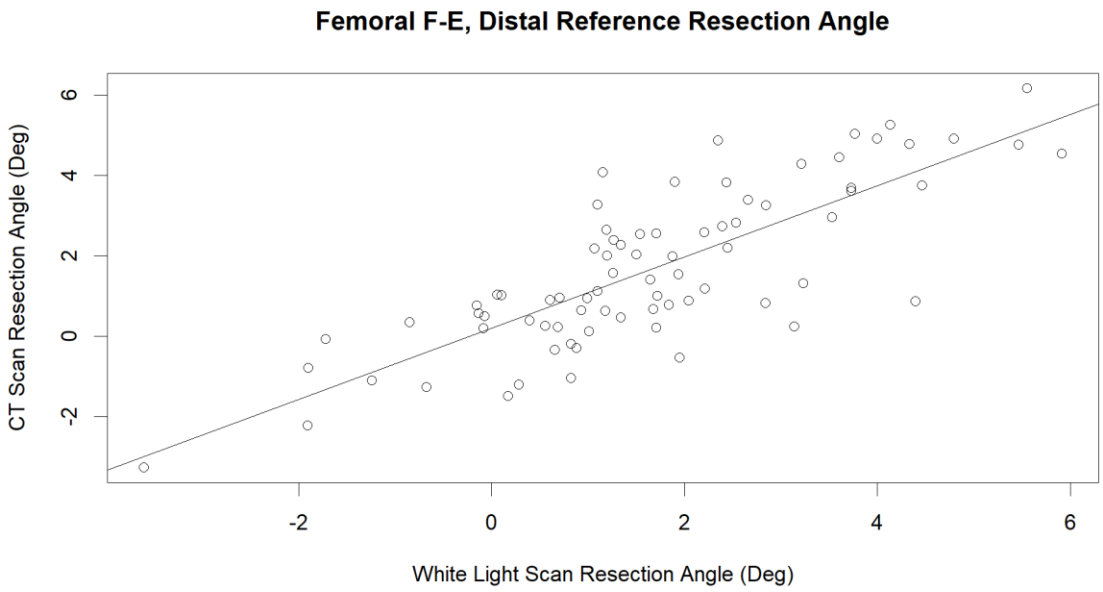

Figure 3.24: Femoral sagittal plane resection agreement between CT and white light scans.

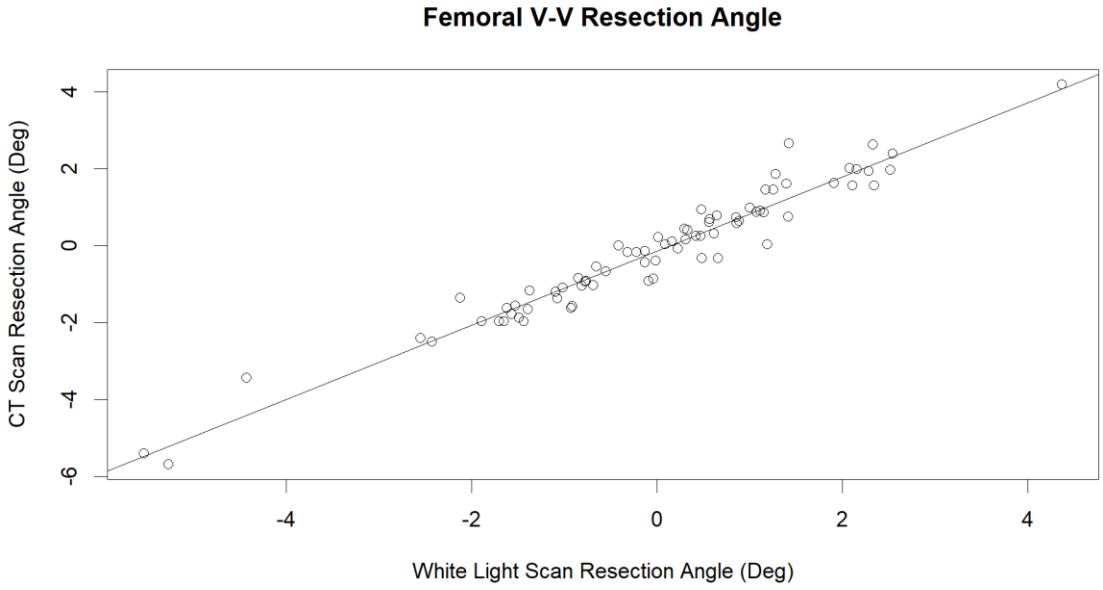

Figure 3.25: Femoral coronal plane resection agreement between CT and white light scans.

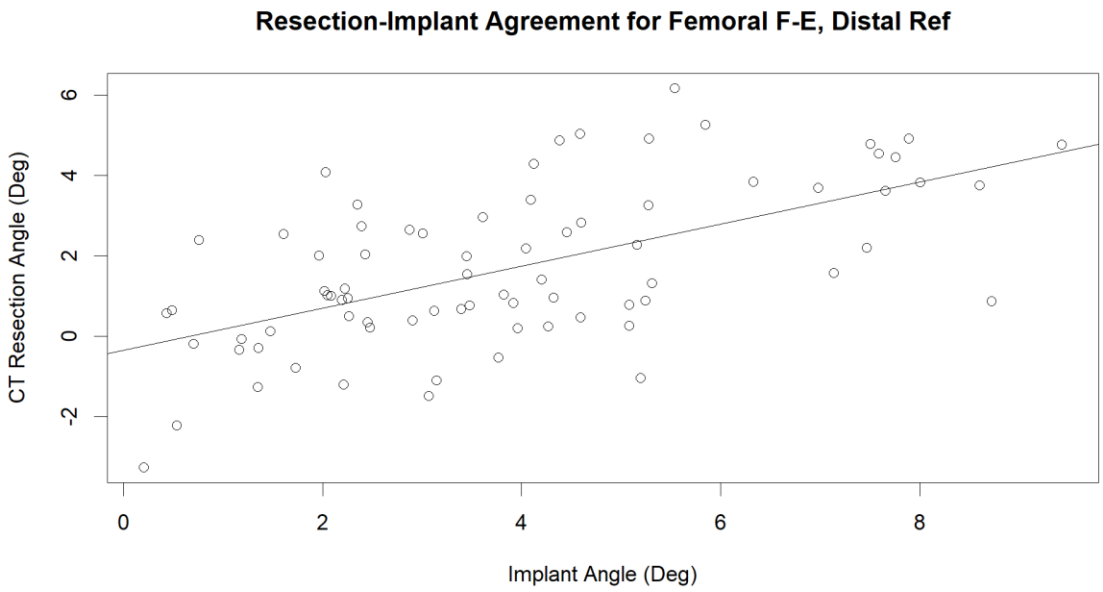

Figure 3.26: Femoral sagittal plane agreement between resection and implant alignment.

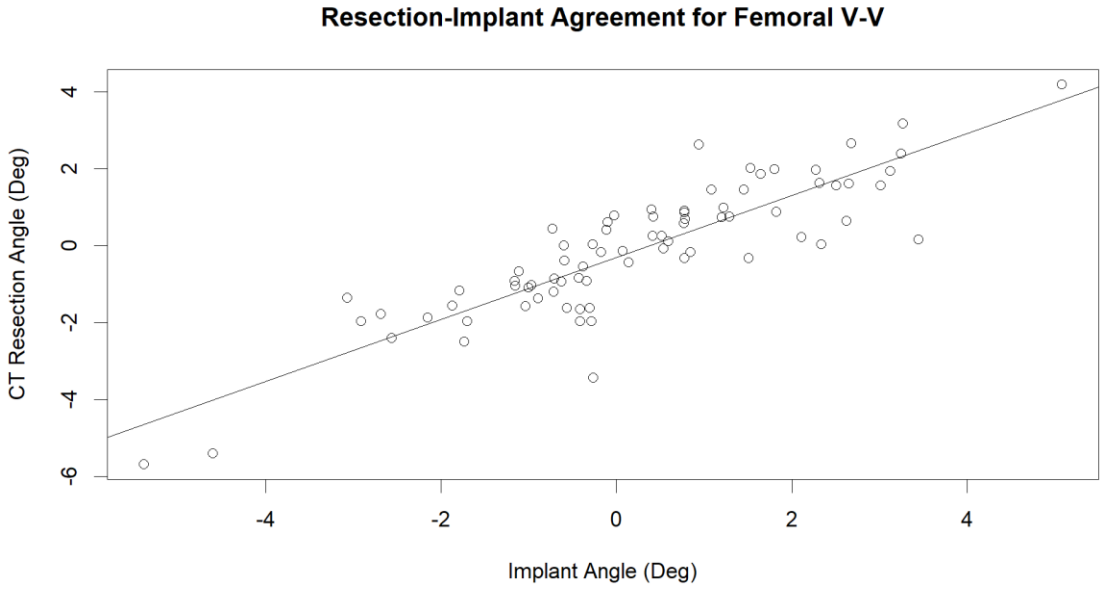

Figure 3.27: Femoral coronal plane agreement between resection and implant alignment.

Table 3.7: Femoral relative resection summary statistics. PRSA, Posterior Resection Angle; ARSA, Anterior Resection Sagittal Angle; APTA, Anterior Posterior Transverse Angle; APSA, Anterior Posterior Sagittal Angle; APRD, Anterior Posterior Resection Distance.

	RATKA			CTKA				
Metric	**Mean ± SD**	**Median**	**Abs. Mean ± SD**	**Mean ± SD**	**Median**	**Abs. Mean ± SD**	**Result**	**p-value**
PRSA (°)	0.56 ± 1.24	0.46	0.95 ± 0.96	0.23 ± 2.93	-0.15	2.08 ± 2.05	Superior	0.001
ARSA (°)	-1.91 ± 1.05	-1.90	1.91 ± 1.05	-1.75 ± 1.51	-1.81	1.92 ± 1.27	Non-Inferior	0.028
APTA (°)	-0.03 ± 1.10	0.09	0.85 ± 0.70	-0.33 ± 0.86	-0.18	0.71 ± 0.58	Non-Inferior	0.007
APSA (°)	-1.35 ± 1.28	-1.13	1.51 ± 1.08	-1.51 ± 3.27	-1.88	2.84 ± 2.18	Superior	0.001
APRD (mm)	-0.16 ± 0.83	-0.16	0.56 ± 0.63	-0.17 ± 1.27	-0.27	0.97 ± 0.82	Superior	0.001

Table 3.8: Resection accuracy descriptive statistics for white light scans.

	RATKA			CTKA				
Metric	**Mean ± SD**	**Median**	**Abs. Mean ± SD**	**Mean ± SD**	**Median**	**Abs. Mean ± SD**	**Result**	**p-value**
FSA, Dist. Ref (°)	1.42 ± 0.99	1.58	1.50 ± 0.86	0.25 ± 2.22	0.35	1.70 ± 1.42	Non-Inferior	0.005
FSA, Post. Ref (°)	0.89 ± 1.23	0.84	1.14 ± 1.00	-0.02 ± 4	-0.18	2.93 ± 2.69	Superior	0.000
FCA (°)	-0.12 ± 0.75	-0.14	0.59 ± 0.47	-0.35 ± 1.70	-0.47	1.39 ± 1.02	Superior	0.000
FRA (°)	0.10 ± 1.15	0.12	0.98 ± 0.59	0.29 ± 1.33	0.36	1.10 ± 0.79	Non-Inferior	0.000
TSA (°)	-0.14 ± 1.61	0.09	1.21 ± 1.05	-0.04 ± 2.24	-0.12	1.65 ± 1.49	Non-Inferior	0.000
TCA (°)	0.47 ± 1.47	0.89	1.28 ± 0.85	1.48 ± 1.91	1.47	1.97 ± 1.38	Superior	0.004

3.5 Discussion

A comparison of mean absolute errors shows that RATKA bone resections and implant alignments are either superior or non-inferior to conventional instrumentation. The robotic surgical system showed significant increased bony resection and implant alignment accuracy and precision in the coronal plane for both the femur and tibia. RATKA showed a 53% and 44% increase in resection accuracy in FCA and TCA respectively and an increase in implant alignment accuracy of 36% and 35% in FICA and TICA respectively compared to CTKA. Frontal plane alignment has been shown as an important factor in preventing implant failure when the tibial tray is positioned perpendicular to the mechanical axis. A tray positioned perpendicular to the mechanical axis distributes loads more evenly between the two condyles compared to a mal-rotated tray. A series of studies were conducted to investigate the TICA of intramedullary and extramedullary guides and found that trays aligned within 2° of the target ranged between 71% to 94% and 82% to 88% respectively [28]. The data shows that the use of a robotic surgical system resulted in 85% of the trays aligned within 2° and 95% of the trays aligned within 3°.

Historically, it has been reported by authors that surgeons have trouble making accurate resections and aligning implants in the sagittal plane compared to the coronal and transverse planes [37,43]. Even though not significant, the mean absolute error improved from 1.92° ± 1.50° to 1.65° ± 1.11° for FSA when referenced from the distal resection; however, significant improvement was found when FSA was referenced from the posterior resection from 3.27° ± 2.51° to 1.21° ± 0.90° and for FISA from 2.49° ± 2.10° in CTKA cases to 1.51° ± 1.08° in RATKA cases.

Other metrics such as the tibial proximal resection (TPR), FISA, proximal resection sagittal angle (PRSA), and anterior-posterior resection distance (APRD) were found to be superior in RATKA than for CTKA. TPR accuracy increased by 60% and FISA accuracy increased by 39 % in RATKA cases. The improvement in FISA may be influenced by improvements in the PRSA and APRD. Because the femoral preparation is comprised of five resections, each of the resections must be accurate relative to the previous cuts for the implanted prosthesis to be congruent with the bony resections; otherwise, the implanted prosthesis may impinge during impaction resulting in a mal-aligned prosthesis. A superior result in PRSA and APRD would explain a better implant fit to the distal femur resulting in improved FISA. All other metrics showed non-inferiority between RATKA and CTKA.

It is also be determined that less outliers were observed in the RATKA cases than the CTKA cases. As outliers are more prone to failure, reducing the number of outliers is another step in achieving more satisfactory TKAs. Most surgeons believe that an acceptable tolerance for implant alignment is ± 3° from the target. In the coronal plane 100% of the femoral and tibial resections are within ± 3° for the RATKA cases, while 92.5% and 80% of the femoral and tibial resections are within ± 3° for the CTKA cases. In the same plane for implant alignment, 94.7% and 95% of femoral and tibial components were oriented within ± 3° for RATKA, while 87.2% and 82.1% of femoral and tibial components were oriented within ± 3° for CTKA.

The rotational alignment in both RATKA and CTKA were analogous. This could be caused from the high precision of locating the posterior condylar axis with posterior

referencing when using conventional tools, so improvement in the transverse plane is limited. On the other hand, locating the most posterior points on the lateral condyle, for the posterior condylar axis, is challenging for the RATKA cases due to the lack of access to the posterior compartment with the stylus because of space occupying osseous and soft tissue structures prior to the tibial osteotomy.

Out of the five resection angle measurements, the metric with the least agreement between the CT and white light scan is FSA referenced from the distal resection (R^2 = 0.639). Theoretically, the correlation coefficient between measures taken with the CT and white light scans should be 1, but errors derived from registration, segmentation, and calculations dimmish the correlation coefficient. The high R^2 values for femoral V-V, femoral I-E, tibial F-E, and tibial V-V show that the linear model explains a large portion of the variability. Agreement between CT and white light scans improved, when FSA was referenced from the posterior resection (R^2 = 0.833). The poor correlation with FSA referenced from the distal resection is attributed to the resolution and segmentation errors of the CT scans. Because the distal resection is closely aligned to the axial CT scan slice, segmentation of the distal resection surface can be noisy and inaccurate compared to resections perpendicular to the axial CT scan slice. The scan slice thickness was 0.6 mm, so a distal resection that deviates less than 0.6 mm cannot be differentiated and will be expressed as a flat plane during segmentation. For example, with a 0.6 mm scan slice thickness and a femoral distal resection A-P dimension of 20 mm, the minimum angular change capable of being observed by the segmentation software is 1.72°. This means that

angular changes of less than 1.72° cannot be differentiated and are segmented as a single voxel on segmentation software. This is visually explained in Figure 3.27.

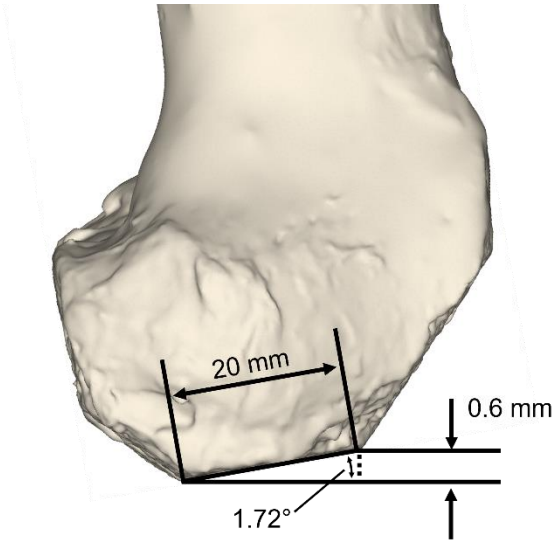

Figure 3.28: Femoral flexion-extension resolution based on axial CT scan slice thickness.

Limitations in this study include possible errors during the registration phase of the study. In the study an initial registration was performed then an ICP algorithm was implemented to finalize the registration. A potential solution to further minimize registration error is to implant fiducial markers prior to the preoperative scan. Because the fiducial markers are rigidly fixed to the bones, a simple singular value decomposition (SVD) algorithm can be used to register the preoperative and postoperative bones together. This could potentially guarantee a more accurate initial registration. Another limitation stems from the scanning equipment used for this study. The resolution of the models generated from the CT scans for the distal resection were large compared to the white light scans. One way to reduce this error is to orient the bones differently and not align the distal resection along the axial slice of the CT scan. This may have caused deviations in the fit plane and the calculated resection angles.

Chapter 4 : Tibial Flatness

4.1 Introduction

Cemented implants have been the standard, but today cementless implants have been increasing in popularity in TKAs for younger patients. As younger patients perform more demanding and load intensive activities, high stresses at the implant-cement interface and bone-cement interface can cause loose wear particles and osteolysis which predates aseptic loosening. In order to avoid particle debris generated at the tibiofemoral joint, orthopaedic surgeons found a new form of fixation.

The initial stability of an implant is affected by the fixation method. Modern implants can be cemented or cementless, where cemented implants are covered in a layer of bone cement, commonly polymethyl methacrylate (PMMA), which fills gaps and voids within the implant-bone interface and anchors the prosthesis to the bone. On the other hand, cementless implants are initially anchored to the bone using a press fit, and fixed long term through bony ingrowth. The press fit takes advantage of the plastic deformation between the bone and the implant to create large normal and frictional forces. The surface of cementless implants is usually manufactured with a porous structure to promote osseointegration (e.g., angiogenesis and osteogenesis) with the prosthesis.

The postoperative tibial resection is considered clinically flat, but at a microscopic level peaks and valleys exist that may be large enough to influence bony ingrowth.

Gaps between the implant-bone interface larger than 500 μm have shown to reduce the quality and rate of bone formation [44]. Since tibial trays are manufactured with a very tight tolerance, bony preparation of the tibia must be made accurately for significant contact between the bone and the implant. As cementless designs have been increasing in popularity, especially in patients younger than 55, the method of long-term fixation for cementless designs is heavily dependent on bony ingrowth.

Bony ingrowth is multifactorial with factors including micromotion, implant topography, biocompatibility, and external load. Lack of bony ingrowth with cementless implants have been associated with higher rates of aseptic loosening [45]. Because the knee joint experiences complex loading throughout flexion and extension, cementless tibial trays fail more often due to micromotion from the combination of shear forces and moments. Large amounts of micromotion inhibit bony ingrowth and acceptable ranges have been reported to be from 28 – 150 μm [46]. Studies suggest that micromotion greater than 150 μm facilitates fibrocartilaginous formation rather than osteogenesis [44].

In a canine study, researchers tested the bony ingrowth of implants with a porous surface and found that contact osteogenesis occurred around the implant for all micromotion groups from 0 to 150 μm of displacement, but bone formation on the surface of the implant was in continuity with surrounding bone in the 0 to 20 μm groups. The groups between 40 μm and 150 μm of micromotion showed implants surrounded with fibrocartilaginous tissue [47].

Surface topography is another influential factor on the rate and quality of bone formation. When bones are remodeled, osteoclasts remove old bone and create a proper

surface for new bone formation. The implant surface must have a similarly complex surface for bone formation as well. The formation of bone, osteogenesis, is not simple and can be broken into two different phenomena, distance osteogenesis and contact osteogenesis. In contact osteogenesis, bone matrix is secreted by active osteoblasts on the surface of the implant and proceeds toward the cut edges of the bone. When bone forms in the opposite direction, from the cut edges of the bone to the implant surface, it is called distance osteogenesis. The formation of immature bone matrix, woven bone, provides secondary stabilization for the implant if both osteogenic processes occur. If contact osteogenesis does not occur due to inadequate implant surface topography, woven bone created from distance osteogenesis cannot interdigitate with the surface of the implant and bone bonding does not occur; therefore, the creation of a complex surface is important in bone bonding and porous surface structures can be created in many ways. One method is sintering, where particles are fused together using pressure and high temperatures. The particles are bonded without melting the material leaving interstitial spaces for osteointegration. Another method is solid state foaming, where the expansion gas bubbles aerate through a material and create a porous structure. During this phase, the porosity, pore size, and pore throat size are important in facilitating contact osteogenesis. Studies have found that implants with larger porosity sizes, around 600 μm, had larger amounts of bony ingrowth at 2 weeks [48].

The component materials can change how the body interacts with the implant. Materials are classified by their biocompatibility and labeled either biotolerant, bioinert, or bioactive materials. Common implant material such as PMMA and stainless steel are

biotolerant, aluminum oxides, titanium (Ti), and cobalt chromium (CrCo) alloys are bioinert, and calcium phosphates and ceramics are bioactive [49]. To theoretically maximize osseointegration, a trabecular structure made with a bioactive material will promote contact osteogenesis hence coatings of calcium phosphates, and popularly hydroxyapatite (HA), have been introduced to create an osteoconductive surface to improve contact osteogenesis and implant fixation.

Flat resections are important to generate maximum bone-implant contact of less than 500 μm apart [50]. A non-planar surface will seat the tibial tray unevenly, leaving sections of the tray with large displacements relative to the peri-prosthetic bone bed. Naturally, the tray will sit on the medial and lateral side of the resection, where harder cancellous bone exists near the cortical wall. Cancellous bone near the center of the resection is naturally softer creating a bowl-like geometry and a zone where potentially large displacements within the implant-bone interface exist. Because high points on an osteotomy naturally exist, a majority of peri-prosthetic contact will occur amid impaction of the tibial tray. Subsidence of the prosthetic will elastically deform and crush weight bearing bony islands, generating surface contact between the peri-prosthetic bone bed.

With conventional instrumentation, a flat surface is achieved using a cutting jig and oscillating saw. As described in Chapter 3, intraoperative guide movement and incorrect pinning can cause resection errors. Plaskos et al., describes popular errors introduced by conventional tools such as the deflection of the resection blade with open slotted cutting jigs. The resection blade, a cantilevered beam, can deflect when the operating surgeon applies a small biasing force on the cutting jig. As a result, slotted cutting jigs have been

proposed as a solution, but errors such as vibrations and contact from the oscillating saw can loosen pin fixation and displace the cutting jig. Another consequence of slotted cutting guides is the use of thin blades. In order to correctly guide the resection, the thin blade must fit within the slot. A decrease in blade thickness correlates to a decreased moment of inertia, and overall blade stiffness, and therefore, increased deflection. Contact with sclerotic bone, an unusual thickening or hardening of the bone, would cause larger deflections for a thinner resection blade which can skive the proximal resection surface. With the elimination of conventional cutting jigs and the use of thicker saw blades in robotic surgical systems, RATKA has been proposed as a solution to reduce intraoperative error during osteotomies.

A metric to quantify surface flatness of the proximal tibial resection has not been established among the orthopaedic community. Flatness metrics have been defined as the standard deviation of measuring points as well as the height above the best fit plane that encompasses 99% of the surface [45,50,51]. Flatness has also been defined by machinists as the smallest distance between two parallel planes, the tolerance zone, that encompasses the measuring points. In a study conducted by Toksvig-Larsen and Ryd (1991), the authors measured the topographic geometry of eight prepared tibial surfaces using a coordinate measuring machine. Plaster-cast negative and positive imprints of the surface resection were created and measured to assess the reproducibility of the method. The maximum roughness, difference between the highest and lowest measuring point, was reported to be 1.05 – 2.39 mm for the bone and 1.22 – 2,30 mm for the imprints and the flatness was reported 0.15 – 0.40 mm and 0.20 – 0.42 for the bone and imprints,

respectively. A study conducted by Delgadillo et al., utilized a laser scanner, a non-contact measurement tool, to capture the surface topography of the tibial osteotomy. To quantify the surface flatness, a plane was fit to the resection surface, and the height above the fit plane was calculated. The flatness of the osteotomy was 1.15 ± 0.10 mm (range 0.56 – 1.81).

This study was performed to compare the surface flatness between RATKA and CTKA. Two measures were taken to quantify the surface flatness of the tibial osteotomy and the distance between the implant-bone interface. It is hypothesized that RATKA cases will have increased surface flatness as well as less distance between the prosthetic and bone bed compared to CTKA cases.

4.2 Methodology

Bilateral TKA was performed on forty pelvis-to-toe cadaveric specimens (Age: 70.4 ± 8.2 years, Height: 67.1 ± 4.1 in., Weight: 132.4 ± 35.8 lbs., BMI: 20.6 ± 4.9). Five board certified orthopaedic surgeons performed all CTKA or RATKA procedures. To avoid handed or side bias, the initial surgical procedure for a lower limb was randomized between CTKA or RATKA, then the contralateral limb would receive the alternate procedure. After TKA, the tibias were denuded of soft tissue and the Artec Space Spider (Artec3D, Luxembourg) was used to optically capture the surface geometry from the resected epiphysis to the distal diaphysis. Afterwards, the bone was impacted with the ATTUNE® Cemented Tibial Base (Depuy Synthes, Warsaw, IN) and another optical white light scan was taken. White light scans of the tibial proximal resection surface were transformed to the implant coordinate system (Figure 3.13). The tibial implant coordinate system was oriented such that a line connecting the most lateral and most medial points

correlates with M-L axis, a line normal to the proximal surface of the tray correlates with the S-I axis, and the vector product between the two lines correlates to the A-P axis. The origin of the implant coordinate system was located at the most anterior point of the proximal surface. The origin was translated 4.1 mm inferiorly to set the origin on the distal surface of the tibial tray.

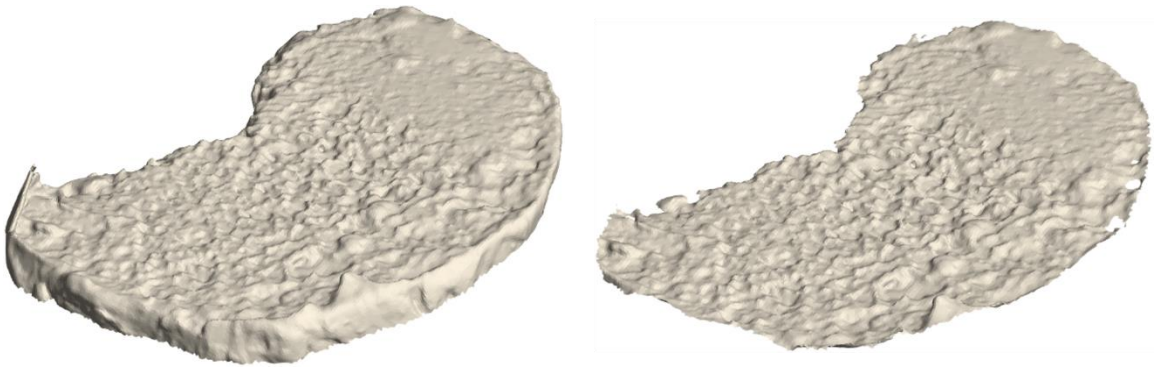

Figure 4.1: Proximal 5 mm of the tibial resection (Left). Proximal 5 mm with removed cortical bone (Right).

The proximal 5 mm of the tibial osteotomy was extracted from solid models generated using the white light scans, and the outer cortical bone was removed (Figure 4.1) using a custom MATLAB (MathWorks, Natick, MA) script. The cortical bone was removed by projecting the proximal resection vertices onto the transverse plane and encompassing the projected vertices within a concave hull. The concave hull was then offset interiorly by 2 mm to remove the cortical bone.

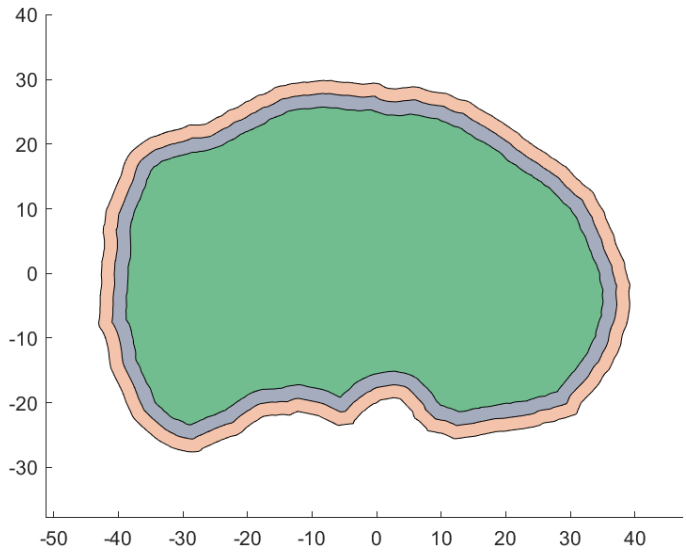

Figure 4.2: Transverse view of convex hulls surrounding the tibial proximal resection. Convex hull offset by 2 mm interiorly (red region). Subsequent convex hull offset creating an annulus (blue region).

In multiple cases, because the metaphysis of the tibia narrows distally towards the diaphysis, a second removal was necessary. For the second removal, another concave hull was created and offset by another 2 mm from the first offset concave hull. To isolate the region between the two offset concave hulls, an annulus, the XOR logic operator was implemented, and the vertices were unprojected from the transverse plane and the standard deviation of the vertices within the annulus was calculated. Vertices were kept within the annulus if they existed within 2.5 standard deviations (98.76%). A 2D median filter, with a kernel size of 5 mm, was then applied to reduce noise during the scanning phase of the white light scan. These steps to remove the cortical bone and filter the proximal surface are important as bony and soft tissue artifacts exist on the resection surface, especially around the cortical bone where soft tissue attaches and posteriorly where unfinished resections are likely to exist.

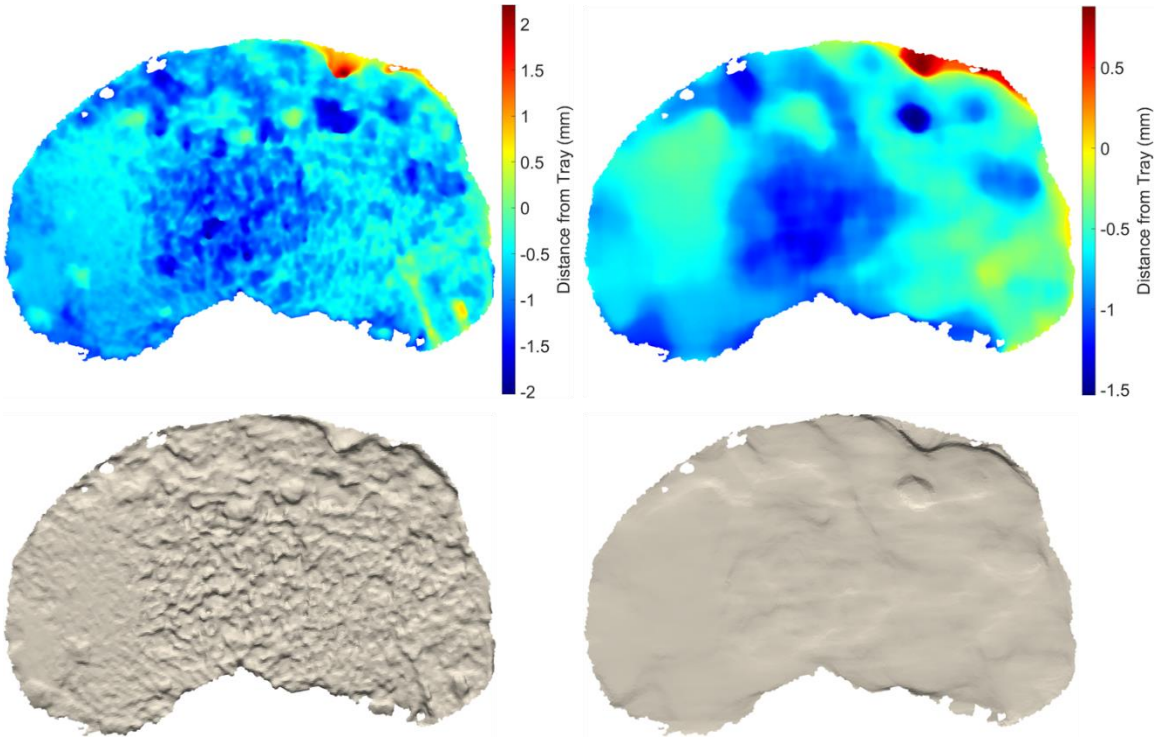

Figure 4.3: Unfiltered proximal resection (Left). Filtered proximal resection (Right). Distance between the tibial tray and proximal resection contours (Top). Proximal resection surface geometry (Bottom).

The proximal resection was then sectioned into seven different regions and several metrics were calculated such as surface flatness and the mean distance between the periprosthetic interface for each section. Each zone is defined by the anatomic location relative to the geometric center of the tibial proximal resection. The Antero-Medial (A-M), Postero-Medial (P-M), Anterior Cruciate Ligament (ACL), Center (C), Posterior Cruciate Ligament (PCL), Antero-Lateral (A-L), and Postero-Medial (P-M) regions are shown in Figure 4.4.

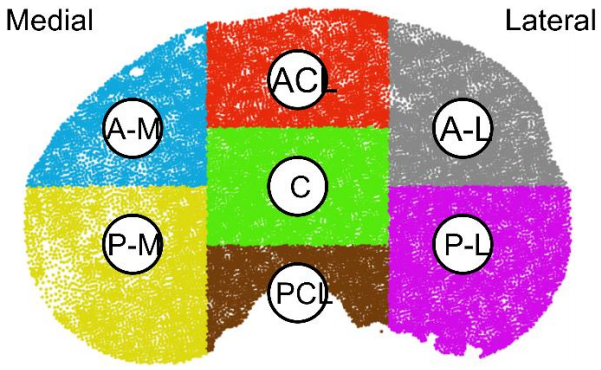

Figure 4.4: Proximal resection regions. Antero-Medial (Blue), Postero-Medial (Yellow), ACL (Red), Center (Green), PCL (Brown), Antero-Lateral (Gray), Postero-Lateral (Purple).

The flatness metric was calculated using the GD&T definition of parallelism. Surface parallelism was defined as a tolerance zone controlled by two planes, where the two planes bound all the surface points and are parallel to a reference datum. The first plane lied on the tallest irregularity and the second plane lied on the deepest irregularity. The height between the two planes was the reported as the parallelism (Figure 4.5). For the rest of the thesis, this metric will be defined as tibial surface flatness.

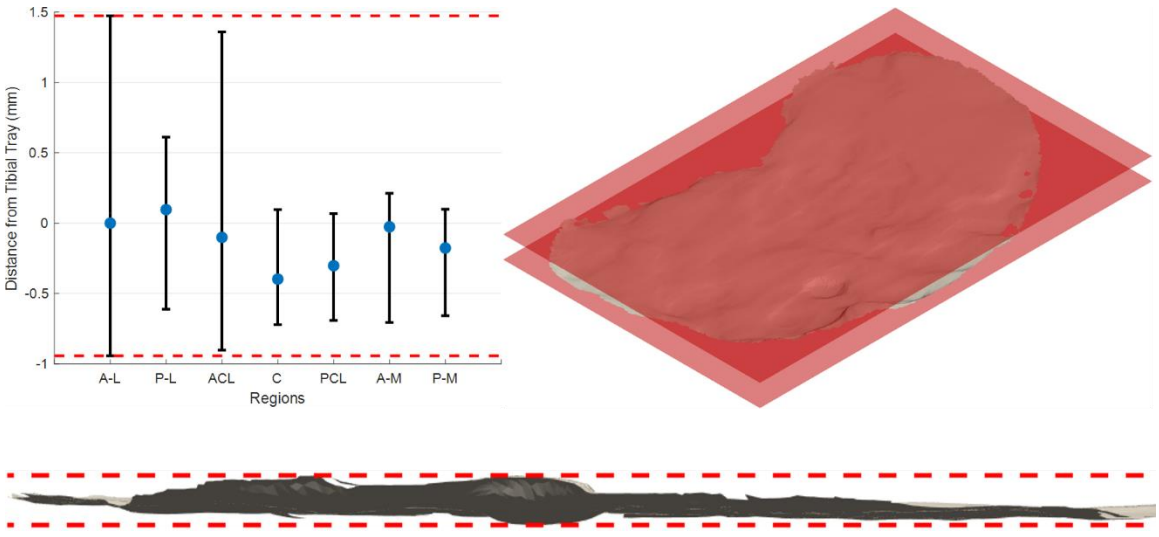

Figure 4.5: Distance between tibial tray and proximal resection error bar plot, surface flatness metric defined by red dotted lines (Top Left). Proximal resection with surface flatness planes in red, isometric view (Top Right). Proximal resection with surface flat.

A second metric was used to quantify gaps within the tibial periprosthetic interface by computing the distance between the distal surface of the tibial tray and the proximal resection. This metric was calculated by computing the height difference between points on the resection surface and a point on the distal surface of the tibial tray. Distances were categorized into five different buckets: < 100 μm, 100 – 200 μm, 200 – 300 μm, 300 – 400 μm, and > 400 μm.

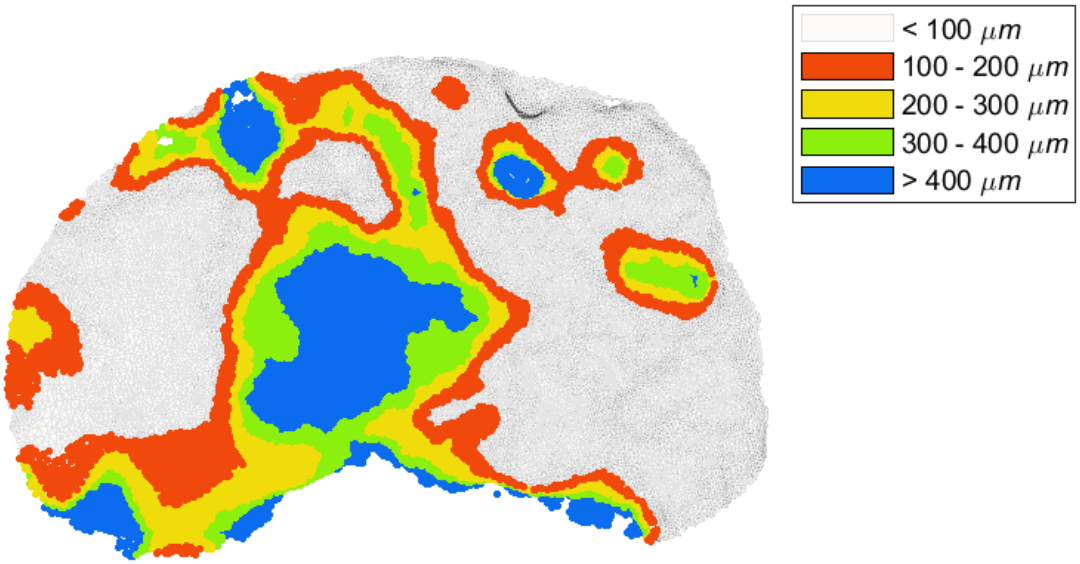

Figure 4.6: Distance between tibial tray and proximal resection contour. (< 100 μm in white, 100 – 200 μm in orange, 200 – 300 μm in yellow, 300 – 400 μm in green, and > 400 μm in blue).

Figure 4.6 maps the categorized distances between the tibial tray and the proximal resection. Visual comparisons between proximal resections is less noisy and simpler with categorized distances. The information displayed using the categorized distances also represents locations of potential bony ingrowth (< 100 μm).

Another analysis was performed to account for the plastic deformation of the cancellous bone during impaction. For this analysis, the region underneath the tibial tray was extracted by superimposing the periphery of the tibial tray onto the surface of the

proximal resection (Figure 4.7) and removing any points outside the tray periphery. Areas above 0 μm are considered to be above the distal surface of the registered implant and will bear a majority of the weight when the tibial tray is impacted. These areas are then plastically deformed until the resulting distance relative to the tibial tray is 0 μm (Figure 4.8).

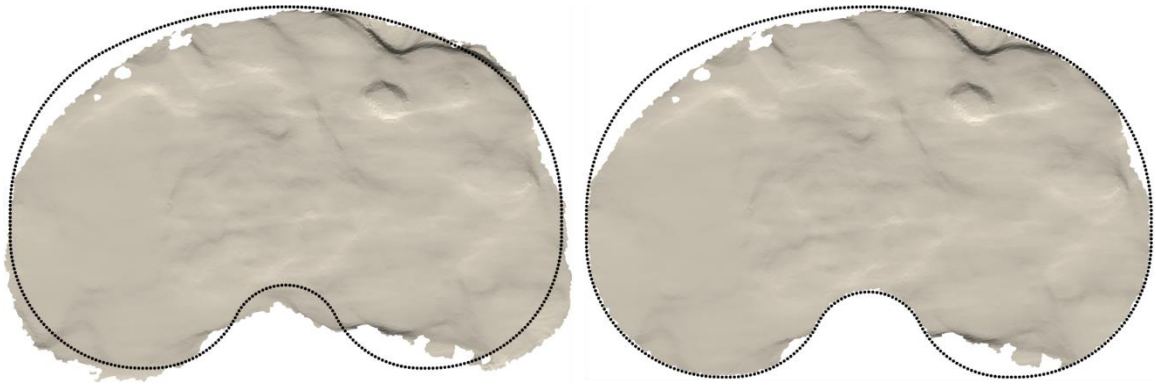

Figure 4.7: Proximal resection overlayed with the periphery of the implanted tibial tray (Left). Isolated proximal resection underneath the tibial tray (Right).

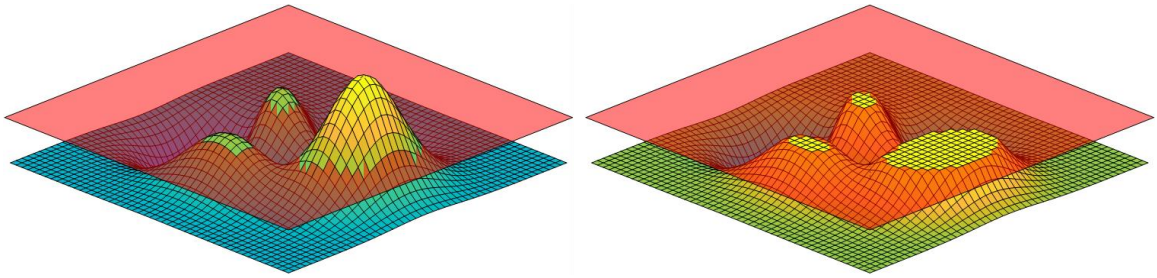

Figure 4.8: Surface peaks prior to plastic deformation (Left)and surface peaks post plastic deformation (Right).

4.2.1 Sign Convention

The sign conventions for this chapter follows the tibial implant coordinate system in Chapter Three. A positive distance corresponds a point proximal to the distal surface of the tray and a negative distance corresponds to a point distal to the distal surface of the tray.

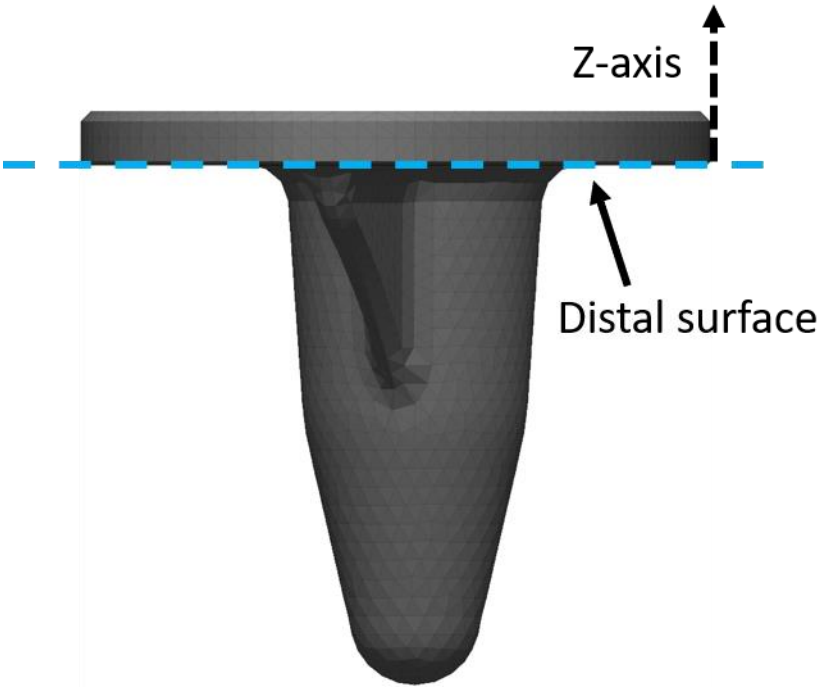

Figure 4.9: Tibial tray distal surface datum and z-axis diagram.

4.2.2 Statistical Methodology

Normality was tested by using the Shapiro-Wilk's test and the homogeneity of variances was tested using Levene's test. Linear regressions and hypothesis testing were then implemented to analyze potential differences between RATKA and CTKA. When testing for the effect of surgical method on the tibial surface flatness or distance within the periprosthetic interface, the region of the tibial resection was controlled for. In another linear regression model, the inputs were the same as the previous model except the region of the tibial resection was not controlled for.

Table 4.1: Null and alternative hypotheses for surface flatness and distance between the tibial tray and resection surface metrics.

Surface Flatness	Distance within Periprosthetic Interface
Ho: There is no difference in tibial surface flatness between RATKA and CTKA cases	Ho: There is no difference in the distance within the periprosthetic interface between RATKA and CTKA cases
Ha: There is a difference in tibial surface flatness between RATKA and CTKA cases	Ha: There is a difference in the distance within the periprosthetic interface between RATKA and CTKA cases

Confidence intervals (CI) with a 95% confidence level (α risk of 0.05) were also calculated to determine significant differences. All statistical tests for this chapter were performed in RStudio (RStudio, Boston, MA).

4.3 Results

Out of the forty cases, two of which, one RATKA and one CTKA case, were removed due to corrupted files. Observing the overall flatness of the resection, the mean flatness for the RATKA group was 3.31 ± 1.47 mm while the mean flatness for the CTKA group was 3.04 ± 1.08 mm. The mean distance between the tray and resection for the RATKA group was 186 ± 129 μm and 195 ± 142 μm for the CTKA group. Statistically significant differences ($p < 0.05$) were not observed between any region.

Table 4.2: Mean values for tibial surface flatness and distance between the tibial tray and the proximal resection for the full tibial resection surface.

	RATKA	CTKA	p-value
Surface Flatness (mm)	3.31 ± 1.47	3.04 ± 1.08	0.36
Mean Tray to Resection Distance (μm)	-186 ± 129	-195 ± 142	0.74

To observe localized effects, the surface flatness was calculated for each of the seven regions on the proximal resection. The surface flatness for RATKA and CTKA cases is summarized in Table 11.

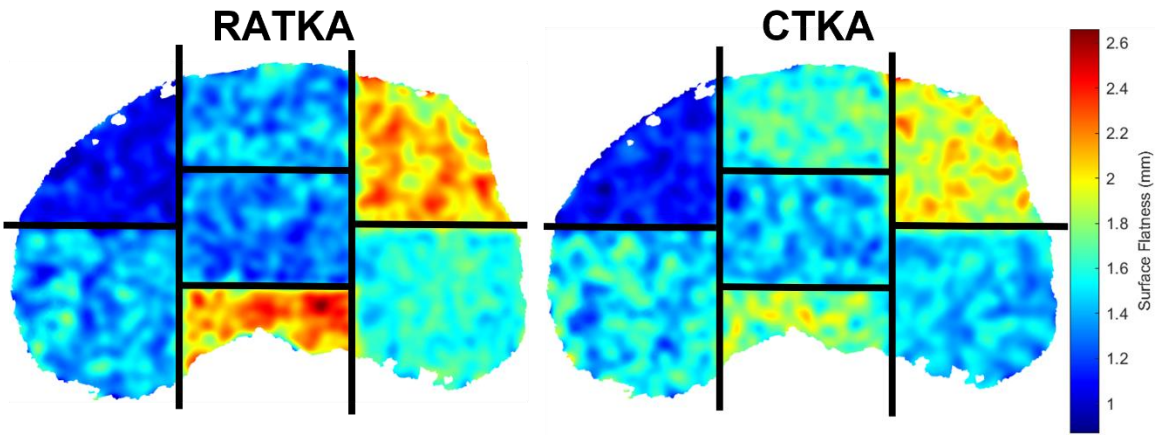

Figure 4.10: Composite image of theoretical resection surface flatness separated by anatomic regions for CTKA (Left) and RATKA (Right). Plots are generated from data in Table 4.3.

Table 4.3: Mean surface flatness between anatomic regions for RATKA and CTKA.

	Mean Resection Surface Flatness (mm)		**p-value**
Region	**RATKA**	**CTKA**	
Antero-Lateral	2.08 ± 1.16	1.93 ± 0.94	0.52
Postero-Lateral	1.57 ± 0.84	1.45 ± 0.61	0.48
ACL	1.38 ± 0.79	1.61 ± 0.74	0.20
Center	1.31 ± 0.95	1.41 ± 0.85	0.65
PCL	2.18 ± 1.51	1.81 ± 1.17	0.23
Antero-Medial	1.08 ± 0.51	1.12 ± 0.48	0.72
Postero-Medial	1.42 ± 0.82	1.52 ± 0.77	0.62

The same regions were used to quantify the distance between the implant and resection surfaces. In the antero-lateral region, the mean distance was 37 ± 243 and -32 ± 270 μm for RATKA and CTKA groups, respectively. In the postero-lateral region, the mean distance was -158 ± 265 and -151 ± 281 μm for RATKA and CTKA groups, respectively. In the ACL region, the mean distance was -228 ± 234 and -224 ± 286 μm for RATKA and CTKA groups, respectively. For the center, PCL, antero-medial, and postero-medial regions, the RATKA and CTKA mean distance values were -487 ± 341 and -525 ± 309 μm, -263 ± 394 and -297 ± 396 μm, -6 ± 179 and -17 ± 209 μm, and -194

± 235 and -132 ± 252 μm respectively. Statistically significant differences ($p < 0.05$) were not observed between any region.

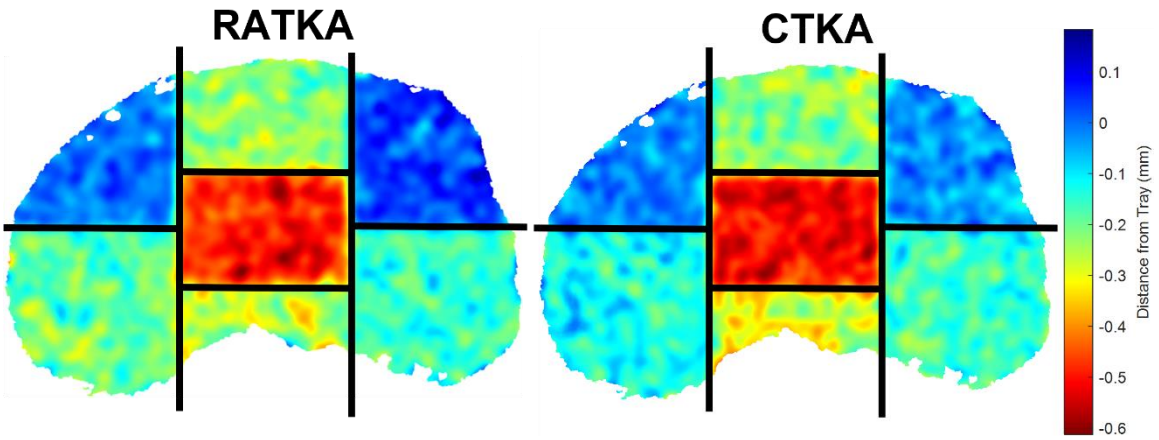

Figure 4.11: Composite image of theoretical distance from the tibial tray separated by anatomic regions for CTKA (Left) and RATKA (Right). Plots are generated from data in Table 4.4.

Table 4.4: Mean distances between the tibial tray and the proximal resection between anatomic regions for RATKA and CTKA.

	Mean Tray to Resection Distance (μm)		**p-value**
Region	**RATKA**	**CTKA**	
Antero-Lateral	37 ± 243	-32 ± 270	0.24
Postero-Lateral	-158 ± 265	-151 ± 281	0.91
ACL	-228 ± 234	-224 ± 286	0.94
Center	-487 ± 341	-525 ± 309	0.61
PCL	-263 ± 394	-297 ± 396	0.70
Antero-Medial	-6 ± 179	-17 ± 209	0.79
Postero-Medial	-194 ± 235	-132 ± 252	0.26

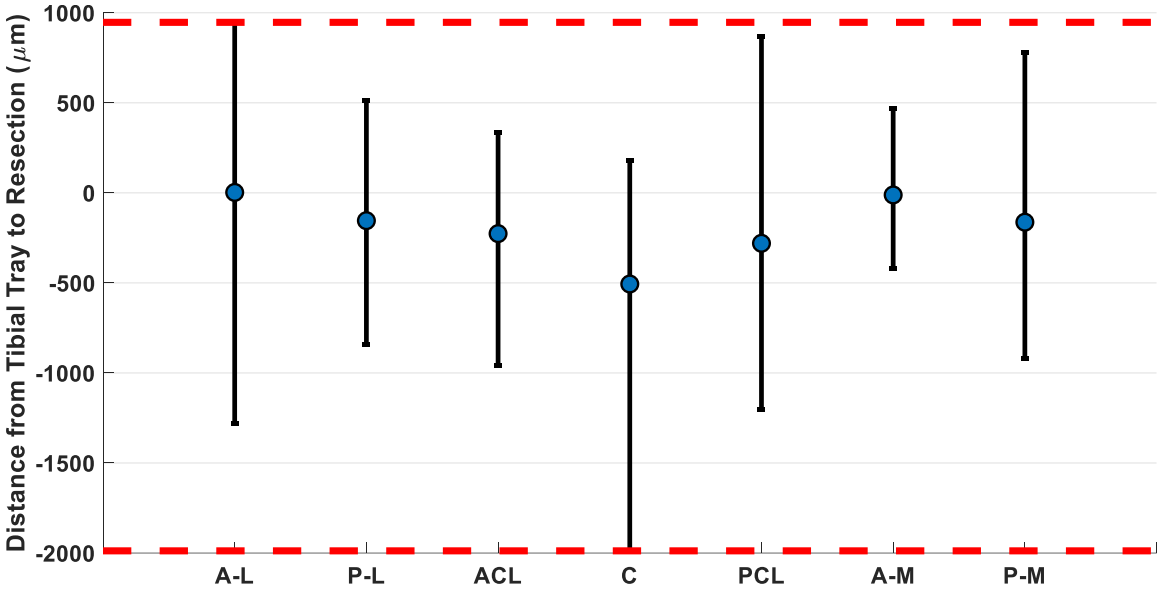

Figure 4.12: Scatter plot of mean distances from tibial tray to resection between anatomic regions (Error bars represent minimum and maximum values).

Table 4.5: One-way ANOVA test showing the variation between mean distance from the tibial tray to the resection surface between anatomic regions.

	Df	Sum Sq.	Mean Sq.	F value	p-value
Regions	6	14.06	2.34	29.11	0.000
Residuals	539	43.40	0.08		

Table 4.6: Mean distance from tibial tray to resection (Top), Post hoc test (Bottom) (shows the mean difference is significant at the 0.05 level).*

Mean Tray to Resection Distance (μm)						
A-L	**P-L**	**ACL**	**C**	**PCL**	**A-M**	**P-M**
2.52 ± 257.72	-154.36 ± 271.43	-226.29 ± 259.74	-506.10 ± 323.80	-280.05 ± 392.67	-11.54 ± 193.24	-162.84 ± 244.26

P-values Between Anatomic Regions for Mean Tray to Resection Distance							
	A-L	**P-L**	**ACL**	**C**	**PCL**	**A-M**	**P-M**
A-L		0.001*	0.000*	0.000*	0.000*	0.757	0.000*
P-L	0.001*		0.114	0.000*	0.006*	0.002*	0.852
ACL	0.000*	0.114		0.000*	0.237	0.000*	0.163
C	0.000*	0.000*	0.000*		0.000*	0.000*	0.000*
PCL	0.000*	0.006*	0.237	0.000*		0.000*	0.010*
A-M	0.757	0.002*	0.000*	0.000*	0.000*		0.001*
P-M	0.000*	0.852	0.163	0.000*	0.010*	0.001*	

Table 4.7: Percentage of total resection surface area within tibial tray distance bounds.

	Percentage of Surface within Distance	
Distances	**RATKA**	**CTKA**
< 100 μm	45.83%	46.85%
100 – 200 μm	12.00%	10.53%
200 – 300 μm	10.36%	8.83%
300 – 400 μm	9.31%	7.92%
> 400 μm	22.51%	25.87%

4.4 Discussion

Each year, the number of TKAs performed around the world has increased, particularly for younger patients. Due to the increased demand for TKA, a need to reduce revision surgeries due to mechanical failures is imperative, such that aseptic loosening of components has driven a large proportion of revision surgeries. Authors believe that improvements in secondary fixation such as bony ingrowth will reduce mechanical loosening of tibial trays. The two metrics we measured that effect bony fixation were: the flatness of the tibial osteotomy and the mean distance from the tibial tray to the tibial osteotomy. Our results show that the surface flatness ($p = 0.36$) and distance between the tibial tray and the proximal resection ($p = 0.74$) were not significantly different between RATKA and CTKA cases. Even though RATKA cases had a larger mean flatness value (3.31 ± 1.47 mm) compared to CTKA cases (3.04 ± 1.08 mm), RATKA cases showed smaller mean distances within the periprosthetic interface (-186 ± 129 μm) compared to CTKA (-195 ± 142 μm). The results also show that the osseous surface after resection using an oscillating saw is not flat and varies with anatomic location ($p < 0.001$). The center of the tibial osteotomy in addition to the region directly anteriorly and posteriorly are elevated inferiorly than the medial and lateral sections. This is accompanied by

another difference between the anterior and posterior section of the tibial resection. The heights of the tibial sections can be ordered from lowest to highest from: Center, ACL and PCL, P-L and P-M, and A-L and A-M. This is supported by the fact that the mean distance from the tray to the anterior region (A-L and A-M) is strictly less than 50 μm, the posterior region (P-L and P-M) is bounded between 100 μm and 200 μm, and the intermediate regions are greater than 200 μm, regardless of resection method. These findings align with Delgadillo et al. and Toksvig-Larsen and Ryd [45,51].

It was also quantified that 45.83% and 46.85% of the proximal resection was less than 100 μm from the distal surface of the tibial tray for RATKA and CTKA cases, respectively. These percentages would theoretically increase from plastic deformation of the trabecular bone when the prosthesis is impacted, as space for initial fixation devices such as posts, keels, and pegs displace bony material. This can be seen in Figure 4.13, where the dotted line represents the keel and post of the tibial tray.

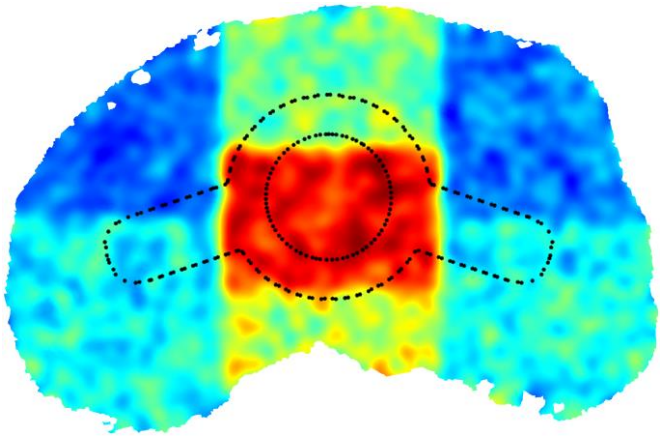

Figure 4.13: Tibial osteotomy surface with an overlayed implanted post and keel.

One limitation within this study consists of allowing surgeons to resurface the tibial osteotomy with the oscillating saw. During tibial preparation in TKA, an initial resection

is performed but not completed. The osseous remnant is then raised to provide clearer visualization of the soft tissue structures and the remainder of the resection is performed. In some cases, the osseous remnant is pulled after the partial resection and bony asperities develop posteriorly, requiring the need to resurface the resection. This technique allows surgeons to protect surrounding soft tissue structures such as the collateral and posterior cruciate ligaments, as poor structural integrity of the posterior cruciate ligament is associated with jeopardized A-P knee translation.

In conclusion, no significant differences were found between the two cohorts, but differences within the groups were found where the mean distance metric shows more prominent gaps on the posterior region (P-L and P-M) than the anterior region (A-L and A-M) of the resection surface. This begs the question whether this phenomenon occurs due to the oscillating saw, surgical technique during resection or implantation, or from natural variation on the topography of the tibial resection.

Chapter 5 : Conclusion

5.1 Final Remarks

The goal of RATKA systems is to improve upon conventional instrumentation to provide better outcomes for patients; therefore, the work presented in this thesis offers an initial investigation on the resection and implant alignment accuracy of the VELYS™ Robotic Assisted Solution compared to conventional instrumentation. Further investigations and significant improvements for RATKA systems will minimize the revision rates for TKAs, reduce outliers, and improve patient satisfaction.

The work from Chapter Three showed significant improvement in resection and implant alignment for both the femur and tibia in the coronal plane. Improvements were also seen in the sagittal plane for the femoral resection, referenced from the posterior resection, femoral component alignment, and femoral relative resections. In conjunction with increased accuracy metrics, precision based metrics also improved. Resection and implant alignment metrics were less prone to be outside the 3°- or 3-mm tolerance for RATKA cases compared to CTKA cases. This chapter gives potential insight to future improvements and investigations for VELYS™ Robotic Assisted Solution in the transverse plane.

Chapter Four showed no statistical differences for the flatness metrics of the proximal tibial osteotomy but did show that flatness varies over the anatomic location of the proximal resection. This chapter stressed the importance of a flat surface for bony

fixation in TKA. We infer that the majority of the tibial flatness error is derived from theresection tooling (oscillating saw) and/or intraoperative tibial resurfacing. More work needs to be performed to isolate the predictive factors effecting the flatness of a tibial osteotomy.

5.2 Future Work

The next step to improve the robotic surgical system is to map the total system error to each subsequent step in the VELYS™ Robotic Assisted Solution TKA surgical procedure. The information gathered from this work would quantify the magnitude of error associated with each step in the surgical procedure and can give engineers and surgeons potential solutions to improve the hardware, software, or surgical technique for VELYS™ Robotic Assisted Solution.

Future work would also consist of gathering clinical data with VELYS™ Robotic Assisted Solution and to measure patient satisfaction rates using a knee scoring system. Without clinical outcomes, it would be difficult to associate the improvement in resection and implant alignment to patient outcomes. Functional clinical data can also be used to quantify preoperative and postoperative differences in knee kinematics during everyday activities such as walking, sitting, standing, leaning, climbing stairs, etc. with the VELYS™ Robotic Assisted Solution.

Another potential study could include comparing various measurement techniques. Because many authors used various techniques to quantify the resection and implant alignment accuracy, a study should be done to compare each method. Methods range from using a planar probe to creating small divots, fiducial markers, into the prosthesis and creating the respective coordinate transformations. These methods should be

compared to the methods used in Chapter Three to provide accurate comparisons between authors. This study would hope to evaluate the different measurement techniques and set a precedence for best practices to measure resection and implant alignment accuracy metrics in the future.

References

[1] Sloan M, Premkumar A, Sheth NP. Projected Volume of Primary Total Joint Arthroplasty in the U.S., 2014 to 2030. J Bone Jt Surg 2018;100:1455–60. https://doi.org/10.2106/JBJS.17.01617.

[2] Losina E, Katz JN. Total knee arthroplasty on the rise in younger patients: Are we sure that past performance will guarantee future success? Bone 2011;23:1–7. https://doi.org/10.1002/art.33371.Total.

[3] Argenson J-N, Boisgard S, Parratte S, Descamps S, Bercovy M, Bonnevialle P, et al. Survival analysis of total knee arthroplasty at a minimum 10 years' follow-up: A multicenter French nationwide study including 846 cases. Orthop Traumatol Surg Res 2013;99:385–90. https://doi.org/10.1016/j.otsr.2013.03.014.

[4] Evans JT, Walker RW, Evans JP, Blom AW, Sayers A, Whitehouse MR. How long does a knee replacement last? A systematic review and meta-analysis of case series and national registry reports with more than 15 years of follow-up. Lancet 2019;393:655–63. https://doi.org/10.1016/S0140-6736(18)32531-5.

[5] Delanois RE, Mistry JB, Gwam CU, Mohamed NS, Choksi US, Mont MA. Current Epidemiology of Revision Total Knee Arthroplasty in the United States. J Arthroplasty 2017;32:2663–8. https://doi.org/10.1016/j.arth.2017.03.066.

[6] Postler A, Lützner C, Beyer F, Tille E, Lützner J. Analysis of Total Knee Arthroplasty revision causes. BMC Musculoskelet Disord 2018;19:55. https://doi.org/10.1186/s12891-018-1977-y.

[7] Kim KT, Lee S, Ko DO, Seo BS, Jung WS, Chang BK. Causes of Failure after

Total Knee Arthroplasty in Osteoarthritis Patients 55 Years of Age or Younger. Knee Surg Relat Res 2014;26:13–9. https://doi.org/10.5792/ksrr.2014.26.1.13.

[8] Lum ZC, Shieh AK, Dorr LD. Why total knees fail-A modern perspective review. World J Orthop 2018;9:60–4. https://doi.org/10.5312/wjo.v9.i4.60.

[9] Plaskos C, Hodgson AJ, Inkpen K, McGraw RW. Bone cutting errors in total knee arthroplasty. J Arthroplasty 2002;17:698–705. https://doi.org/10.1054/arth.2002.33564.

[10] Walker LC, Clement ND, Ghosh KM, Deehan DJ. What is a balanced knee replacement? EFORT Open Rev 2018;3:614–9. https://doi.org/10.1302/2058-5241.3.180008.

[11] Lawrence RC, Felson DT, Helmick CG, Arnold LM, Choi H, Deyo RA, et al. Estimates of the prevalence of arthritis and other rheumatic conditions in the United States: Part II. Arthritis Rheum 2008;58:26–35. https://doi.org/10.1002/art.23176.

[12] Neogi T. The epidemiology and impact of pain in osteoarthritis. Osteoarthr Cartil 2013;21:1145–53. https://doi.org/10.1016/j.joca.2013.03.018.

[13] Zhang Y, Jordan JM. Epidemiology of Osteoarthritis. Clin Geriatr Med 2010;26:355–69. https://doi.org/10.1016/j.cger.2010.03.001.

[14] Rivière C, Iranpour F, Auvinet E, Howell S, Vendittoli P-A, Cobb J, et al. Alignment options for total knee arthroplasty: A systematic review. Orthop Traumatol Surg Res 2017;103:1047–56. https://doi.org/10.1016/j.otsr.2017.07.010.

[15] Inacio MCS, Paxton EW, Graves SE, Namba RS, Nemes S. Projected increase in

total knee arthroplasty in the United States – an alternative projection model. Osteoarthr Cartil 2017;25:1797–803. https://doi.org/10.1016/j.joca.2017.07.022.

[16] Cram P, Lu X, Kates SL, Singh JA, Li Y, Wolf BR. Total knee arthroplasty volume, utilization, and outcomes among medicare beneficiaries, 1991-2010. JAMA - J Am Med Assoc 2012;308. https://doi.org/10.1001/2012.jama.11153.

[17] Choi Y-J, Ra HJ. Patient Satisfaction after Total Knee Arthroplasty. Knee Surg Relat Res 2016;28:1–15. https://doi.org/10.5792/ksrr.2016.28.1.1.

[18] Amanatullah DF, Di Cesare PE, Meere PA, Pereira GC. Identification of the Landmark Registration Safe Zones During Total Knee Arthroplasty Using an Imageless Navigation System. J Arthroplasty 2013;28:938–42. https://doi.org/10.1016/j.arth.2012.12.013.

[19] Maderbacher G, Matussek J, Keshmiri A, Greimel F, Baier C, Grifka J, et al. Rotation of intramedullary alignment rods affects distal femoral cutting plane in total knee arthroplasty. Knee Surgery, Sport Traumatol Arthrosc 2018;26:3311–6. https://doi.org/10.1007/s00167-018-4875-9.

[20] Kim Y-H, Park J-W, Kim J-S, Park S-D. The relationship between the survival of total knee arthroplasty and postoperative coronal, sagittal and rotational alignment of knee prosthesis. Int Orthop 2014;38:379–85. https://doi.org/10.1007/s00264-013-2097-9.

[21] Gromov K, Korchi M, Thomsen MG, Husted H, Troelsen A. What is the optimal alignment of the tibial and femoral components in knee arthroplasty? Acta Orthop 2014;85:480–7. https://doi.org/10.3109/17453674.2014.940573.

[22] Rivière C, Lazic S, Boughton O, Wiart Y, Vïllet L, Cobb J. Current concepts for aligning knee implants: patient-specific or systematic? EFORT Open Rev 2018;3:1–6. https://doi.org/10.1302/2058-5241.3.170021.

[23] Jiri G, Goodman SB, Konttinen YT, Wimmer MA, Holinka M. Osteolysis Around Total Knee Arthroplasty: A Review of Pathogenetic Mechanisms. Bone 2008;23:1–7. https://doi.org/10.1016/j.actbio.2013.05.005.OSTEOLYSIS.

[24] Rodriguez-Merchan EC. Instability following Total Knee Arthroplasty. HSS Journal® Musculoskelet J Hosp Spec Surg 2011;7:273–8. https://doi.org/10.1007/s11420-011-9217-0.

[25] Petersen W, Rembitzki IV, Brüggemann G-P, Ellermann A, Best R, Koppenburg AG, et al. Anterior knee pain after total knee arthroplasty: a narrative review. Int Orthop 2014;38:319–28. https://doi.org/10.1007/s00264-013-2081-4.

[26] Yoo JD, Kim NK. Periprosthetic Fractures Following Total Knee Arthroplasty. Knee Surg Relat Res 2015;27:1–9. https://doi.org/10.5792/ksrr.2015.27.1.1.

[27] Stucinskas J, Robertsson O, Sirka A, Lebedev A, Wingstrand H, Tarasevicius S. Moderate varus/valgus malalignment after total knee arthroplasty has little effect on knee function or muscle strength. Acta Orthop 2015;86:728–33. https://doi.org/10.3109/17453674.2015.1059689.

[28] Jeffcote B, Shakespeare D. Varus/valgus alignment of the tibial component in total knee arthroplasty. Knee 2003;10:243–7. https://doi.org/10.1016/S0968-0160(02)00101-1.

[29] Mattei L, Pellegrino P, Calò M, Bistolfi A, Castoldi F. Patient specific

instrumentation in total knee arthroplasty: a state of the art. Ann Transl Med 2016;4:126–126. https://doi.org/10.21037/atm.2016.03.33.

[30] Sassoon A, Nam D, Nunley R, Barrack R. Systematic Review of Patient-specific Instrumentation in Total Knee Arthroplasty: New but Not Improved. Clin Orthop Relat Res 2015;473:151–8. https://doi.org/10.1007/s11999-014-3804-6.

[31] Sheetz KH, Claflin J, Dimick JB. Trends in the Adoption of Robotic Surgery for Common Surgical Procedures. JAMA Netw Open 2020;3:e1918911. https://doi.org/10.1001/jamanetworkopen.2019.18911.

[32] Bae DK, Song SJ. Computer Assisted Navigation in Knee Arthroplasty. Clin Orthop Surg 2011;3:259. https://doi.org/10.4055/cios.2011.3.4.259.

[33] Perlick L, Bäthis H, Tingart M, Perlick C, Grifka J. Navigation in total-knee arthroplastyCT-based implantation compared with the conventional technique. Acta Orthop Scand 2004;75:464–70. https://doi.org/10.1080/00016470410001259-1.

[34] Bäthis H, Perlick L, Tingart M, Lüring C, Perlick C, Grifka J. Radiological results of image-based and non-image-based computer-assisted total knee arthroplasty. Int Orthop 2004;28:87–90. https://doi.org/10.1007/s00264-003-0533-y.

[35] Martin A, von Strempel A. Two-year Outcomes of Computed Tomography-based and Computed Tomography Free Navigation for Total Knee Arthroplasties. Clin Orthop Relat Res 2006;449:275–82. https://doi.org/10.1097/01.blo.0000218738.69247.d8.

[36] Daines BK, Dennis DA. Gap Balancing vs. Measured Resection Technique in

Total Knee Arthroplasty. Clin Orthop Surg 2014;6:1. https://doi.org/10.4055/cios.2014.6.1.1.

[37] Hampp E, Chughtai M, Scholl L, Sodhi N, Bhowmik-Stoker M, Jacofsky D, et al. Robotic-Arm Assisted Total Knee Arthroplasty Demonstrated Greater Accuracy and Precision to Plan Compared with Manual Techniques. J Knee Surg 2019;32:239–50. https://doi.org/10.1055/s-0038-1641729.

[38] Figueroa F, Wakelin E, Twiggs J, Fritsch B. Comparison between navigated reported position and postoperative computed tomography to evaluate accuracy in a robotic navigation system in total knee arthroplasty. Knee 2019;26:869–75. https://doi.org/10.1016/j.knee.2019.05.004.

[39] Casper M, Mitra R, Khare R, Jaramaz B, Hamlin B, McGinley B, et al. Accuracy assessment of a novel image-free handheld robot for Total Knee Arthroplasty in a cadaveric study. Comput Assist Surg 2018;23:14–20. https://doi.org/10.1080/24699322.2018.1519038.

[40] Parratte S, Price AJ, Jeys LM, Jackson WF, Clarke HD. Accuracy of a New Robotically Assisted Technique for Total Knee Arthroplasty: A Cadaveric Study. J Arthroplasty 2019;34:2799–803. https://doi.org/10.1016/j.arth.2019.06.040.

[41] Han M, Liow L, Chin PL. Total Knee Arthroplasty Technique: TSolution One (Robodoc). Cham: Springer International Publishing; 2019. https://doi.org/10.1007/978-3-030-16593-2.

[42] Khare R, Jaramaz B, Hamlin B, Urish KL. Implant orientation accuracy of a hand-held robotic partial knee replacement system over conventional technique in a

cadaveric test. Comput Assist Surg 2018;23:8–13. https://doi.org/10.1080/24699322.2018.1484167.

[43] Bäthis H, Perlick L, Tingart M, Perlick C, Lüring C, Grifka J. Intraoperative cutting errors in total knee arthroplasty. Arch Orthop Trauma Surg 2005;125:16–20. https://doi.org/10.1007/s00402-004-0759-1.

[44] Kuzyk PR, Schemitsch EH. The basic science of peri-implant bone healing. Indian J Orthop 2011;45:108. https://doi.org/10.4103/0019-5413.77129.

[45] Delgadillo LE, Jones HL, Ismaily SK, Han S, Noble PC. How Flat Is the Tibial Osteotomy in Total Knee Arthroplasty? J Arthroplasty 2020;35:870–6. https://doi.org/10.1016/j.arth.2019.10.007.

[46] Cross MJ, Spycher J. Cementless fixation techniques in joint replacement. Jt. Replace. Technol., Elsevier; 2008, p. 190–211. https://doi.org/10.1533/9781845694807.2.190.

[47] Jasty M, Bragdon C, Burke D, O'Connor D, Lowenstein J, Harris WH. In Vivo Skeletal Responses to Porous-Surfaced Implants Subjected to Small Induced Motions*. J Bone Jt Surg (American Vol 1997;79:707–14. https://doi.org/10.2106/00004623-199705000-00010.

[48] Taniguchi N, Fujibayashi S, Takemoto M, Sasaki K, Otsuki B, Nakamura T, et al. Effect of pore size on bone ingrowth into porous titanium implants fabricated by additive manufacturing: An in vivo experiment. Mater Sci Eng C 2016;59:690–701. https://doi.org/10.1016/j.msec.2015.10.069.

[49] Kienapfel H, Sprey C, Wilke A, Griss P. Implant fixation by bone ingrowth. J

Arthroplasty 1999;14:355–68. https://doi.org/10.1016/S0883-5403(99)90063-3.

[50] Toksvig-Larsen S, Ryd L. Surface flatness after bone cutting: A cadaver study of tibial condyles. Acta Orthop Scand 1991;62:15–8. https://doi.org/10.3109/17453679108993084.

[51] Toksvig-Larsen S, Ryd L. Preparation Characteristics During Total Following Knee Arthioplasty. J Arthroplasty 1994;9:63–6.

Appendix

Additional Figures for Chapter Three

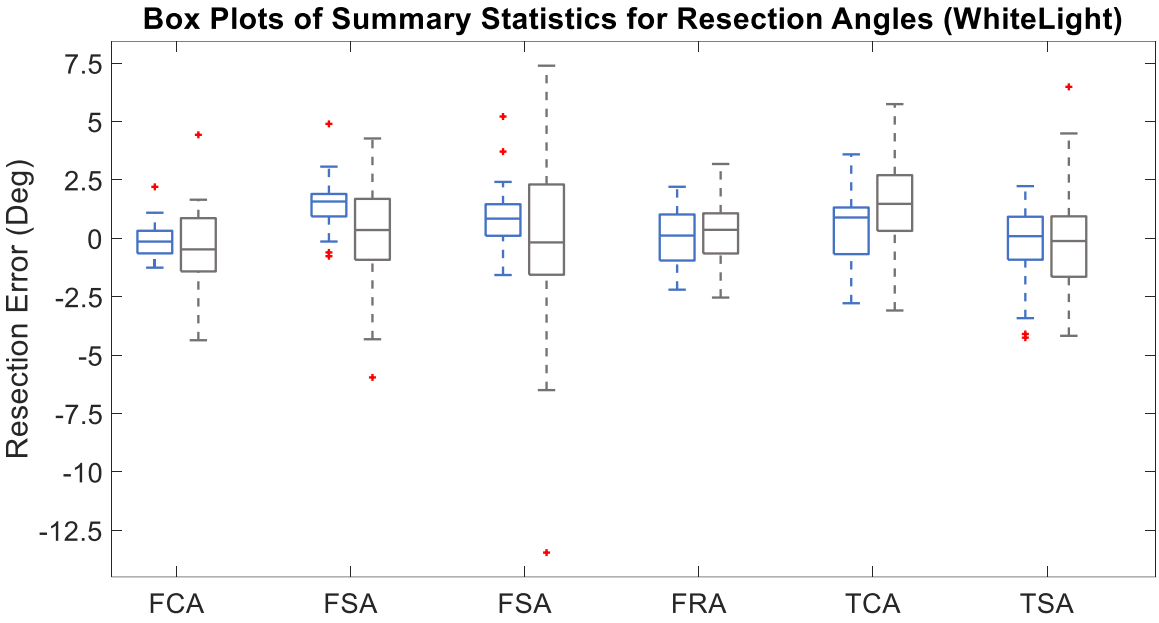

Figure A.1: Box plots showing summary statistics of resection angles (white light scans). Central mark represents the median and red dots denote outliers (Data outside 1.5 IQR).

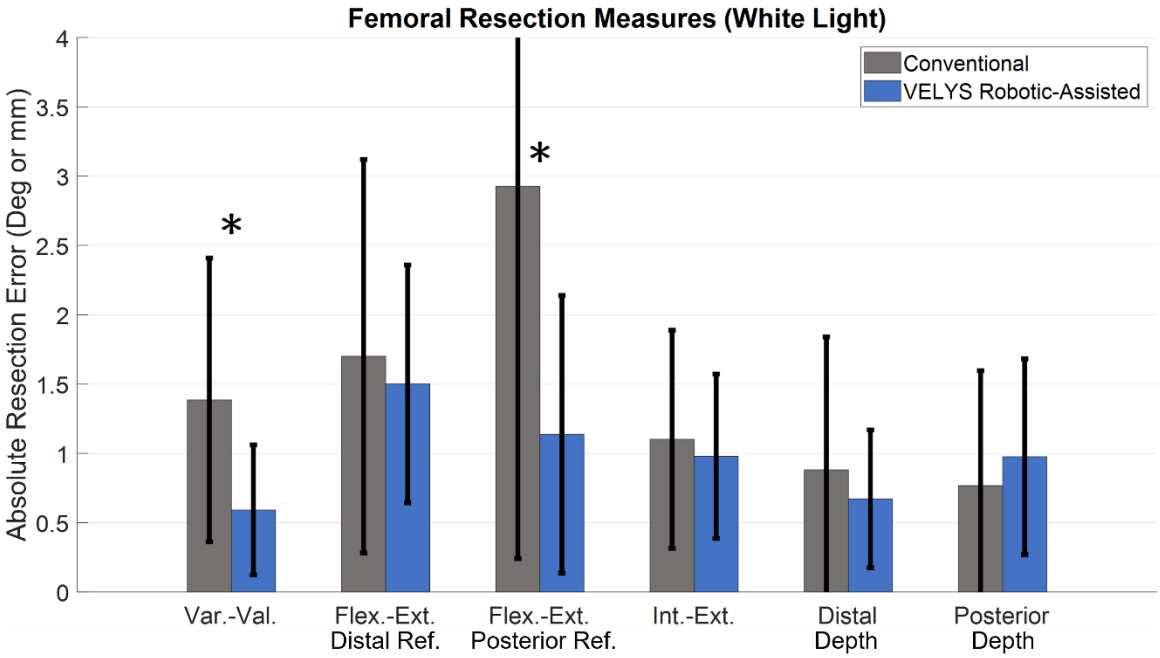

Figure A.2: Femoral resection measures based on white light scans (denotes statistically significant results at 95% CI).*

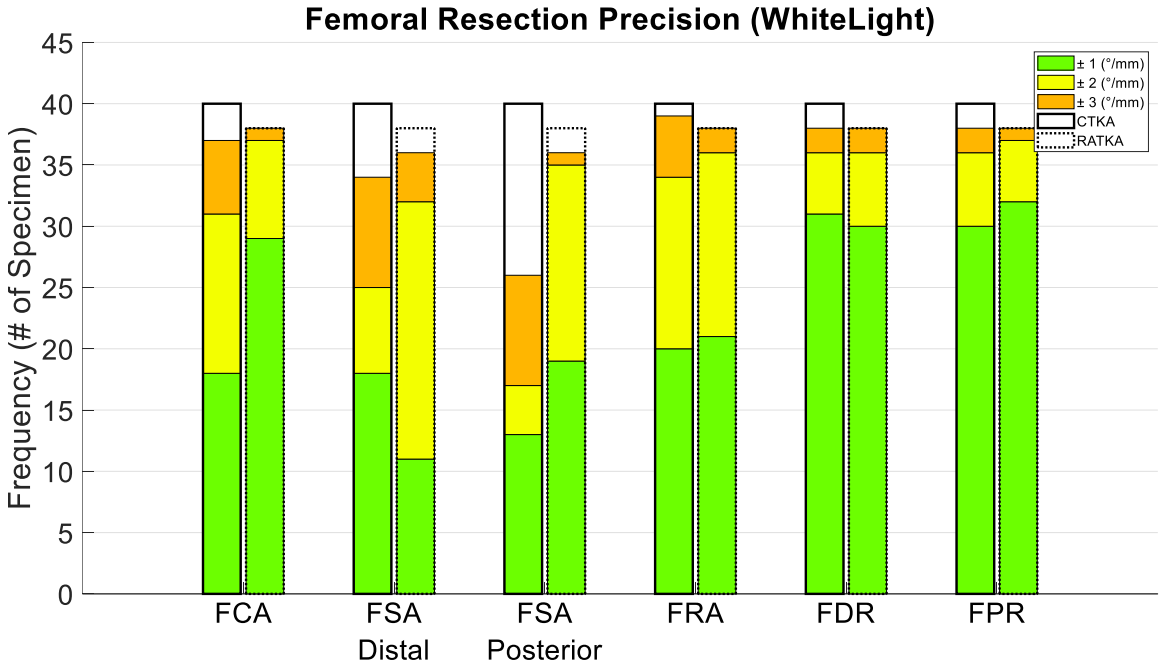

Figure A.3: Stacked bar chart of femoral resection accuracy metrics (white light scans) within ±1 (green), ±2 (yellow), and ±3 (orange) degrees or mm.

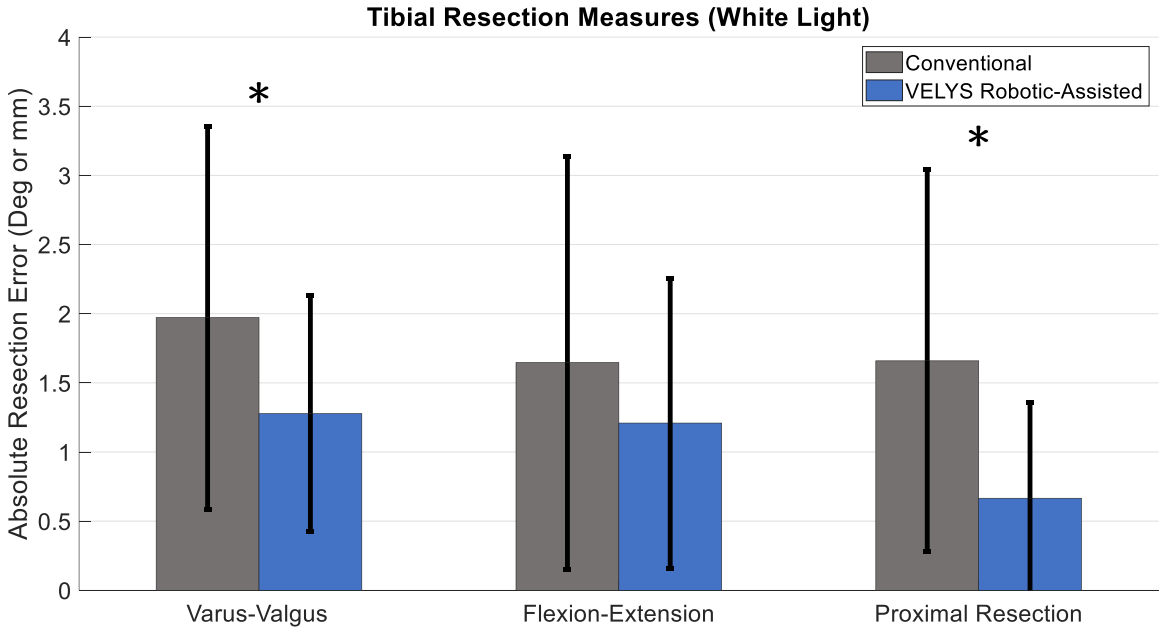

Figure A.4: Tibial resection measures based on white light scans (denotes a statistically significant result at 95% CI).*

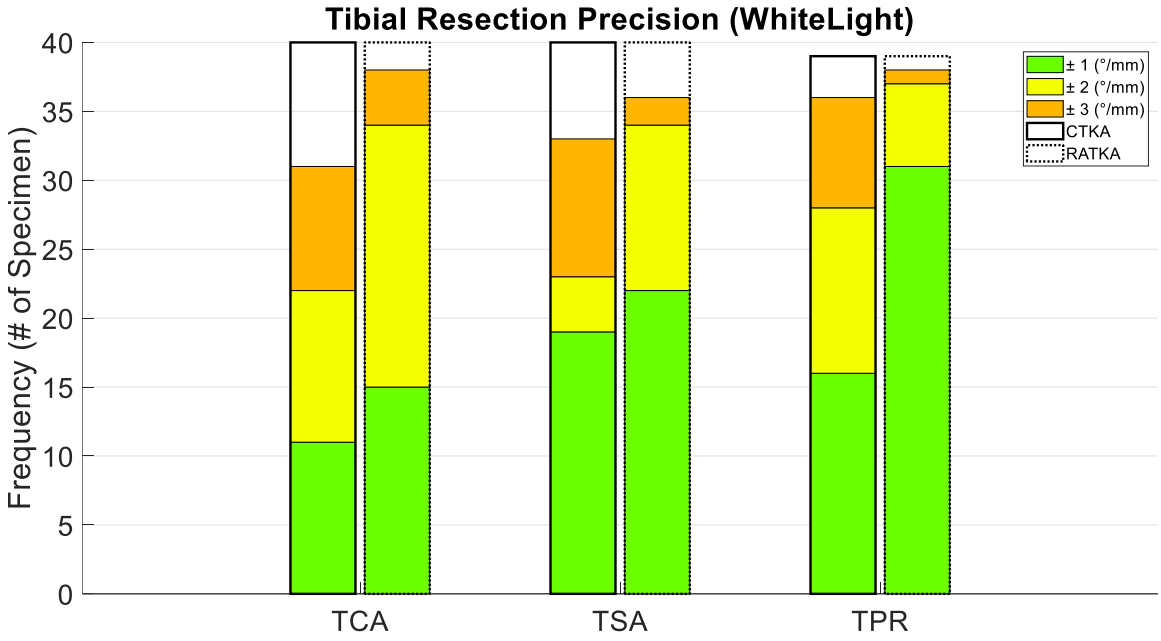

Figure A.5: Stacked bar chart of tibial resection accuracy metrics (white light scans) within ±1 (green), ±2 (yellow), and ±3 (orange) degrees or mm.

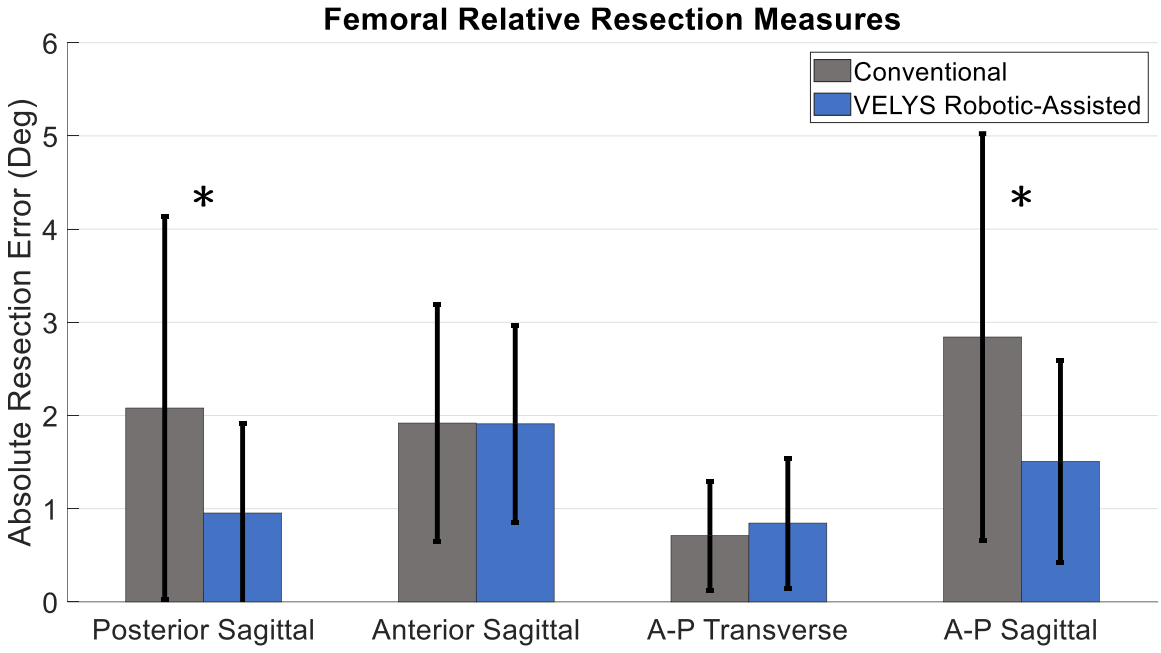

Figure A.6: Femoral relative resection measures based on postoperative CT scans (indicates RTKA superiority at a 95% CI).*

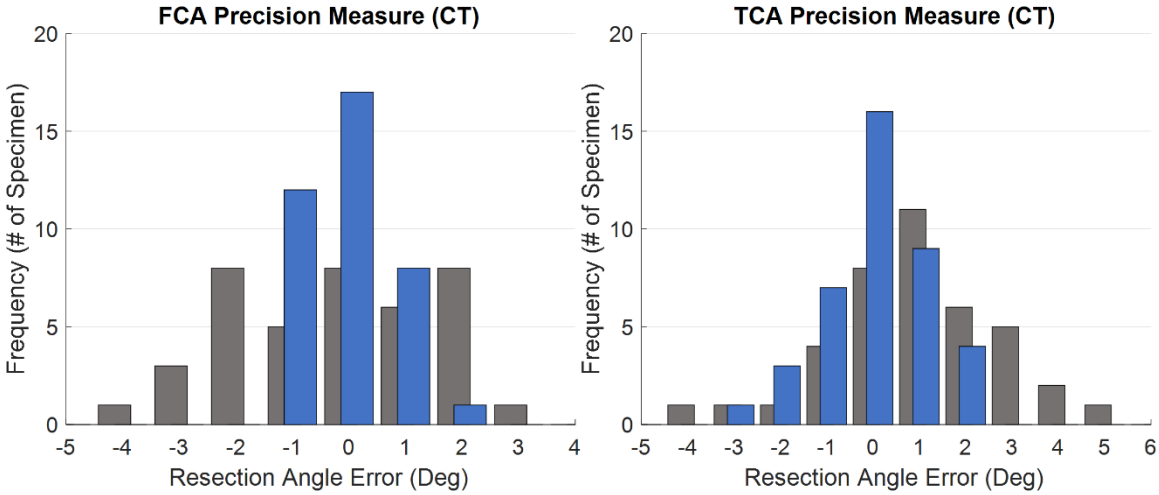

Figure A.7: Coronal plane resection precision histograms for the femur based on postoperative CT scans (Left) and tibia (Right).

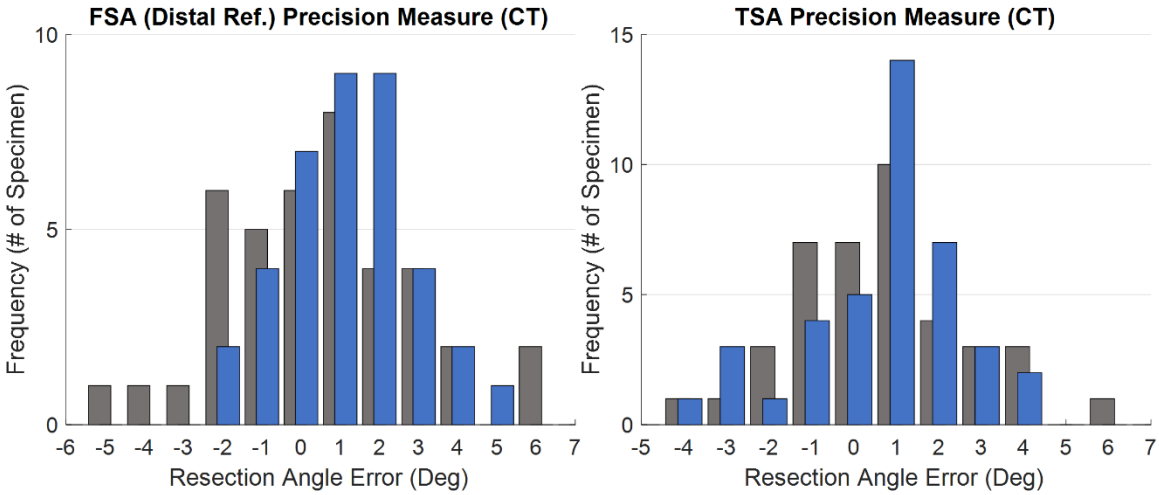

Figure A.8: Coronal plane implant alignment precision histograms for the femur based on postoperative CT scans (Left) and tibia (Right).

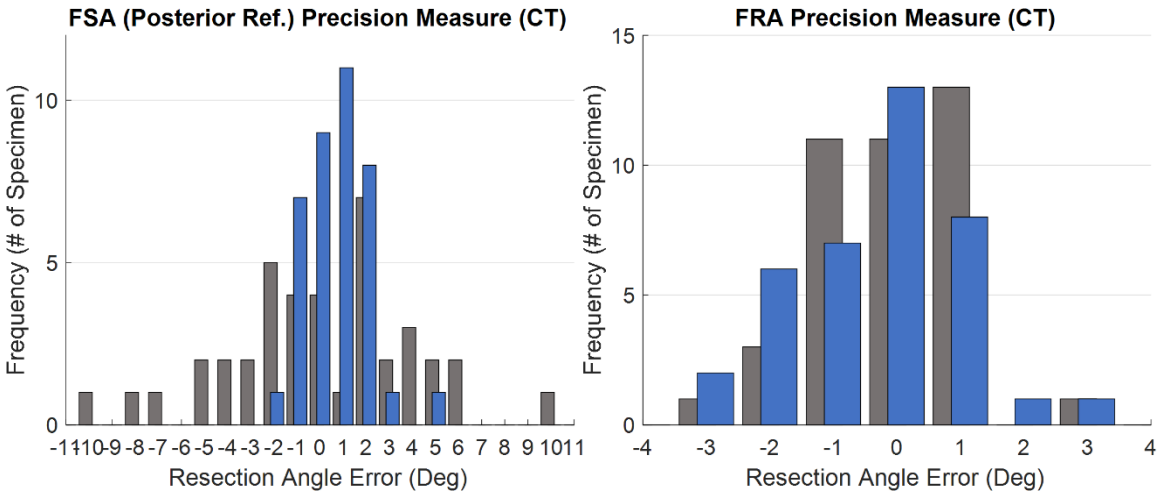

Figure A.9: Femoral sagittal posterior reference (Left) and transverse (Right) plane precision histograms.

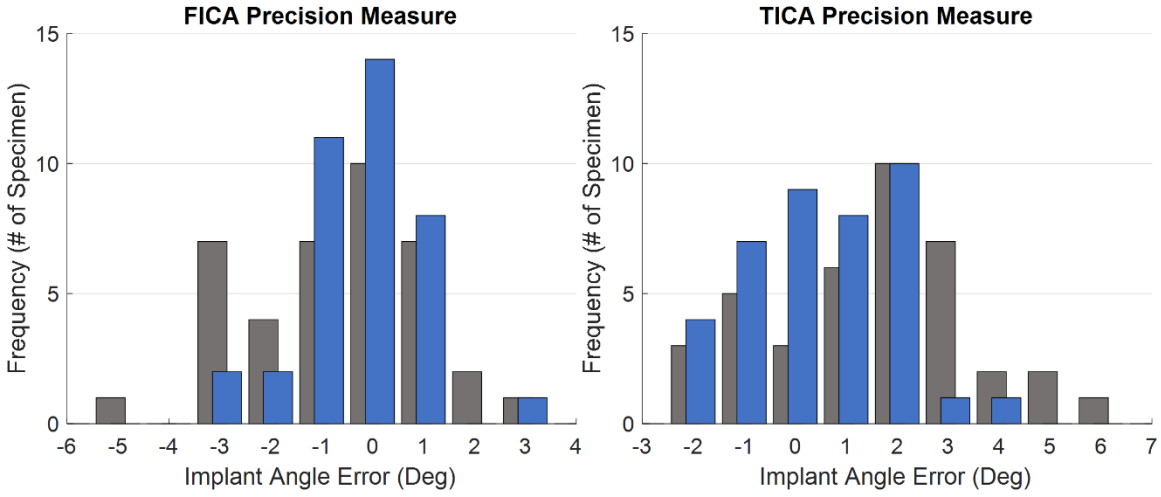

Figure A.10: Sagittal plane implant alignment precision histograms for the femur (Left) and tibia (Right).

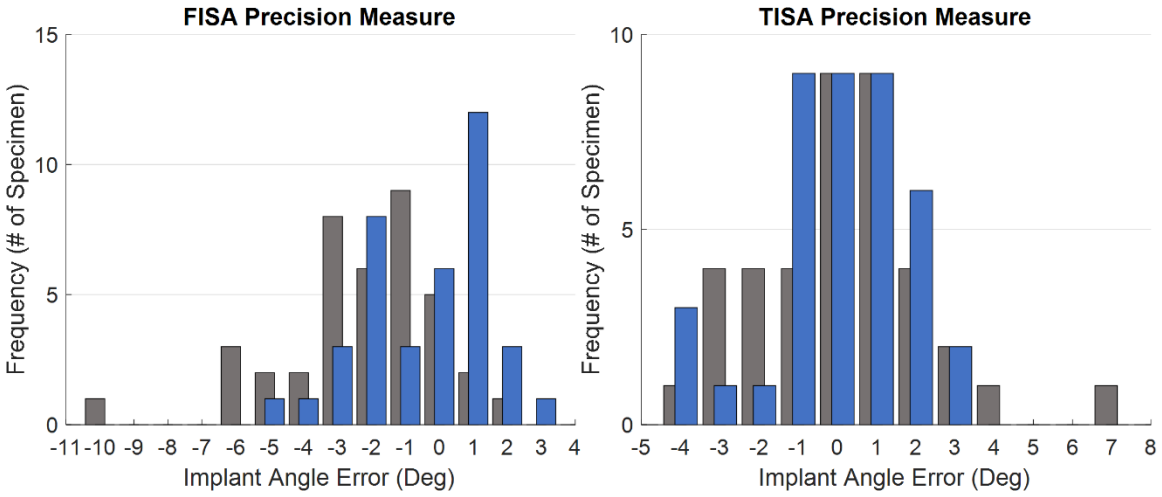

Figure A.11: Transverse plane implant alignment precision histograms for the femur (Left) and tibia (Right).

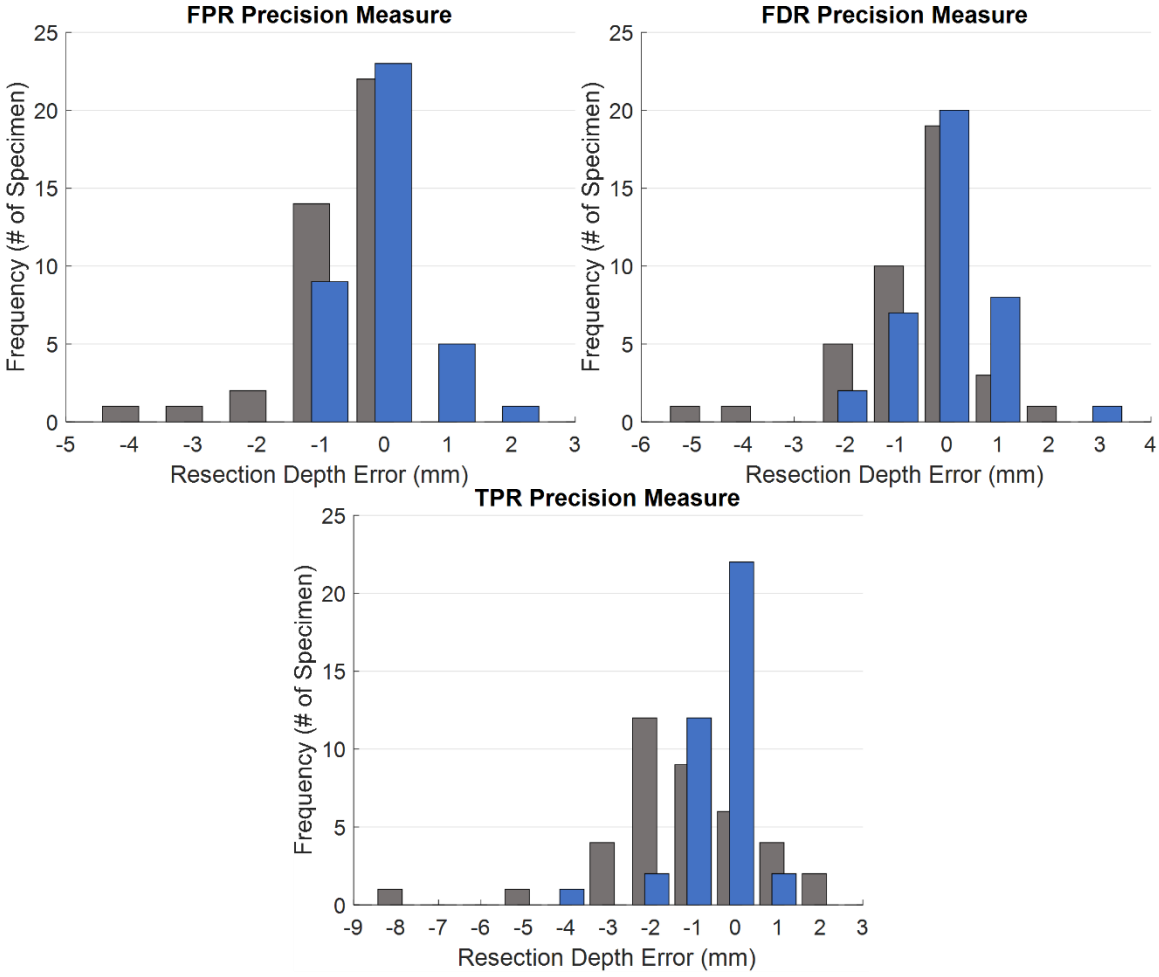

Figure A.12: Posterior, distal, and transverse resection depth precision histograms.

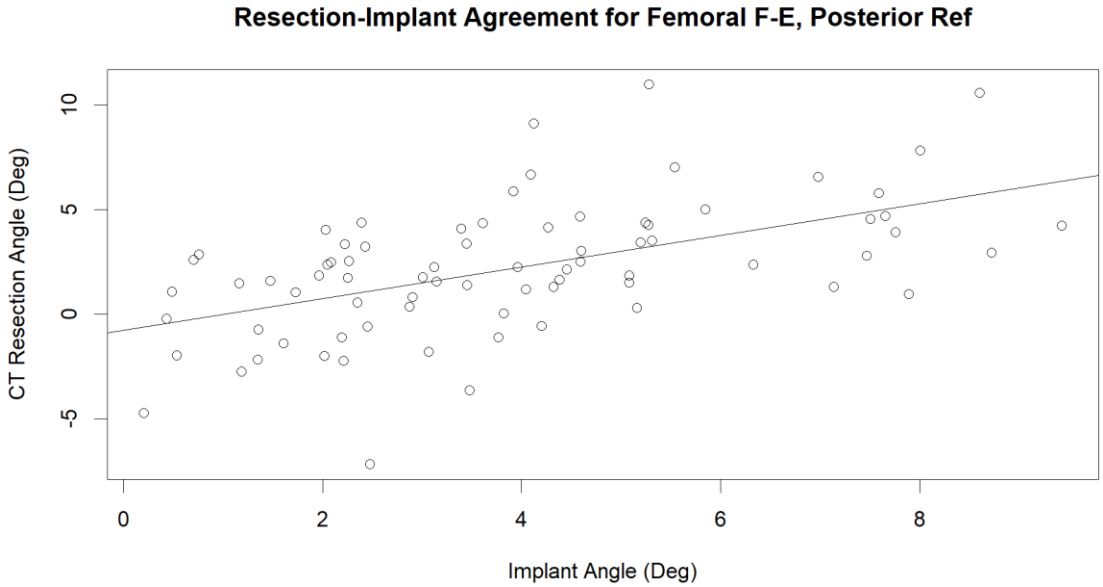

Figure A.13: Femoral sagittal plane posterior reference resection agreement between CT and white light scans.

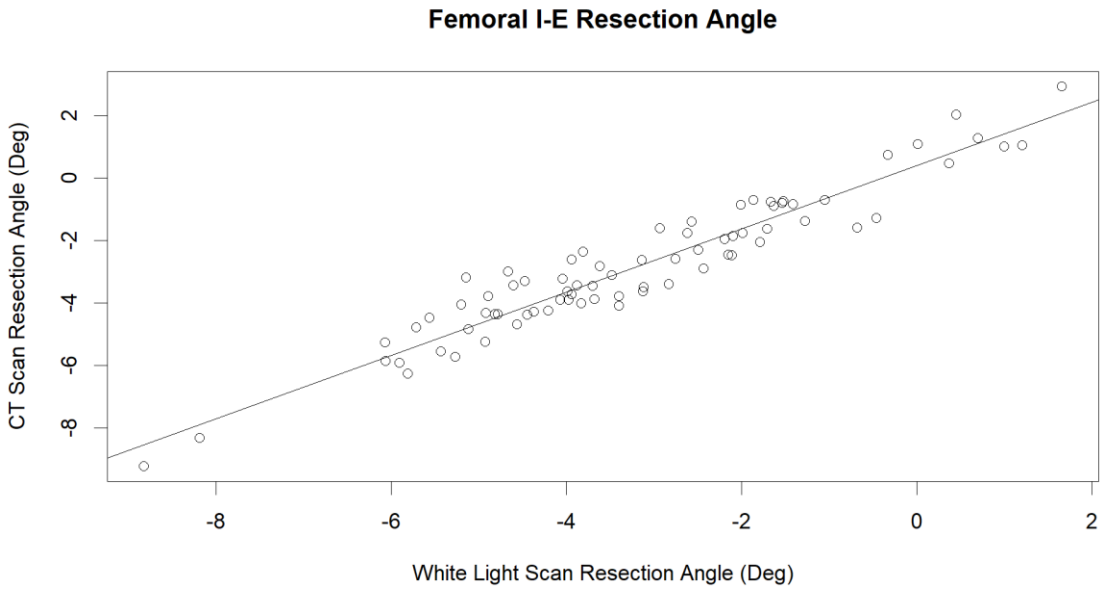

Figure A.14: Femoral transverse plane resection agreement between CT and white light scans.

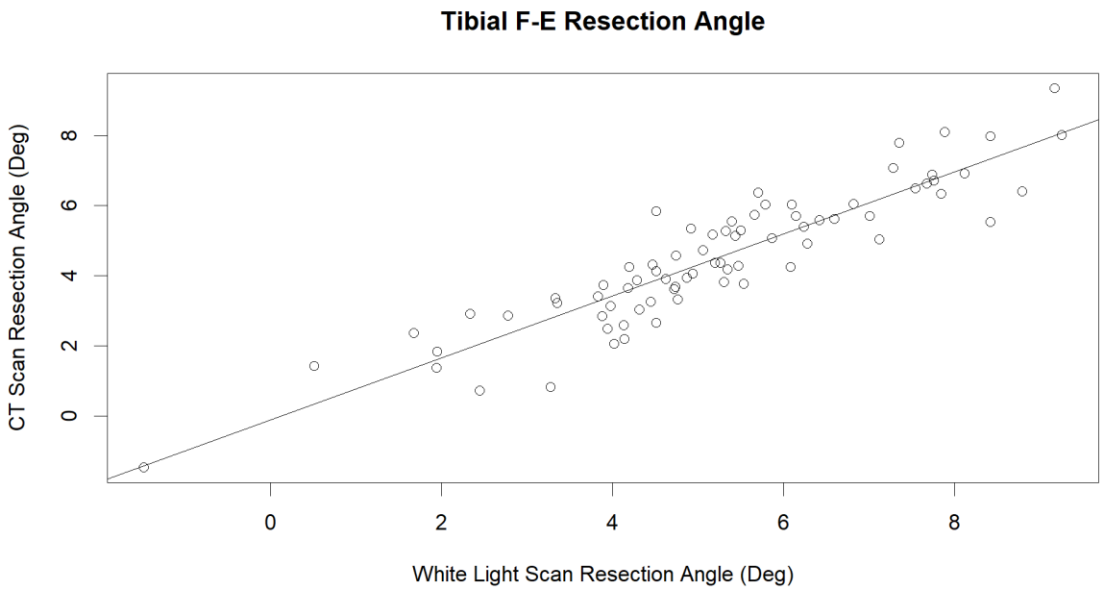

Figure A.15: Tibial transverse plane resection agreement between CT and white light scans.

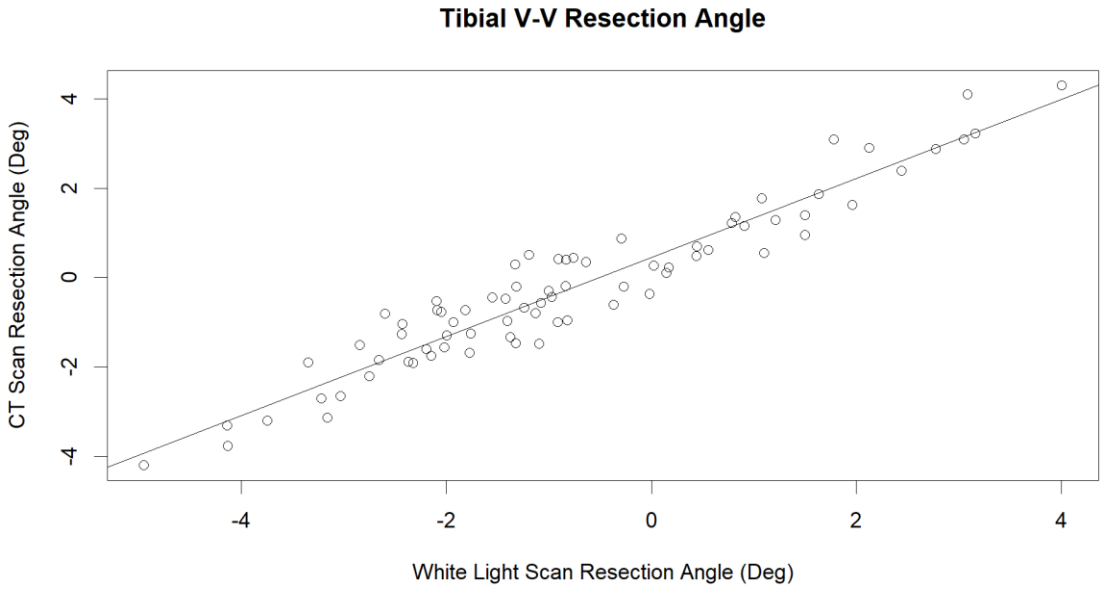

Figure A.16: Tibial coronal plane resection agreement between CT and white light scans.

Table A.1: Angle agreement between white light scan resection and implant alignment expressed as an adjusted correlation coefficient.

Metric	Adjusted R^2
Femoral F-E (Distal Ref.)	0.538
Femoral F-E (Posterior Ref.)	0.269
Femoral V-V	0.766
Femoral I-E	0.839
Tibial F-E	0.859
Tibial V-V	0.945

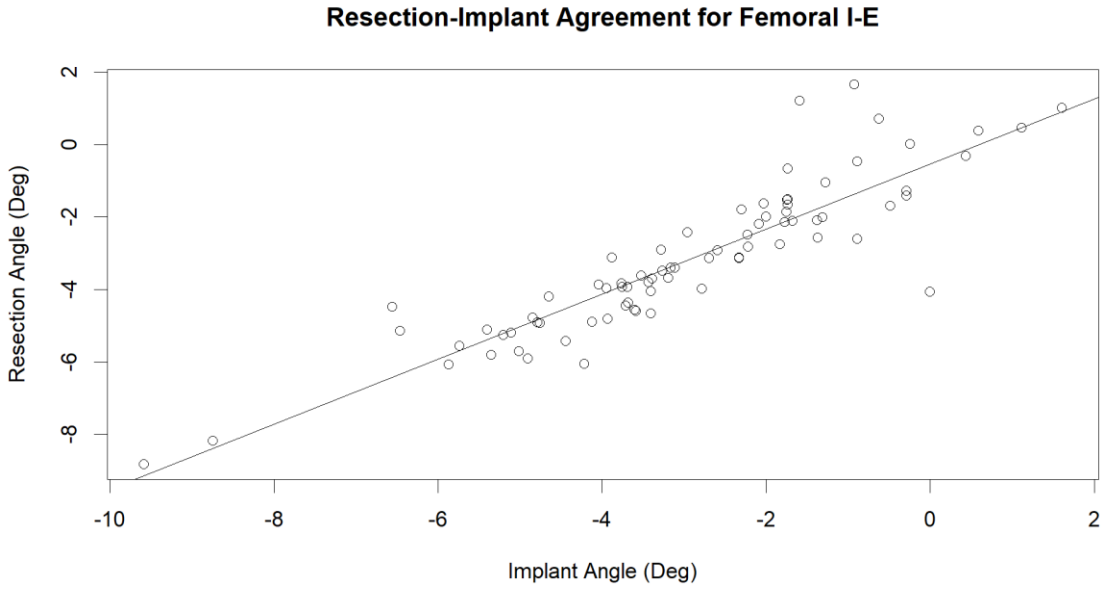

Figure A.17: Femoral transverse plane agreement between resection and implant alignment.

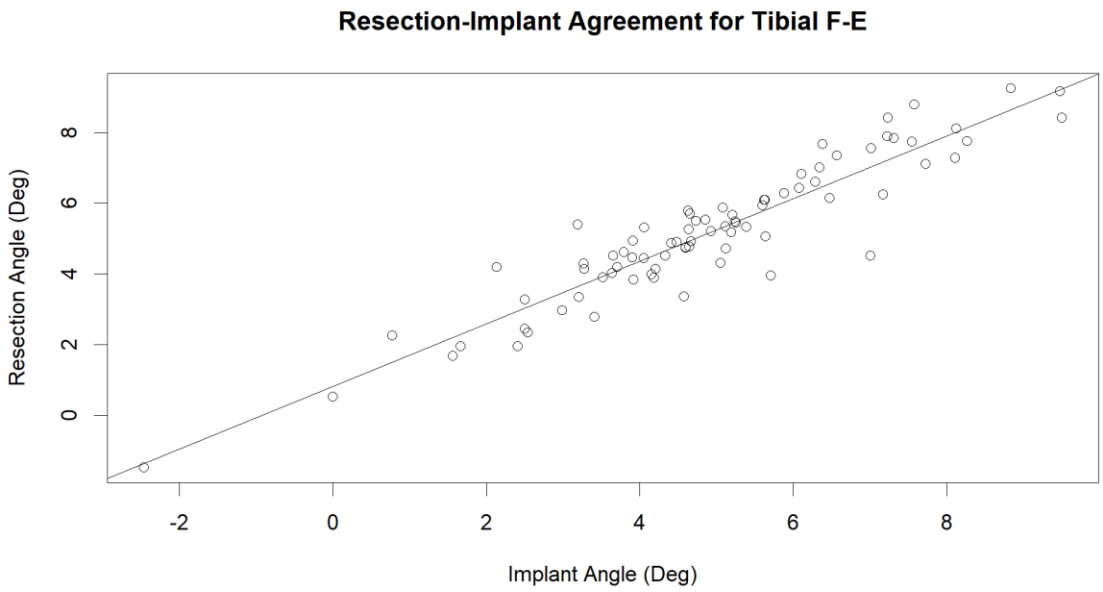

Figure A.18: Tibial sagittal plane agreement between resection and implant alignment.

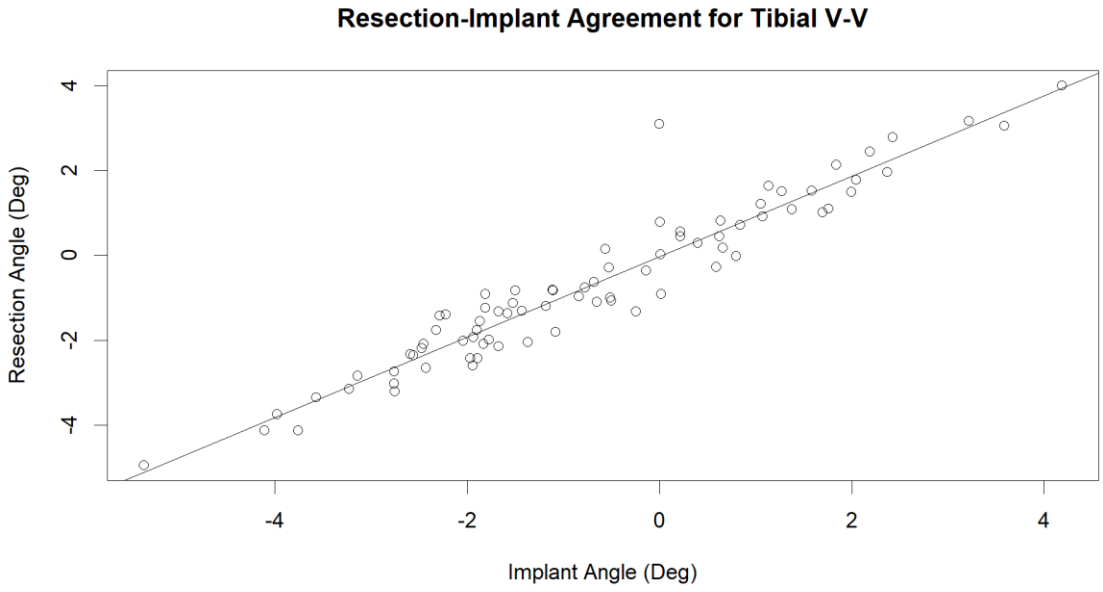

Figure A.19: Tibial coronal plane agreement between resection and implant alignment.

Additional Figures for Chapter Four

Table A.2: Mean values for tibial surface flatness and distance between tibial tray and proximal resection for entire proximal resection surface with plastic deformation.

	RATKA	CTKA	p-value
Surface Flatness (mm)	1.63 ± 0.72	1.66 ± 0.98	0.88
Mean Tray to Resection Distance (μm)	-0.27 ± 0.12	-0.28 ± 0.12	0.61

Table A.3: Mean values for tibial surface flatness for resection surface regions with plastic deformation.

	Resection Surface Flatness (mm)		p-value
Region	**RATKA**	**CTKA**	
Antero-Lateral	0.91 ± 0.73	0.94 ± 0.66	0.85
Postero-Lateral	0.95 ± 0.65	0.94 ± 0.58	0.94
ACL	0.98 ± 0.74	1.04 ± 0.65	0.71
Center	1.21 ± 0.91	1.27 ± 0.82	0.76
PCL	1.12 ± 0.71	1.05 ± 0.45	0.61
Antero-Medial	0.56 ± 0.45	0.69 ± 0.39	0.16
Postero-Medial	0.86 ± 0.60	0.85 ± 0.39	0.98

Table A.4: Mean values for distance between tibial tray and proximal resection for resection surface regions with plastic deformation.

	Mean Tray to Resection Distance (μm)		p-value
Region	**RATKA**	**CTKA**	
Antero-Lateral	-0.13 ± 0.16	-0.16 ± 0.22	0.45
Postero-Lateral	-0.23 ± 0.23	-0.23 ± 0.21	0.95
ACL	-0.27 ± 0.19	-0.29 ± 0.24	0.73
Center	-0.49 ± 0.34	-0.54 ± 0.29	0.50
PCL	-0.40 ± 0.25	-0.41 ± 0.27	0.96
Antero-Medial	-0.11 ± 0.11	-0.13 ± 0.11	0.44
Postero-Medial	-0.25 ± 0.18	-0.21 ± 0.18	0.36

MATLAB Code to Calculate Resection Angles

```
%% Main Script for Resection Angle Analysis
%% Description
% This script is used to perform the Resection Angle Accuracy for Velys and
% Conventional cases.
% The script imports anatomical landmarks, robotic planned points, Pre/Post Op
% CT data, and White Light data.
%% Steps
% 1.) User picks a surgeon with associated cases to analyze
% 2.) Memory is pre-allocated for structures "data"
% 3.) Start analysis by looping through cases
```

```
% 4.) Sort anatomical landmarks given by variable "landmarksList"
% 5.) Read in STL files and convert from triangulation class to structures
% For both Femur and Tibia
% 6.) Create anatomical TM and apply to Pre/Post Op CT and WhiteLight data
% 7.) Create PostOp and WhiteLight to PreOp CT TM through ICP
% 8.) Apply respective ICP TM to PostOp and White Light data
% For all resections
% 9.) Apply respective TM (anatomical and ICP) to resections
% 10.) Fit planes to resections and create intersections with anatomical planes
% 11.) Calculate angles using dot product definition and assign clinically conventions
%% Clear all Data
clear; clc; close all;
%% Create Paths, Constants, and Lists

myFolder = pwd;                     % Searches for current working directory
addpath('functions');               % Add sub folders to current search path
k = strfind(myFolder,'MATLAB');     % Find the "MATLAB" string
PATH = myFolder(1:k - 1);             % Parse away everything after "StreamLine"

analysisType = 'CT';        % Options Include 'CT' or 'WhiteLight'

surgeonList = {'Green','Wright','Swank','Smith','Heoffel'};

for countsl = 5:length(surgeonList)
surgeon = surgeonList{countsl};

% surgeon = 'Wright';               % Options are Green, Wright, Swank, Smith, Heoffel,
and Test

switch surgeon
    case 'Green'
        specimen =
{'C200610L','C200610R','C200617L','C200617R','C200624L','C200624R','C200630L','C200630R',
'C200640L','C200640R','C200656L','C200656R','C200659L','C200659R','C200666L','C200666R'};
% Greens Cases
    case 'Wright'
        specimen =
{'S201490L','S201490R','I200572L','I200572R','I200607L','I200607R','I200620L','I200620R',
'I200624L','I200624R','F200747L','F200747R','F200881L','F200881R','F200882L','F200882R'};
% Wrights Cases
    case 'Swank'
        specimen =
{'L200888L','L200888R','L200997L','L200997R','S201318L','S201318R','S201343L','S201343R',
'S201350L','S201350R','S201408L','S201408R','S201411L','S201411R','S201461L','S201461R'};
% Swanks Cases
    case 'Smith'
        specimen =
{'F200870L','F200870R','F200873L','F200873R','F200875L','F200875R','F200877L','F200877R',
'F200894L','F200894R','F200889L','F200889R','S201497L','S201497R','S201533L','S201533R'};
% Smiths Cases
    case 'Heoffel'
        specimen =
{'S201193L','S201193R','S201240L','S201240R','S201253L','S201253R','S201300L','S201300R',
'S201326L','S201326R','S201471L','S201471R','S201488L','S201488R','S201500L','S201500R'};
% Heoffels Cases
    case 'Test'
        specimen = {'F200894L','F200894R'};
    otherwise
        error('Error')
end

cutPlanes =
{'Anterior','Anterior_Distal','Distal','Posterior_Distal','Posterior','Proximal'};      %
List of Resection Planes
bone = {'Femur','Tibia'};       % List of Bones
```

```
landmarksList =
{'Ankle_Center','Malleolus_Center','Femoral_Head','Femur_Medial_Epicondyle','Femur_Latera
l_Epicondyle',...

'Femur_Anterior_Cortex_Point','Tibia_Anterior_Medial_Plateau','Tibia_Posterior_Medial_Pla
teau','Tibia_Anterior_Lateral_Plateau','Tibia_Posterior_Lateral_Plateau',...

'Femur_Center','Tibia_Center','Tibia_Medial_Tubercle','Tibia_Lateral_Tubercle'};   %
Forces Anatomical Landmarks in Boxes.txt to be read in this order

%% Pre-Allocate Empty Structures

tempStructs = struct('vertices',[],'faces',[],'TMvertices',[]);      % Create parent
structure with empty structures vertices, faces, and TMvertices
tempStructc =
struct('vertices',[],'faces',[],'TMvertices',[],'Distance',[],'Normal',zeros(1,3),'Point'
,zeros(1,3));        % Create parent structure with empty structures vertices, faces,
TMvertices, Distance, Normal, and Point
for counts = length(specimen):-1:1      % Create Final Size of Structure on 1st Iteration
    data(counts).ID = 'Specimen ID';                    % Allocate memory for ID
    data(counts).AnatLandmarks = zeros(14,3);           % Allocate memory for Anatomical
Landmarks
    data(counts).PlanningPoints = zeros(30,3);          % Allocate memory for Planning
Points

    % Allocate memory for Femur and Tibia
    data(counts).Femur =
struct('PreOpCT1',tempStructs,'PreOpCT2',tempStructs,'PostOpCT',tempStructs,'WhiteLight',
tempStructs,'TM_GtoA',zeros(4),'TM_LtoC',zeros(4),'TM_PtoP',zeros(4),'Angles',struct('FE'
,0,'VV',0,'IE',0,'aFE',0));
    data(counts).Tibia =
struct('PreOpCT1',tempStructs,'PreOpCT2',tempStructs,'PostOpCT',tempStructs,'WhiteLight',
tempStructs,'TM_GtoA',zeros(4),'TM_LtoC',zeros(4),'TM_PtoP',zeros(4),'Angles',struct('FE'
,0,'VV',0));

    % Allocate memory for Resection Planes
    for countc = length(cutPlanes):-1:1
        data(counts).CutPlanes.(cutPlanes{countc}) = tempStructc;
    end
end

%% Analysis Starts Here

for counts = 1:length(specimen)     % Start Specimen Loop

    if mod(counts,2) == 1       % Odd = Left
        chirality = 'Left';
    elseif mod(counts,2) == 0   % Even = Right
        chirality = 'Right';
    end

    data(counts).ID = [specimen{counts}];       % Fill ID with Specimen Name

    % Load in Anatomical Landmarks
    fid = fopen([PATH,'Boxes_ScriptLog/',specimen{counts},'_Boxes.txt']);
    tempAnatLandmarks = textscan(fid,'%s %f %f %f','Delimiter',',');
    fclose(fid);

    % Organize Anatomical Landmarks by landmarksList
    for countl = 1:length(landmarksList)
        myLandmark = landmarksList{countl};
        for counta = 1:size(tempAnatLandmarks{1,1},1)
            testLandmark = tempAnatLandmarks{1}{counta};
            if strcmp(myLandmark,testLandmark)
                x = tempAnatLandmarks{2}(counta);
                y = tempAnatLandmarks{3}(counta);
                z = tempAnatLandmarks{4}(counta);
```

```
                data(counts).AnatLandmarks(countl,:) = [x,y,z];
            end
        end
    end

    % Load in Planning Points
    data(counts).PlanningPoints =
readExp([PATH,'Boxes_ScriptLog/',specimen{counts},'_ScriptLog.txt']);

    for countc = 1:length(cutPlanes)        % Start Resection Plane Loop

        switch analysisType
            case 'CT'
                tempCut =
stlread([PATH,'PostOp_CT_Analysis/Cut_Planes/',specimen{counts},'_',cutPlanes{countc},'_'
,'Cut.stl']);     % Read in Resection Planes
            case 'WhiteLight'
                tempCut =
stlread([PATH,'White_Light_Analysis/Cut_Planes/',specimen{counts},'_',cutPlanes{countc},'
_','Cut.stl']);     % Read in Resection Planes
            otherwise
                error('Could not determine type of analysis');
        end

        data(counts).CutPlanes.(cutPlanes{countc}).vertices =
zeros(size(tempCut.Points));           % Pre-allocate Contents of Fields
        data(counts).CutPlanes.(cutPlanes{countc}).faces =
zeros(size(tempCut.ConnectivityList));

        data(counts).CutPlanes.(cutPlanes{countc}).vertices = tempCut.Points;        %
Convert stlread Structures to write friendly structures
        data(counts).CutPlanes.(cutPlanes{countc}).faces = tempCut.ConnectivityList;
    end

    for countb = 1:length(bone)     % Start Bone Loop
        tempPreOpCT1 =
stlread([PATH,'PostOp_CT_Analysis/PreOp_CT_Mod/',specimen{counts},'_',bone{countb},'_PreO
p_CT_Mod.stl']);            % Load in Modified PreOp CT Nodes for PostOp Analysis
        tempPreOpCT2 =
stlread([PATH,'White_Light_Analysis/PreOp_CT_Mod/',specimen{counts},'_',bone{countb},'_Pr
eOp_CT_Mod.stl']);          % Load in Modified PreOp CT Nodes for WhiteLight Analysis
        tempPostOpCT =
stlread([PATH,'PostOp_CT_Analysis/PostOp_CT_Mod/',specimen{counts},'_',bone{countb},'_Pos
tOp_CT_Mod.stl']);          % Load in Modified PostOp CT Nodes
        tempWhiteLight =
stlread([PATH,'White_Light_Analysis/White_Light_Mod/',specimen{counts},'_',bone{countb},'
_Laser_Mod.stl']);        % Load in Modified WhiteLight Nodes

        tempPreOpCTOG =
stlread([PATH,'PreOp_CT/',specimen{counts},'_',bone{countb},'_PreOp_Full.stl']);
% Load in Original PreOp CT Nodes
        tempPostOpCTOG =
stlread([PATH,'PostOp_CT_Analysis/PostOp_CT_Registered/',specimen{counts},'_',bone{countb
},'_PostOp_CT.stl']);     % Load in Original PostOp CT Nodes
        tempWhiteLightOG =
stlread([PATH,'White_Light_Analysis/White_Light_Registered/',specimen{counts},'_',bone{co
untb},'_Laser.stl']);   % Load in Original WhiteLight Nodes

        if strcmp(bone{countb},'Femur')         % Conditional Statement for Femur
            % Allocate memory for vertices and faces for modified data
            data(counts).Femur.PreOpCT1.vertices = zeros(size(tempPreOpCT1.Points));
            data(counts).Femur.PreOpCT1.faces =
zeros(size(tempPreOpCT1.ConnectivityList));
            data(counts).Femur.PreOpCT1.TMvertices = zeros(size(tempPreOpCT1.Points));
            data(counts).Femur.PreOpCT2.vertices = zeros(size(tempPreOpCT2.Points));
            data(counts).Femur.PreOpCT2.faces =
zeros(size(tempPreOpCT2.ConnectivityList));
            data(counts).Femur.PreOpCT2.TMvertices = zeros(size(tempPreOpCT2.Points));
```

```
            data(counts).Femur.PostOpCT.vertices = zeros(size(tempPostOpCT.Points));
            data(counts).Femur.PostOpCT.faces =
zeros(size(tempPostOpCT.ConnectivityList));
            data(counts).Femur.PostOpCT.TMvertices = zeros(size(tempPostOpCT.Points));
            data(counts).Femur.WhiteLight.vertices = zeros(size(tempWhiteLight.Points));
            data(counts).Femur.WhiteLight.faces =
zeros(size(tempWhiteLight.ConnectivityList));
            data(counts).Femur.WhiteLight.TMvertices =
zeros(size(tempWhiteLight.Points));

            % Allocate memory for vertices and faces for original data
            data(counts).Femur.PreOpCT1.OGvertices = zeros(size(tempPreOpCTOG.Points));
            data(counts).Femur.PreOpCT1.OGfaces =
zeros(size(tempPreOpCTOG.ConnectivityList));
            data(counts).Femur.PreOpCT1.OGTMvertices = zeros(size(tempPreOpCTOG.Points));
            data(counts).Femur.PostOpCT.OGvertices = zeros(size(tempPostOpCTOG.Points));
            data(counts).Femur.PostOpCT.OGfaces =
zeros(size(tempPostOpCTOG.ConnectivityList));
            data(counts).Femur.PostOpCT.OGTMvertices =
zeros(size(tempPostOpCTOG.Points));
            data(counts).Femur.WhiteLight.OGvertices =
zeros(size(tempWhiteLightOG.Points));
            data(counts).Femur.WhiteLight.OGfaces =
zeros(size(tempWhiteLightOG.ConnectivityList));
            data(counts).Femur.WhiteLight.OGTMvertices =
zeros(size(tempWhiteLightOG.Points));

            % Convert Triangulation Class to structure
            data(counts).Femur.PreOpCT1.vertices = tempPreOpCT1.Points;
            data(counts).Femur.PreOpCT1.faces = tempPreOpCT1.ConnectivityList;
            data(counts).Femur.PreOpCT2.vertices = tempPreOpCT2.Points;
            data(counts).Femur.PreOpCT2.faces = tempPreOpCT2.ConnectivityList;
            data(counts).Femur.PostOpCT.vertices = tempPostOpCT.Points;
            data(counts).Femur.PostOpCT.faces = tempPostOpCT.ConnectivityList;
            data(counts).Femur.WhiteLight.vertices = tempWhiteLight.Points;
            data(counts).Femur.WhiteLight.faces = tempWhiteLight.ConnectivityList;

            data(counts).Femur.PreOpCT1.OGvertices = tempPreOpCTOG.Points;
            data(counts).Femur.PreOpCT1.OGfaces = tempPreOpCTOG.ConnectivityList;
            data(counts).Femur.PostOpCT.OGvertices = tempPostOpCTOG.Points;
            data(counts).Femur.PostOpCT.OGfaces = tempPostOpCTOG.ConnectivityList;
            data(counts).Femur.WhiteLight.OGvertices = tempWhiteLightOG.Points;
            data(counts).Femur.WhiteLight.OGfaces = tempWhiteLightOG.ConnectivityList;

            [data(counts).Femur.TM_GtoA] =
anatomicalTM(data(counts).AnatLandmarks,bone{countb},data(counts).PlanningPoints,chiralit
y);      % Create Anatomical TM

            % Apply Inverse Transformation to Pre/Post Op CT and WhiteLight vertices
            [data(counts).Femur.PreOpCT1.TMvertices] =
iTransformNodes(data(counts).Femur.PreOpCT1.vertices,data(counts).Femur.TM_GtoA);
            [data(counts).Femur.PreOpCT1.OGTMvertices] =
iTransformNodes(data(counts).Femur.PreOpCT1.OGvertices,data(counts).Femur.TM_GtoA);
            [data(counts).Femur.PreOpCT2.TMvertices] =
iTransformNodes(data(counts).Femur.PreOpCT2.vertices,data(counts).Femur.TM_GtoA);
            [data(counts).Femur.PostOpCT.TMvertices] =
iTransformNodes(data(counts).Femur.PostOpCT.vertices,data(counts).Femur.TM_GtoA);
            [data(counts).Femur.PostOpCT.OGTMvertices] =
iTransformNodes(data(counts).Femur.PostOpCT.OGvertices,data(counts).Femur.TM_GtoA);
            [data(counts).Femur.WhiteLight.TMvertices] =
iTransformNodes(data(counts).Femur.WhiteLight.vertices,data(counts).Femur.TM_GtoA);
            [data(counts).Femur.WhiteLight.OGTMvertices] =
iTransformNodes(data(counts).Femur.WhiteLight.OGvertices,data(counts).Femur.TM_GtoA);

            [data(counts).Femur.TM_PtoP] =
icpTM(data(counts).Femur.PreOpCT1.TMvertices,data(counts).Femur.PostOpCT.TMvertices);
% Create ICP TM for Pre/Post Op data
```

```
            [data(counts).Femur.TM_LtoC] =
icpTM(data(counts).Femur.PreOpCT2.TMvertices,data(counts).Femur.WhiteLight.TMvertices);
% Create ICP TM for Pre/WhiteLight data

            % Apply ICP Transformation to PostOp CT and WhiteLight vertices
            [data(counts).Femur.PostOpCT.TMvertices] =
fTransformNodes(data(counts).Femur.PostOpCT.TMvertices,data(counts).Femur.TM_PtoP);
            [data(counts).Femur.PostOpCT.OGTMvertices] =
fTransformNodes(data(counts).Femur.PostOpCT.OGTMvertices,data(counts).Femur.TM_PtoP);
            [data(counts).Femur.WhiteLight.TMvertices] =
fTransformNodes(data(counts).Femur.WhiteLight.TMvertices,data(counts).Femur.TM_LtoC);
            [data(counts).Femur.WhiteLight.OGTMvertices] =
fTransformNodes(data(counts).Femur.WhiteLight.OGTMvertices,data(counts).Femur.TM_LtoC);

            for countc = 1:length(cutPlanes) - 1        % Start Resection Plane Loop for
Femur (Anterior to Posterior)

                [data(counts).CutPlanes.(cutPlanes{countc}).TMvertices] =
iTransformNodes(data(counts).CutPlanes.(cutPlanes{countc}).vertices,data(counts).Femur.TM
_GtoA);        % Perform Anatomical Alignment of PostOpCT Resection Planes
                switch analysisType
                    case 'CT'
                        [data(counts).CutPlanes.(cutPlanes{countc}).TMvertices] =
fTransformNodes(data(counts).CutPlanes.(cutPlanes{countc}).TMvertices,data(counts).Femur.
TM_PtoP);      % Perform ICP Alignment of PostOpCT Resection Planes
                    case 'WhiteLight'
                        [data(counts).CutPlanes.(cutPlanes{countc}).TMvertices] =
fTransformNodes(data(counts).CutPlanes.(cutPlanes{countc}).TMvertices,data(counts).Femur.
TM_LtoC);      % Perform ICP Alignment of WhiteLight Resection Planes
                    otherwise
                        error('Error Determining Type of Analysis')
                end

[data(counts).CutPlanes.(cutPlanes{countc}).Distance,data(counts).CutPlanes.(cutPlanes{co
untc}).Normal,data(counts).CutPlanes.(cutPlanes{countc}).Point] =
resectionPlanes(data(counts).CutPlanes.(cutPlanes{countc}).TMvertices);         % Affine
Fit Plane and Quantify Distance

                switch cutPlanes{countc}
                    case 'Anterior'
                        % If normal for Anterior Plane is pointing posteriorly, flip the
normal to point anteriorly
                        if data(counts).CutPlanes.Anterior.Normal(2) < 0
                            data(counts).CutPlanes.Anterior.Normal = -
data(counts).CutPlanes.Anterior.Normal;
                        end

                        tempNorm = data(counts).CutPlanes.Anterior.Normal;
                        tempNorm(1) = 0; tempNorm = tempNorm/norm(tempNorm);    % Project
onto Sagittal Plane and Create Unit Vector
                        data(counts).Femur.Angles.Anterior2SI =
acosd(dot(tempNorm,[0,0,1]));
                    case 'Distal'
                        % If normal for Distal Plane is pointing inferiorly, flip the
normal to point superiorly
                        if data(counts).CutPlanes.Distal.Normal(3) < 0
                            data(counts).CutPlanes.Distal.Normal = -
data(counts).CutPlanes.Distal.Normal;
                        end

                        tempNorm = data(counts).CutPlanes.Distal.Normal;
                        tempNorm(2) = 0; tempNorm = tempNorm/norm(tempNorm);    % Project
onto Coronal Plane and Create Unit Vector
                        data(counts).Femur.Angles.VV = acosd(dot(tempNorm,[0,0,1]));

                        tempNorm = data(counts).CutPlanes.Distal.Normal;
                        tempNorm(1) = 0; tempNorm = tempNorm/norm(tempNorm);    % Project
onto Sagittal Plane and Create Unit Vector
```

```
                        data(counts).Femur.Angles.FE = acosd(dot(tempNorm,[0,0,1]));
                    case 'Posterior'
                        % If normal for Posterior Plane is pointing posteriorly, flip the
normal to point anteriorly
                        if data(counts).CutPlanes.Posterior.Normal(2) < 0
                            data(counts).CutPlanes.Posterior.Normal = -
data(counts).CutPlanes.Posterior.Normal;
                        end

                        tempNorm = data(counts).CutPlanes.Posterior.Normal;
                        tempNorm(3) = 0; tempNorm = tempNorm/norm(tempNorm);    % Project
onto Axial Plane and Create Unit Vector
                        data(counts).Femur.Angles.IE = acosd(dot(tempNorm,[0,1,0]));

                        % Temporarily flip normal to point posteriorly
                        if data(counts).CutPlanes.Posterior.Normal(2) > 0
                            tempNorm = -data(counts).CutPlanes.Posterior.Normal;
                        end

                        tempNorm(1) = 0; tempNorm = tempNorm/norm(tempNorm);    % Project
onto Sagittal Plane and Create Unit Vector
                        data(counts).Femur.Angles.Posterior2SI =
acosd(dot(tempNorm,[0,0,1]));    % Calculate Angle between Posterior Normal and SI
                    otherwise
                end

            end % End Resection Plane Loop

            % Set Clinically Correct Signs for Rotations
            if data(counts).CutPlanes.Distal.Normal(2) < 0
                data(counts).Femur.Angles.FE = -data(counts).Femur.Angles.FE;
            end

            switch chirality
                case 'Left'
                    if data(counts).CutPlanes.Distal.Normal(1) > 0
                        data(counts).Femur.Angles.VV = -data(counts).Femur.Angles.VV;
                    end
                    if data(counts).CutPlanes.Posterior.Normal(1) < 0
                        data(counts).Femur.Angles.IE = -data(counts).Femur.Angles.IE;
                    end
                case 'Right'
                    if data(counts).CutPlanes.Distal.Normal(1) < 0
                        data(counts).Femur.Angles.VV = -data(counts).Femur.Angles.VV;
                    end
                    if data(counts).CutPlanes.Posterior.Normal(1) > 0
                        data(counts).Femur.Angles.IE = -data(counts).Femur.Angles.IE;
                    end
            end

            % Solve for Anatomical Axis for Femur
            tempPlanningPoints =
iTransformNodes(data(counts).PlanningPoints,data(counts).Femur.TM_GtoA);       %
Transform Planning Points to Anatomical CoSys
            anatAxis = tempPlanningPoints(25,:) - tempPlanningPoints(24,:); anatAxis =
anatAxis/norm(anatAxis);  % Create Unit Vector in Anatomical CoSys
            anatAxis(1) = 0; anatAxis = anatAxis/norm(anatAxis);
            data(counts).Femur.Angles.aFE = acosd(dot(anatAxis,[0,0,1]));     % Solve for
angle between SI axis and Projected Vector to Sagittal Plane

            % Set Clinically Correct Signs for Anatomic Axis (FE component)
            if anatAxis(2) < 0
                data(counts).Femur.Angles.aFE = - data(counts).Femur.Angles.aFE;
            end

        elseif strcmp(bone{countb},'Tibia')         % Conditional Statement for Tibia
            % Allocate memory for vertices and faces for modified data
            data(counts).Tibia.PreOpCT1.vertices = zeros(size(tempPreOpCT1.Points));
```

```
            data(counts).Tibia.PreOpCT1.faces =
zeros(size(tempPreOpCT1.ConnectivityList));
            data(counts).Tibia.PreOpCT1.TMvertices = zeros(size(tempPreOpCT1.Points));
            data(counts).Tibia.PreOpCT2.vertices = zeros(size(tempPreOpCT2.Points));
            data(counts).Tibia.PreOpCT2.faces =
zeros(size(tempPreOpCT2.ConnectivityList));
            data(counts).Tibia.PreOpCT2.TMvertices = zeros(size(tempPreOpCT2.Points));
            data(counts).Tibia.PostOpCT.vertices = zeros(size(tempPostOpCT.Points));
            data(counts).Tibia.PostOpCT.faces =
zeros(size(tempPostOpCT.ConnectivityList));
            data(counts).Tibia.PostOpCT.TMvertices = zeros(size(tempPostOpCT.Points));
            data(counts).Tibia.WhiteLight.vertices = zeros(size(tempWhiteLight.Points));
            data(counts).Tibia.WhiteLight.faces =
zeros(size(tempWhiteLight.ConnectivityList));
            data(counts).Tibia.WhiteLight.TMvertices =
zeros(size(tempWhiteLight.Points));

            % Allocate memory for vertices and faces for original data
            data(counts).Tibia.PreOpCT1.OGvertices = zeros(size(tempPreOpCTOG.Points));
            data(counts).Tibia.PreOpCT1.OGfaces =
zeros(size(tempPreOpCTOG.ConnectivityList));
            data(counts).Tibia.PreOpCT1.OGTMvertices = zeros(size(tempPreOpCTOG.Points));
            data(counts).Tibia.PostOpCT.OGvertices = zeros(size(tempPostOpCTOG.Points));
            data(counts).Tibia.PostOpCT.OGfaces =
zeros(size(tempPostOpCTOG.ConnectivityList));
            data(counts).Tibia.PostOpCT.OGTMvertices =
zeros(size(tempPostOpCTOG.Points));
            data(counts).Tibia.WhiteLight.OGvertices =
zeros(size(tempWhiteLightOG.Points));
            data(counts).Tibia.WhiteLight.OGfaces =
zeros(size(tempWhiteLightOG.ConnectivityList));
            data(counts).Tibia.WhiteLight.OGTMvertices =
zeros(size(tempWhiteLightOG.Points));

            % Convert Triangulation Class to structure
            data(counts).Tibia.PreOpCT1.vertices = tempPreOpCT1.Points;
            data(counts).Tibia.PreOpCT1.faces = tempPreOpCT1.ConnectivityList;
            data(counts).Tibia.PreOpCT2.vertices = tempPreOpCT2.Points;
            data(counts).Tibia.PreOpCT2.faces = tempPreOpCT2.ConnectivityList;
            data(counts).Tibia.PostOpCT.vertices = tempPostOpCT.Points;
            data(counts).Tibia.PostOpCT.faces = tempPostOpCT.ConnectivityList;
            data(counts).Tibia.WhiteLight.vertices = tempWhiteLight.Points;
            data(counts).Tibia.WhiteLight.faces = tempWhiteLight.ConnectivityList;

            data(counts).Tibia.PreOpCT1.OGvertices = tempPreOpCTOG.Points;
            data(counts).Tibia.PreOpCT1.OGfaces = tempPreOpCTOG.ConnectivityList;
            data(counts).Tibia.PostOpCT.OGvertices = tempPostOpCTOG.Points;
            data(counts).Tibia.PostOpCT.OGfaces = tempPostOpCTOG.ConnectivityList;
            data(counts).Tibia.WhiteLight.OGvertices = tempWhiteLightOG.Points;
            data(counts).Tibia.WhiteLight.OGfaces = tempWhiteLightOG.ConnectivityList;

            [data(counts).Tibia.TM_GtoA] =
anatomicalTM(data(counts).AnatLandmarks,bone{countb},data(counts).PlanningPoints,chiralit
y);     % Create Anatomical TM

            % Apply Inverse Transformation to Pre/Post Op CT and WhiteLight vertices
            [data(counts).Tibia.PreOpCT1.TMvertices] =
iTransformNodes(data(counts).Tibia.PreOpCT1.vertices,data(counts).Tibia.TM_GtoA);
            [data(counts).Tibia.PreOpCT1.OGTMvertices] =
iTransformNodes(data(counts).Tibia.PreOpCT1.OGvertices,data(counts).Tibia.TM_GtoA);
            [data(counts).Tibia.PreOpCT2.TMvertices] =
iTransformNodes(data(counts).Tibia.PreOpCT2.vertices,data(counts).Tibia.TM_GtoA);
            [data(counts).Tibia.PostOpCT.TMvertices] =
iTransformNodes(data(counts).Tibia.PostOpCT.vertices,data(counts).Tibia.TM_GtoA);
            [data(counts).Tibia.PostOpCT.OGTMvertices] =
iTransformNodes(data(counts).Tibia.PostOpCT.OGvertices,data(counts).Tibia.TM_GtoA);
            [data(counts).Tibia.WhiteLight.TMvertices] =
iTransformNodes(data(counts).Tibia.WhiteLight.vertices,data(counts).Tibia.TM_GtoA);
```

```
            [data(counts).Tibia.WhiteLight.OGTMvertices] =
iTransformNodes(data(counts).Tibia.WhiteLight.OGvertices,data(counts).Tibia.TM_GtoA);

            [data(counts).Tibia.TM_PtoP] =
icpTM(data(counts).Tibia.PreOpCT1.TMvertices,data(counts).Tibia.PostOpCT.TMvertices);
% Create ICP TM for Pre/Post Op data
            [data(counts).Tibia.TM_LtoC] =
icpTM(data(counts).Tibia.PreOpCT2.TMvertices,data(counts).Tibia.WhiteLight.TMvertices);
% Create ICP TM for Pre/WhiteLight data

            [data(counts).Tibia.PostOpCT.TMvertices] =
fTransformNodes(data(counts).Tibia.PostOpCT.TMvertices,data(counts).Tibia.TM_PtoP);
            [data(counts).Tibia.PostOpCT.OGTMvertices] =
fTransformNodes(data(counts).Tibia.PostOpCT.OGTMvertices,data(counts).Tibia.TM_PtoP);
            [data(counts).Tibia.WhiteLight.TMvertices] =
fTransformNodes(data(counts).Tibia.WhiteLight.TMvertices,data(counts).Tibia.TM_LtoC);
            [data(counts).Tibia.WhiteLight.OGTMvertices] =
fTransformNodes(data(counts).Tibia.WhiteLight.OGTMvertices,data(counts).Tibia.TM_LtoC);

            [data(counts).CutPlanes.(cutPlanes{end}).TMvertices] =
iTransformNodes(data(counts).CutPlanes.(cutPlanes{end}).vertices,data(counts).Tibia.TM_Gt
oA);        % Perform Anatomical Alignment of PostOpCT Resection Planes

            switch analysisType
                case 'CT'
                    [data(counts).CutPlanes.(cutPlanes{end}).TMvertices] =
fTransformNodes(data(counts).CutPlanes.(cutPlanes{end}).TMvertices,data(counts).Tibia.TM_
PtoP);      % Perform ICP Alignment of PostOpCT Resection Planes
                case 'WhiteLight'
                    [data(counts).CutPlanes.(cutPlanes{end}).TMvertices] =
fTransformNodes(data(counts).CutPlanes.(cutPlanes{end}).TMvertices,data(counts).Tibia.TM_
LtoC);      % Perform ICP Alignment of WhiteLight Resection Planes
                otherwise
                    error('Error Determining Type of Analysis')
            end


[data(counts).CutPlanes.(cutPlanes{end}).Distance,data(counts).CutPlanes.(cutPlanes{end})
.Normal,data(counts).CutPlanes.(cutPlanes{end}).Point] =
resectionPlanes(data(counts).CutPlanes.(cutPlanes{end}).TMvertices);         % Affine Fit
Plane and Quantify Distance

            % If normal for Proximal Plane is pointing inferiorly, flip the normal to
point superiorly (Should assist FE and VV)
            if data(counts).CutPlanes.Proximal.Normal(3) < 0
                data(counts).CutPlanes.Proximal.Normal = -
data(counts).CutPlanes.Proximal.Normal;
            end

            tempNorm = data(counts).CutPlanes.Proximal.Normal;
            tempNorm(2) = 0; tempNorm = tempNorm/norm(tempNorm);    % Project onto
Coronal Plane and Create Unit Vector
            data(counts).Tibia.Angles.VV = acosd(dot(tempNorm,[0,0,1]));

            tempNorm = data(counts).CutPlanes.Proximal.Normal;
            tempNorm(1) = 0; tempNorm = tempNorm/norm(tempNorm);    % Project onto
Sagittal Plane and Create Unit Vector
            data(counts).Tibia.Angles.FE = acosd(dot(tempNorm,[0,0,1]));

            % Set Clinically Correct Signs for Rotations
            if data(counts).CutPlanes.Proximal.Normal(2) > 0
                data(counts).Tibia.Angles.FE = -data(counts).Tibia.Angles.FE;
            end

            switch chirality
                case 'Left'
                    if data(counts).CutPlanes.Proximal.Normal(1) < 0
                        data(counts).Tibia.Angles.VV = -data(counts).Tibia.Angles.VV;
```

```
                    end
                case 'Right'
                    if data(counts).CutPlanes.Proximal.Normal(1) > 0
                        data(counts).Tibia.Angles.VV = -data(counts).Tibia.Angles.VV;
                    end
            end
        end    % End Femur/Tibia Conditional Statement
    end        % End Bone Loop
end            % End Specimen Loop

disp(['Finished Surgeon: ',num2str(countsl),'/5'])

%% Save Variables

switch analysisType
    case 'CT'
        save([PATH,'MATLAB/MainIO/variables/','dataBatch',surgeon,'.mat'],'data')
    case 'WhiteLight'

save([PATH,'MATLAB/MainIO/variables/','dataBatch',surgeon,'WhiteLight.mat'],'data')
    otherwise
        error('There was trouble saving the data')
end

end
```